**AGRICULTURAL UNIVERSITY OF ATHENS**
**DEPARTMENT OF ANIMAL SCIENCE**
**LABORATORY OF ANATOMY**
**& PHYSIOLOGY OF FARM ANIMALS**

**PhD Thesis**

# Advanced laboratory and Point Of Service technologies for the optimization of livestock biosecurity

**Georgios A. Manesis**

Supervisor:
Ioannis Bossis, Professor Aristotle University of Thessaloniki

Advisory committee:
Ioannis Bossis, Professor, Aristotle University of Thessaloniki
Athanasios Gelasakis, Assistant Professor, Agricultural University of Athens
Georgios Theodorou, Assistant Professor, Agricultural University of Athens

**ATHENS**
**2023**

**AGRICULTURAL UNIVERSITY OF ATHENS**
**DEPARTMENT OF ANIMAL SCIENCE**
**LABORATORY OF ANATOMY**
**& PHYSIOLOGY OF FARM ANIMALS**

**PhD Thesis**

# Advanced laboratory and Point Of Service technologies for the optimization of livestock biosecurity

# Καινοτόμες εργαστηριακές μέθοδοι και τεχνολογίες διαγνωστικών συσκευών πεδίου για τη βελτιστοποίηση της βιοασφάλειας στα αγροτικά ζώα

**Georgios A. Manesis**

Examination committee:
Ioannis Bossis, Professor, Aristotle University of Thessaloniki
Athanasios Gelasakis, Assistant Professor, Agricultural University of Athens
Georgios Theodorou, Assistant Professor, Agricultural University of Athens
Ioannis Politis, Professor, Agricultural University of Athens
George P. Laliotis, Assistant Professor, Agricultural University of Athens
Georgios Vatzias, Assistant Professor, Aristotle University of Thessaloniki
Georgios Michailidis, Associate Professor, Aristotle University of Thessaloniki

**Advanced laboratory and Point Of Service technologies for the optimization of livestock biosecurity**

*Department of Animal Science*
*Laboratory of Anatomy & Physiology of Farm Animals*

# ABSTRACT

The swine industry accounts for approximately 35% of the global meat production. EU is the second biggest producer of pork meat after China and the largest exporter of pork products. European policies promote greener and more sustainable agriculture and food systems and are expected to reshape the legislation relevant to the pig sector, including animal health and welfare.

To meet the surging demand for animal products and reduce production costs, modern farming systems are focused on intensification and higher stocking density. However, increased stocking density can accelerate pathogen transmission. On top of that, vast globalized trade networks and insufficient surveillance programs further exacerbate disease outbreaks and the emergence of transboundary infectious agents. Among them, viral diseases can be devastating to the swine sector due to (i) their transmission dynamics, (ii) the lack of effective treatments, (iii) the limited vaccine availability and efficiency, and (iv) the absence of monitoring systems and the lack of coordinated preventive measures. Porcine Parvovirus 1 (PPV1), Porcine Circovirus type 2 (PCV-2), Porcine Reproductive and Respiratory Syndrome Virus (PRRSV), Swine Influenza A (SIV), African Swine Fever Virus (ASFV) and Classical Swine Fever Virus (CSFV) are among the most important viral diseases affecting swine due to their socioeconomic impact, wide expansion and/or severity.

The time from disease onset to laboratory confirmation of the etiologic agent may vary from days to up to a month. For this reason, advanced laboratory technologies and biosensors have been gradually integrated in Point Of Service (POS) diagnostic devices to provide timely diagnosis, optimize livestock biosecurity and tackle animal diseases. These diagnostics are defined as analytical devices and other tests capable of providing rapid diagnosis on-site without the need of core laboratories. The available POS applications for animal diseases could be classified in two broad categories, paper-based diagnostics and microfluidic devices.

The main objectives of this thesis were the development of the analytical protocol and the initial validation of a novel microfluidic Lab-on-Chip analyzer for the rapid and reliable detection of major swine viral pathogens at the POS setting. The state-of-the-art POS

diagnostic system targeted the six swine viruses mentioned earlier. The system utilized microfluidics and Photonic Integrated Circuit (PIC) sensors for the label-free detection of viral antigens.

The device followed a modular approach to efficiently integrate its components into a single, portable diagnostic platform weighing around 45 kg, with a size of about 40×50×60 cm. The dimensions and weight provided refer to a fully functional and autonomous device that include communication hardware and software, fully functional display and operational controls and waste containers, and a sterilization and sanitation module with a UV-C unit. The new diagnostic device can be divided into three functional subsystems: 1) the mechanics/microfluidics subsystem consisting of (i) a fluid delivery syringe system, (ii) motors, (iii) a microfluidics channel, (iv) a waste tank, and (v) a Peltier element, 2) the optics subsystem consisting of (i) a tunable laser, (ii) optic fibers, (iii) a photodiode and (iv) the biosensors, namely the Photonic Integrated Circuits (PICs) on silicon nitride, and 3) the firmware subsystem consisting of (i) the microcontroller and its software, (ii) an arduino data logger, and (iii) an SD card. Features such as system operation, analysis progress, data collection/storage, and results were monitored via an Android application. The assay for the detection of the six viruses could be completed within 60 min. Minimal handling and training was required for the operation of the device. The device also allowed multiplexing.

The biosensors used in the novel device utilized 8 ring resonators with immobilized antibodies (MREs) on their surfaces for the capturing of the viral particles. The capture of viral antigens via the antibodies resulted in a localized change in the refractive index which extended beyond the sensor's surface. This change in the refractive index modified the resonant wavelength of the ring resonators upon laser excitation, causing a signal shift that was detected by the photodiode and was associated with the presence of the targeted viral particles.

The analysis protocol of the novel POS device included five consecutive steps: i) the buffer step, ii) the sample step, iii) the washing step, iv) the regeneration step and v) the final washing step. Two main buffers, phosphate buffered saline (PBS) and 2-(N-morpholino) ethanesulfonic acid (MES), supplemented with Bovine Serum Albumin (BSA), were selected for viral detection. Data analysis was performed using a case-specific algorithm which incorporated the LOWESS (Locally Weighted Scatterplot Smoothing) algorithm, and a novel software for PC, written in Python. The same shift calculation algorithm was also accessible through an Android application (in a tablet) and an online platform.

Reference and complex biological samples (oral fluids and sera), collected from swine farms, were used to validate the device. All samples were tested with conventional PCR assays to confirm their status (positive or negative) and positive samples (containing the targeted viruses) were quantified using SYBR Green-based real-time PCR assays.

To estimate the Limit of Detection (LOD) of the novel device, six serial 3-fold dilutions of the reference samples were used starting from $10^8$ viral genome copies/mL for PPV1, PCV-2, PPRSV and CSF and from $10^7$ viral genome copies/mL for SIV and ASF. Moreover, the LOD of ASF functionalized sensors in sera was tested using six serial 3-fold dilutions (range of $10^7$ – $3.3 \times 10^4$ viral genome copies/mL). Receiver operating characteristic (ROC) curves were drawn. The area under the curve (AUC) along with its 95% confidence intervals (95% CI) for all the studied viruses were calculated. Sensitivity, specificity, accuracy and precision were also calculated. Additionally, the positive likelihood ratio (PLR), negative likelihood ratio (NLR), and diagnostic odds ratio (DOR) were computed for each virus to assess the performance of the device. Calibrators (samples) were classified into three categories, negatives, positives, and weakly positives. For the classification of device measurements to True Positives (TP), True Negatives (TN), False Positives (FP), and False Negatives (FN) and the subsequent calculation of the performance metrics, the optimal thresholds of the ROC curve analysis were used. Considering that each ring resonator functions independently, the validation of the POC device was conducted at the ring level.

The novel device achieved LOD values ranging from $3.3 \times 10^4$ viral genome copies/mL for ASF and SIV to $3.3 \times 10^5$ viral genome copies/mL for PCV-2, PRRSV and CSF. The LOD of PPV1 functionalized sensors was higher reaching approximately $10^6$ viral genome copies/mL. In general, PIC performance was satisfactory at ring level. PPV1 and PCV-2 functionalized sensors showed sensitivity of 68.60% and 69.50%, specificity of 77.10% and 70.30%, accuracy of 73.30% and 69.95%, precision of 71.08% and 63.33%, PLR of 3.00 and 2.34, NLR of 0.41 and 0.43, DOR values of 7.38 and 5.39 and AUC values of 0.820 and 0.742, respectively. PPRSV functionalized sensors achieved a sensitivity of 83.50%, specificity of 77.80%, accuracy of 80.50%, precision of 77.60%, PLR of 3.76, NLR of 0.21, DOR of 17.66, and AUC values of 0.812. The respective values for SIV functionalized sensors were 81.80%, 82.20%, 82.00%, 84.90%, 4.60, 0.22, 20.81, and 0.816. ASF and CSF functionalized sensors showed sensitivity of 80.79% and 79.00%, specificity of 88.46% and 79.07%, accuracy of 81.92% and 79.04%, precision of 97.60% and 68.70%, PLR of 7.00 and 3.77, NLR of 0.22 and 0.27, DOR values of 32.25 and 14.21 and AUC values of 0.832 and 0.830, respectively. At first glance, PRRSV, SIV, ASF and CSF sensors seemed to outperform PPV1 and PCV-2 sensors in

terms of sensitivity, specificity and likelihood ratios, however, the 95% CIs of the aforementioned metrics overlapped, indicating that the recorded differences were not statistically significant. PRRSV, SIV, ASF and CSF sensors showed statistically significant higher DOR values than PCV-2 sensors, whereas only PRRSV and ASF sensors had statistically significant higher DOR values than PPV1 sensors. DOR value differences between PPV1 and PCV-2 sensors, as well as between PRRSV, SIV, ASF and CSF, were not statistically significant.

In the present work, photonic, microfluidic, signal processing, data collection/analysis and communication technologies were integrated into a single, portable device for the detection of swine viral diseases in oral fluids and serum samples. This is the first attempt to exploit PICs for the detection of swine pathogens in the POS setting, paving the way for the development of the next generation of animal diagnostics. The integration of modern nanomaterials, microfabrication technologies, instrumentation designs and sensors into POS devices and tests present exciting opportunities for the non-intrusive, real-time monitoring of animal health, behavior, and physiology.

The first validation data showed the novel device is a promising tool with satisfactory performance that can potentially reduce the time and costs required for the diagnosis of swine viral diseases, and at the same time enable rapid and local decision making for the implementation of evidence-based disease control measures. The device failed to quantify the viral load in the tested samples. Future research will focus on reducing the current system limitations, increase multiplexing, implement large-scale field validation studies, and increase the Technology Readiness Level (TRL) of the device for successful commercialization. The development and the commercialization of advanced POS devices through the exploitation of recent technological breakthroughs is expected to overcome the current limitations of POS methodologies such as portability, complexity, sample pretreatment, multiplexing and insufficient validation, and finally realize the translation of cutting-edge laboratory techniques to accessible and user-friendly devices and tests that improve the biosecurity, resilience, and sustainability of animal farming.

**Scientific field:** Diagnostics

**Keywords:** Point of Service, Point of Care (POC) diagnostics, Swine viral diseases, Photonic Integrated Circuits (PICs), Microfluidics

**Καινοτόμες εργαστηριακές μέθοδοι και τεχνολογίες διαγνωστικών συσκευών πεδίου για την βελτιστοποίηση της βιοασφάλειας στα αγροτικά ζώα**

*Τμήμα Επιστήμης Ζωικής Παραγωγής*
*Εργαστήριο Ανατομίας & Φυσιολογίας Αγροτικών Ζώων*

# ΠΕΡΙΛΗΨΗ

Η σημασία της χοιροτροφίας τονίζεται από το γεγονός ότι το χοιρινό κρέας αγγίζει σχεδόν το 35% της παραγωγής κρέατος σε παγκόσμιο επίπεδο. Το 2020 η εκτροφή χοίρων ανήλθε σε 150 εκατομμύρια ζώα και απέδωσε 23.8 εκατομμύρια τόνους χοίρειου κρέατος, ποσότητα που αντιστοιχεί περίπου το μισό της συνολικής παραγωγής κρέατος στην Ευρωπαϊκή Ένωση (ΕΕ). Η ΕΕ είναι ο δεύτερος μεγαλύτερος παραγωγός κρέατος μετά την Κίνα, και ο κύριος εξαγωγέας χοιρινού παγκοσμίως. Η χοιροτροφία στην Ευρώπη υπόκειται σε αρκετά νομοθετικά πλαίσια συμπεριλαμβανομένης της Κοινής Αγροτικής Πολιτικής (ΚΑΠ), τα οποία ρυθμίζουν την προστασία του περιβάλλοντος, την ασφάλεια των τροφίμων και την δημόσια υγεία, την παράγωγή οργανικών προϊόντων καθώς και την υγεία και την ευζωία των ζώων. Η νέα ΚΑΠ σε συνδυασμό με την Ευρωπαϊκή Πράσινη Συμφωνία και την στρατηγική «Από το Αγρόκτημα στο Πιάτο», προάγει την φιλικότερη στο περιβάλλον και βιώσιμη παραγωγή τροφίμων, ενώ αναμένεται να αναδιαμορφώσει την ισχύουσα νομοθεσία για την παραγωγή χοίρειου κρέατος καθώς και για την υγεία και ευζωία των ζώων.

Για να ανταπεξέλθουν στην αυξανόμενη ζήτηση ζωικών προϊόντων και παράλληλα να μειώσουν το κόστος παραγωγής, τα σύγχρονα συστήματα εκτροφής εστιάζουν στην εντατικοποίηση, στις αυξημένες εισροές και στην μεγαλύτερη πυκνότητα εκτροφής. Παρόλα αυτά, η αύξηση της πυκνότητας εκτροφής μπορεί να επιταχύνει την μετάδοση παθογόνων, θέτοντας σε κίνδυνο την υγεία και την ευζωία των ζώων. Επιπροσθέτως, τα εκτενή, διεθνή εμπορικά δίκτυα και η ελλιπής επιδημιολογική επιτήρηση των λοιμωδών νοσημάτων των ζώων εντείνουν την έξαρση επιδημιών και την ανάδυση νέων παθογόνων. Ανάμεσα σε αυτά τα παθογόνα, τα ιογενή νοσήματα μπορεί να είναι καταστροφικά για την χοιροτροφία λόγω των κάτωθι αιτιών: i) της δυναμικής της μετάδοσης τους, ii) της έλλειψης αποτελεσματικών θεραπειών, iii) του περιορισμένου αριθμού διαθέσιμων εμβολίων και της ενίοτε μειωμένης αποτελεσματικότητάς τους και iv) των περιορισμένων συστημάτων επιδημιολογικής επιτήρησης καθώς και την έλλειψη συντονισμένων μέτρων για την επιτυχή διαχείρισή τους. Ο Παρβοϊός τύπου 1 (Porcine Parvovirus 1 – PPV1), ο Κυκλοϊός τύπου 2 (Porcine Circovirus type 2 - PCV-2), το Αναπαραγωγικό και Αναπνευστικό Σύνδρομο των Χοίρων (Porcine Reproductive and Respiratory Syndrome Virus - PRRSV), η γρίπη των χοίρων τύπου Α (Swine

Influenza A - SIV), η Αφρικανική Πανώλη των Χοίρων (African Swine Fever Virus - ASFV) και η Κλασσική Πανώλη των Χοίρων (Classical Swine Fever Virus - CSFV) είναι ανάμεσα στα σημαντικότερα ιογενή νοσήματα των χοίρων λόγω του κοινωνικοοικονομικού τους αντικτύπου, της εξάπλωσής τους και της δριμύτητάς τους.

Δεδομένου ότι ο χρόνος που απαιτείται από την έναρξη της νόσησης ως την εργαστηριακή επιβεβαίωση του αιτιολογικού παράγοντα μπορεί να κυμαίνεται μεταξύ ημερών ως και ενός μηνός, προηγμένες εργαστηριακές τεχνολογίες και βιοαισθητήρες ενσωματώνονται σταδιακά σε διαγνωστικές συσκευές πεδίου για την παροχή έγκαιρης διάγνωσης, την βελτιστοποίηση της βιοσφάλειας των ζώων και κατ' επέκταση την αντιμετώπιση των ασθενειών των ζώων. Ως διαγνωστικές συσκευές πεδίου ορίζονται οι συσκευές ανάλυσης και οι δοκιμές που είναι ικανές να παράσχουν γρήγορα διάγνωση στο πεδίο χωρίς να απαιτείται άλλος εργαστηριακός εξοπλισμός. Οι διαθέσιμες συσκευές πεδίου για τις ασθένειες των ζώων μπορούν να καταταχτούν σε δύο ευρείς κατηγορίες, διαγνωστικές συσκευές βασιζόμενες στο διηθητικό χαρτί και διαγνωστικές συσκευές μικρορευστομηχανικών στοιχείων.

Οι διαγνωστικές συσκευές βασιζόμενες στο χαρτί εκμεταλλεύονται τις ιδιότητες της κυτταρίνης και της νιτροκυτταρίνης για την δημιουργία του σώματος στο οποίο λαμβάνει χώρα η ανίχνευση των μορίων-στόχων. Τα υλικά αυτά καθορίζουν το πορώδες, την επιφανειακή χημεία και τις οπτικές ιδιότητες των διαγνωστικών συσκευών βασιζόμενων στο χαρτί. Αυτές οι ιδιότητες είναι συνυφασμένες με τις επιδόσεις και την αποτελεσματικότητα αυτών των διαγνωστικών. Επί του παρόντος, μηχανισμοί όπως χημικές αντιδράσεις, ηλεκτροχημικές αντιδράσεις, χημειοφωταύγεια και ηλεκτροχημειοφωταύγεια συνδυάζονται με τεχνικές ανάλυσης εικόνας για την ανίχνευση των μορίων-στόχων στις διαγνωστικές συσκευές βασιζόμενες στο χαρτί. Αντισώματα, αντιγόνα, ολιγονουκλεοτίδια και απταμερή χρησιμοποιούνται κατά κόρον ως Στοιχεία Μοριακής Αναγνώρισης (Molecular Recognition Elements - MREs). Οι διαγνωστικές συσκευές βασιζόμενες στο χαρτί μπορούν να ταξινομηθούν περαιτέρω σε δοκιμαστικές ταινίες (dipstick and strip tests) και σε δοκιμές πλευρικής ροής (Lateral Flow Assays - LFAs). Χαρακτηριστικοί αντιπρόσωποι της πρώτης κατηγορίας είναι οι δοκιμαστικές ταινίες pH και αντιβιοτικών στο γάλα και της δεύτερης κατηγορίας το τεστ εγκυμοσύνης και η ταχεία δοκιμή αντιγόνου για Covid-19.

Από την άλλη, οι διαγνωστικές συσκευές μικρορευστομηχανικών στοιχείων εκμεταλλεύονται δίκτυα μικροδιαύλων για τον χειρισμό των ρευστών και την ανάλυσή τους σε επίπεδο μικρόλιτρου ή νανόλιτρου. Ο χειρισμός και η ανάλυση των μορίων-στόχων γίνεται

σε ειδικά σχεδιασμένους μικρορευστομηχανικούς διαύλους και θαλάμους. Η ροή των ρευστών στις ολοκληρωμένες συσκευές μικρορευστομηχανικών στοιχείων πραγματοποιείται μέσω του τριχοειδούς φαινομένου ή μέσω αντλιών. Οι συγκεκριμένες συσκευές απαιτούν μικρότερο όγκο δειγμάτων και αντιδραστηρίων και είναι κατά γενικό κανόνα μικρότερες σε μέγεθος. Αυτά τα πλεονεκτήματα τις κάνουν ευκολότερες στην χρήση και μειώνουν το κόστος λειτουργίας τους σε σχέση με τις συμβατικές εργαστηριακές δοκιμές. Επίσης, οι ολοκληρωμένες συσκευές μικρορευστομηχανικών στοιχείων δεν απαιτούν εξειδικευμένο προσωπικό για την χρήση τους, μειώνουν την πιθανότητα ανθρώπινου λάθους και είναι ταχύτερες. Οι συγκεκριμένες συσκευές μπορούν να ταξινομηθούν σε μικροσυστήματα συνολικής ανάλυσης (micro total analysis systems - μTAS), γνωστά ως «εργαστήρια σε τσιπ» (“lab-on-a-chip” - LOC), και σε αναλυτικές συσκευές μικρορευστομηχανικών στοιχείων βασιζόμενες στο χαρτί.

Τα μικροσυστήματα συνολικής ανάλυσης είναι ικανά να εκτελέσουν πλήθος εργαστηριακών δοκιμών (Αλυσιδωτή Αντίδραση Πολυμεράσης – PCR, ισοθερμική ενίσχυση μέσω βρόχου – LAMP, ενίσχυση κυλιόμενου κύκλου – RCA κτλ.) ενσωματώνοντας όλα τα απαραίτητα βήματα των αναλύσεων σε μια μοναδική πλατφόρμα. Ο πυρήνας αυτών των συσκευών είναι το τσιπ ανίχνευσης (βιοαισθητήρας) όπου η αναλυτική διαδικασία και η βιοαναγνώριση των μορίων-στόχων λαμβάνει χώρα. Τα τσιπ ανίχνευσης συνήθως κατασκευάζονται από γυαλί, χαλαζία, πυρίτιο ή πολυμερή υλικά. Τρεις κύριοι παράγοντες καθορίζουν την αποτελεσματικότητα των τσιπ ανίχνευσης, ο σχεδιασμός των μικρορευστομηχανικών στοιχείων, η μορφή και η κατασκευή του κύριου σώματος της συσκευής και η συνάφεια και η συγγένεια των Στοιχείων Μοριακής Αναγνώρισης προς τα μόρια-στόχους. Η επιλογή των κατάλληλων Στοιχείων Μοριακής Αναγνώρισης επηρεάζει σε μεγάλο βαθμό τις επιδόσεις αυτών των διαγνωστικών συσκευών. Η ανίχνευση των μορίων-στόχων τυπικά πραγματοποιείται με την χρήση οπτικών και ηλεκτροχημικών μεθόδων, αισθητήρων μαγνητικής αντίστασης (magneto-resistive sensors - GMR), μέτρησης ακουστικών κυμάτων, φασματοσκοπίας μάζας και πυρηνικού μαγνητικού συντονισμού.

Οι αναλυτικές συσκευές μικρορευστομηχανικών στοιχείων βασιζόμενες στο χαρτί συνδυάζουν τα χαρακτηριστικά τόσο των μικροσυστημάτων συνολικής ανάλυσης όσο και των διαγνωστικών συσκευών βασιζόμενων στο χαρτί, χρησιμοποιώντας οικονομικά υλικά (χαρτί) και απλές διαδικασίες παραγωγής. Σε αντίθεση με τις απλές διαγνωστικές συσκευές βασιζόμενες στο χαρτί, οι χάρτινες συσκευές μικρορευστομηχανικών στοιχείων επιτρέπουν τον ακριβή χειρισμό μικρών ποσοτήτων ρευστών, διευκολύνοντας έτσι τη μετάφραση περίπλοκων δοκιμών σε διαγνωστικές συσκευές πεδίου. Η κίνηση των υγρών γίνεται μέσω

τριχοειδών φαινομένων, οπότε δεν απαιτείται κάποια πηγή ενέργειας ή μηχανικές βαλβίδες και αντλίες. Παρόλα αυτά, απαιτείται η κατασκευή των μικρορευστομηχανικών διαύλων μέσω της δημιουργίας υδρόφοβων φραγμών (απόφραξη των πόρων του χαρτιού). Η δημιουργία των υδρόφοβων φραγμών είναι υψίστης σημασίας καθώς καθορίζει το μήκος και το πλάτος των μικρορευστομηχανικών διαύλων και κατ' επέκταση τις ιδιότητες της διαγνωστικής συσκευής. Από τη σκοπιά των μηχανισμών ανίχνευσης των μορίων-στόχων, η συγκεκριμένη κατηγορία διαγνωστικών συσκευών είναι συμβατή με ποτενσιομετρικούς, φθοριομετρικούς και χρωματομετρικούς αισθητήρες, θερμιδομετρικές και ενζυματικές μεθόδους, μεθόδους χημειοφωταύγειας και ηλεκτροχημειοφωταύγειας, φθορίζοντα νανοσωματίδια κβαντικής κουκκίδας και μεταλλικά σύμπλοκα.

Ως βιοαισθητήρες ορίζονται οι αισθητήρες που χρησιμοποιούν βιολογικά μόρια ακινητοποιημένα στην επιφάνεια τους που είναι ικανά να αναγνωρίσουν μόρια-στόχους ενδεικτικά μικροοργανισμών ή παθολογικών καταστάσεων. Αυτά τα βιολογικά μόρια είναι γνωστά ως βιοϋποδοχείς. Ευρέως χρησιμοποιούμενοι βιοϋποδοχείς είναι τα αντισώματα, το RNA και το DNA, οι γλυκάνες, οι λεκτίνες, τα ένζυμα, διάφοροι συμπαράγοντες, ιστοί ή κύτταρα. Η βιοαναγνώριση μετατρέπεται σε μετρήσιμα σήματα μέσω ειδικών μετατροπέων που επιτρέπουν την ανίχνευση και την ποσοτικοποίηση των μορίων-στόχων. Οι βιοαισθητήρες, βάσει της μεθοδολογίας που γίνεται η μετατροπή της βιοαναγνώρισης σε μετρήσιμο σήμα, μπορούν να κατηγοριοποιηθούν σε οπτικούς, ηλεκτροχημικούς, πιεζοηλεκτρικούς, μαγνητικούς, θερμικούς, ραδιενεργούς, και μηχανικούς.

Οι κύριοι στόχοι της παρούσας διδακτορικής διατριβής περιλαμβάνουν την ανάπτυξη του πρωτοκόλλου ανάλυσης και την πιστοποίηση μίας νέας διαγνωστικής συσκευής πεδίου βασιζόμενης σε ένα μικροσύστημα συνολικής ανάλυσης (LOC) για την ταχεία διάγνωση ιογενών νοσημάτων των χοίρων. Η νέα διαγνωστική συσκευή στόχευε στην ανίχνευση των έξι προαναφερθέντων ιογενών νοσημάτων και ενσωματώνει μικρορευστομηχανικά στοιχεία και Φωτονικά Ολοκληρωμένα Κυκλώματα για την απευθείας ανίχνευση των ιικών αντιγόνων σε βιολογικά δείγματα.

Η διαγνωστική συσκευή είχε ενσωματωμένα όλα της τα δομικά στοιχεία σε μία φορητή πλατφόρμα, συνολικού βάρους 45 κιλών και μεγέθους 40×50×60 εκατοστών. Οι ανωτέρω διαστάσεις και το βάρος αφορούν την πλήρως αυτόνομη και λειτουργική διαγνωστική συσκευή συμπεριλαμβανομένων του μηχανολογικού εξοπλισμού, της δεξαμενής για τις απορροές μετά την ολοκλήρωση της ανάλυσης καθώς και το σύστημα αποστείρωσης υπεριώδους (UV-C) ακτινοβολίας. Η νέα διαγνωστική συσκευή μπορεί να χωριστεί σε τρία

κύρια υποσυστήματα: 1) το μηχανικό/μικρορευστομηχανικό υποσύστημα που αποτελούνταν από i) ένα σύστημα μεταφοράς υγρών με την χρήση συρίγγων, ii) κινητήρες, iii) μικρορευστομηχανικούς διαύλους, iv) δεξαμενή απόρριψης και v) μία συστοιχία Peltier, 2) το οπτικό υποσύστημα που αποτελούνταν από i) ένα ρυθμιζόμενο λέιζερ, ii) οπτικές ίνες, iii) φωτοδίοδο και iv) τους βιοαισθητήρες Φωτονικών Ολοκληρωμένων Κυκλωμάτων, και τέλος 3) το υλικολογισμικό υποσύστημα που αποτελούνταν από i) ένα μικροχειριστήριο και το λογισμικό του, ii) ένα καταγραφέα δεδομένων Arduino και iii) μια κάρτα μνήμης. Η λειτουργία του συστήματος, η πρόοδος της αναλυτικής διαδικασίας, η συλλογή και αποθήκευση των δεδομένων και η καταγραφή των αποτελεσμάτων ελέγχονταν μέσω μιας εφαρμογής Android. Η ανάλυση μπορούσε να ολοκληρωθεί εντός 60 λεπτών. Για τη χρήση της συσκευής δεν απαιτούνταν σημαντικοί χειρισμοί ούτε και η εκπαίδευση των τελικών χρηστών.

Τα φωτονικά ολοκληρωμένα κυκλώματα, οι βιοαισθητήρες της νέας συσκευής, χρησιμοποιούσαν 8 δακτυλίους με ακινητοποιημένα αντισώματα στην επιφάνειά τους για την σύλληψη των ιικών αντιγόνων από τα βιολογικά δείγματα. Ακολουθούμενης της διέγερσής τους υπό συνεχές μήκος κύματος διαμέσου του λέιζερ, κάθε δακτύλιος «δονούνταν» σε ένα μόνο συγκεκριμένο μήκος κύματος, παγιδεύοντας αυτό το μήκος κύματος του φωτός στο εσωτερικό του και παρεμποδίζοντάς το να φτάσει στην φωτοδίοδο. Ως αποτέλεσμα, δημιουργείτο μια μείωση της έντασης του φωτός στο συγκεκριμένο μήκος κύματος της «δόνησης» των δακτυλίων. Η σύλληψη των ιικών αντιγόνων στην επιφάνεια των δακτυλίων μέσω των αντισωμάτων οδηγούσε σε τοπική αλλαγή του συντελεστή διάθλασης του βιοαισθητήρα. Αυτή η αλλαγή του συντελεστή διάθλασης μεταφραζόταν σε αλλαγή της «συχνότητας δόνησης» των δακτυλίων και κατ' επέκταση σε αλλαγή του μήκους κύματος που παγιδεύεται σε αυτούς. Έτσι, η μετατόπιση του σήματος (αλλαγή του παγιδευμένου μήκους κύματος) σχετίζεται άμεσα με τη σύλληψη των ιικών αντιγόνων από τα αντισώματα.

Η αναλυτική διαδικασία της νέας διαγνωστικής συσκευής πεδίου περιελάμβανε πέντε διαδοχικά βήματα: i) εισαγωγή ρυθμιστικού διαλύματος, ii) εισαγωγή του δείγματος, iii) έκπλυση, iv) αναγέννηση του βιαοσθητήρα και v) τελική έκπλυση. Δύο κύρια ρυθμιστικά διαλύματα, φυσιολογικός ορός στον οποίο έχει προστεθεί ρυθμιστικό διάλυμα φωσφορικών ιόντων (PBS) και ρυθμιστικό διάλυμα 2-(N-μορφολινο)εθανοθειικού οξέος (MES), συμπληρώθηκαν με βόεια λευκωματίνη ορού και χρησιμοποιήθηκαν για την ανίχνευση των ιικών αντιγόνων. Η ανάλυση των δεδομένων πραγματοποιήθηκε με τη χρήση ειδικά διαμορφωμένου αλγορίθμου που περιλάβανε τον αλγόριθμο LOWESS, και νέου λογισμικού για υπολογιστές σε γλώσσα προγραμματισμού Python. Ο ίδιος αλγόριθμος για την ανάλυση

των δεδομένων ήταν προσβάσιμος από τον τελικό χρήστη μέσω μιας εφαρμογής Android και μιας διαδικτυακής πλατφόρμας.

Πρότυπα δείγματα αναφοράς για τους έξι ιούς και σύνθετα βιολογικά δείγματα (σίελος και οροί αίματος), συλλεγμένα από χοιροτροφικές εκμεταλλεύσεις, χρησιμοποιήθηκαν για την πιστοποίηση της συσκευής. Όλα τα δείγματα δοκιμάστηκαν με συμβατική PCR για την επιβεβαίωση της απουσίας ή παρουσίας των ιικών σωμάτιων. Επιπροσθέτως, τα θετικά δείγματα ποσοτικοποιήθηκαν με τη χρήση PCR πραγματικού χρόνου βασιζόμενης στην μοριακή χρωστική SYBR Green.

Για τον υπολογισμό του ορίου ανίχνευσης της νέας συσκευής, χρησιμοποιήθηκαν έξι διαδοχικές αραιώσεις των πρότυπων δειγμάτων σε σίελο σε συγκεντρώσεις που άρχιζαν από $10^8$ ιικά αντίγραφα/mL για τους ιούς PPV1, PCV-2, PPRSV και CSF και από $10^7$ ιικά αντίγραφα/mL για τους ιούς SIV και ASF. Επιπροσθέτως, το όριο ανίχνευσης του ιού ASF μελετήθηκε και σε δείγματα ορού αίματος χρησιμοποιώντας πάλι έξι διαδοχικές αραιώσεις στο εύρος $10^7$ – $3.3 \times 10^4$ ιικών αντιγράφων/mL. Επίσης έγινε ανάλυση των χαρακτηριστικών καμπυλών λειτουργίας δέκτη (receiver operating characteristic curves - ROC), εκτίμηση των περιοχών κάτω από την καμπύλη (Area Under the Curve - AUC) και υπολογισμός των 95% διαστημάτων εμπιστοσύνης (95% confidence intervals - 95% CI) για καθένα από τους ιούς. Ακόμη υπολογίστηκαν για κάθε νόσημα η ευαισθησία, η ειδικότητα, η ακρίβεια (accuracy), η πιστότητα (precision), ο θετικός λόγος πιθανοφάνειας (positive likelihood ratio - PLR), ο αρνητικός λόγος πιθανοφάνειας (negative likelihood ratio - NLR) και ο διαγνωστικός σχετικός λόγος συμπληρωματικών πιθανοτήτων (diagnostic odds ratio - DOR) με σκοπό την αξιολόγηση της διαγνωστικής συσκευής, χρησιμοποιώντας αρνητικά, θετικά και ασθενώς θετικά δείγματα. Για τον υπολογισμό των ανωτέρω μέτρων της διαγνωστικής επίδοσης της νέας συσκευής, τα αποτελέσματα κατηγοριοποιήθηκαν σε αληθώς θετικά (True Positives - TP), αληθώς αρνητικά (True Negatives - TN), ψευδώς θετικά (False Positives - FP), και ψευδώς αρνητικά (False Negatives - FN) με βάση τα βέλτιστα κατώφλια σήματος που ταυτοποιήθηκαν με τις καμπύλες ROC. Ο υπολογισμός των μέτρων και η πιστοποίηση της συσκευής έγινε σε επίπεδο δακτυλίου των αισθητήρων, καθώς κάθε δακτύλιος λειτουργεί ανεξάρτητα.

Οι τιμές των ορίων ανίχνευσης της νέας συσκευής κυμαίνονταν από $3.3 \times 10^4$ ιικά αντίγραφα/mL για τους ιούς ASF και SIV ως $3.3 \times 10^5$ ιικά αντίγραφα/mL για τους ιούς PCV-2, PRRSV και CSF. Το όριο ανίχνευσης για τον ιό PPV1 ήταν υψηλότερο, περίπου $10^6$ ιικά αντίγραφα/mL. Σε γενικές γραμμές η επίδοση της νέας συσκευής και των βιοαισθητήρων σε

επίπεδο δακτυλίου ήταν ικανοποιητική. Για τους ιούς PPV1 και PCV-2, η συσκευή εμφάνισε αντιστοίχως ευαισθησία 68.60% και 69.50%, ειδικότητα 77.10% και 70.30%, ακρίβεια 73.30% και 69.95%, πιστότητα 71.08% και 63.33%, PLR 3.00 και 2.34, NLR 0.41 και 0.43, DOR 7.38 και 5.39 και τιμές AUC 0.820 και 0.742. Για τον ιό PPRSV η συσκευή έδειξε ευαισθησία 83.50%, ειδικότητα 77.80%, ακρίβεια 80.50%, πιστότητα 77.60%, PLR 3.76, NLR 0.21, DOR 17.66, και τιμές AUC 0.812. Οι αντίστοιχες τιμές για τον ιό SIV ήταν 81.80%, 82.20%, 82.00%, 84.90%, 4.60, 0.22, 20.81, and 0.816. Ακόμη για του ιούς ASF και CSF (κατ' αντιστοιχία) η συσκευή εμφάνισε τιμές ευαισθησίας, 80.79% και 79.00%, ειδικότητας 88.46% και 79.07%, ακρίβειας 81.92% και 79.04%, πιστότητας 97.60% και 68.70%, PLR 7.00 και 3.77, NLR 0.22 και 0.27, DOR 32.25 και 14.21 και AUC 0.832 και 0.830. Εκ πρώτης όψεως, φαίνεται ότι η συσκευή είχε καλύτερες επιδόσεις για του ιούς PRRSV, SIV, ASF και CSF σε σχέση με τις επιδόσεις των ιών PPV1 και PCV-2 τόσο για την ευαισθησία και την ειδικότητα όσο και τους λόγους πιθανοφάνειας. Παρόλα αυτά, τα 95% διαστήματα εμπιστοσύνης αλληλοκαλύπτονταν, αποδεικνύοντας ότι οι διαφορές στις επιδόσεις δεν ήταν στατιστικά σημαντικές. Η συσκευή είχε στατιστικώς σημαντικά μεγαλύτερες επιδόσεις όσον αφορά τον διαγνωστικό σχετικό λόγο συμπληρωματικών πιθανοτήτων DOR για τους ιούς PRRSV, SIV, ASF και CSF σε σχέση με τον ιό PCV-2, ενώ σε σχέση με τον ιό PPV1 η διαφορά παρέμενε στατιστικώς σημαντική μόνο για τους ιούς PRRSV και ASF. Οι διαφορές των τιμών DOR αναμεταξύ των ιών PRRSV, SIV, ASF και CSF και αναμεταξύ των ιών PPV1 και PCV-2 δεν ήταν στατιστικώς σημαντική.

Στην παρούσα εργασία, φωτονικά ολοκληρωμένα κυκλώματα, μικρορευστομηχανικά στοιχεία και τεχνολογίες τηλεπικοινωνιών και πληροφορικής ενσωματώθηκαν σε μία φορητή συσκευή για την ανίχνευση ιογενών νοσημάτων των χοίρων σε δείγματα σιέλου και ορού αίματος. Μάλιστα, η παρούσα αποτελεί την πρώτη προσπάθεια χρήσης φωτονικών ολοκληρωμένων κυκλωμάτων για την ανίχνευση ικών παθογόνων στο πεδίο, ανοίγοντας τον δρόμο για την ανάπτυξη διαγνωστικών συσκευών πεδίου νέας γενιάς στην ζωική παραγωγή. Η ανάπτυξη νανοϋλικών και τεχνολογιών μικροκατασκευής, ο συνδυασμός τους με καινοτόμα όργανα και αισθητήρες και η ενσωμάτωσή τους σε διαγνωστικές συσκευές πεδίου παρουσιάζουν νέες δυνατότητες για την μη παρεμβατική παρακολούθηση σε πραγματικό χρόνο της υγείας των ζώων, της συμπεριφοράς και της φυσιολογίας τους.

Τα πρώτα πειραματικά δεδομένα για την πιστοποίηση της νέας διαγνωστικής συσκευής πεδίου υποδεικνύουν ότι η συσκευή έχει ικανοποιητικές επιδόσεις, μπορεί να μειώσει τον χρόνο και το κόστος που απαιτείται για την διάγνωση των ιογενών νοσημάτων των χοίρων και παράλληλα μπορεί να επιτρέψει την ταχεία λήψη αποφάσεων σε τοπικό επίπεδο για την

εφαρμογή μέτρων ελέγχου των νοσημάτων με βάση επιστημονικά δεδομένα. Παρόλο που η συσκευή είναι ένα πολλά υποσχόμενο εργαλείο, δεν μπορούσε να χρησιμοποιηθεί για την ποσοτικοποίηση των δειγμάτων. Μελλοντικές έρευνες θα πρέπει να επικεντρωθούν στην επίλυση των προβλημάτων και των περιορισμών του παρόντος συστήματος, στην αύξηση των ασθενειών-στόχων, στην εκτέλεση περισσότερων δοκιμών πιστοποίησης σε πραγματικές συνθήκες πεδίου και στην αύξηση του επιπέδου τεχνολογικής ετοιμότητας (Technology Readiness Level - TRL) της συσκευής για την επιτυχή εμπορική της εκμετάλλευση. Η ανάπτυξη και η εμπορική εκμετάλλευση προηγμένων διαγνωστικών συσκευών πεδίου μέσω της αξιοποίησης νέων τεχνολογικών επιτευγμάτων αναμένεται να υπερσκελίσει τις προκλήσεις που αντιμετωπίζουν αυτές οι συσκευές όπως η περιορισμένη φορητότητα, η πολυπλοκότητα, η ανάγκη επεξεργασίας των δειγμάτων, ο περιορισμένος αριθμός των μορίων-στόχων για κάθε δοκιμή και η ανεπαρκής πιστοποίησή τους. Τέλος, η αξιοποίηση των νέων τεχνολογικών επιτευγμάτων αναμένεται να μεταφράσει διάφορες καινοτόμες εργαστηριακές τεχνικές σε προσβάσιμες και φιλικές προς τον τελικό χρήστη διαγνωστικές συσκευές πεδίου που θα ενισχύσουν την βιοασφάλεια, την ανθεκτικότητα και την βιωσιμότητα της Ζωικής Παραγωγής.

**Επιστημονική περιοχή:** Διαγνωστικά

**Λέξει κλειδιά:** Διαγνωστικές συσκευές πεδίου, ιογενή νοσήματα χοίρων, φωτονικά ολοκληρωμένα κυκλώματα, μικρορρευστονική

# ΔΗΛΩΣΗ ΕΡΓΟΥ

Ο κάτωθι υπογεγραμμένος, Μάνεσης Γεώργιος δηλώνω ότι το κείμενο της μελέτης αποτελεί δικό μου, μη υποβοηθούμενο πόνημα. Υποβάλλεται σε μερική εκπλήρωση των απαιτήσεων για την απόκτηση Διδακτορικού Διπλώματος του Γεωπονικού Πανεπιστημίου Αθηνών. Δεν έχει υποβληθεί ποτέ πριν για οιοδήποτε λόγο ή για εξέταση σε οποιοδήποτε άλλο πανεπιστήμιο ή εκπαιδευτικό ίδρυμα της χώρας ή του εξωτερικού.

Με την άδειά μου, η παρούσα εργασία ελέγχθηκε από την Εξεταστική Επιτροπή μέσα από λογισμικό ανίχνευσης λογοκλοπής που διαθέτει το ΓΠΑ και διασταυρώθηκε η εγκυρότητα και η πρωτοτυπία της.

Μάνεσης Γεώργιος

---

Αρχική Σύνθεση Τριμελούς Συμβουλευτικής Επιτροπής

Επιβλέπων: Ιωάννης Μπόσης, Καθηγητής, ΑΠΘ
Μέλη: Αθανάσιος Γελασάκης, Επίκουρος Καθηγητής, ΓΠΑ
Λεωνίδας Λεοντίδης, Καθηγητής, Πανεπιστήμιο Θεσσαλίας

Αντικατάσταση του Καθηγητή Λεωνίδα Λεοντίδη από τον Επίκουρο Καθηγητή Γεώργιο Θεοδώρου με βάση την απόφαση της Συνέλευσης του Τμήματος ΕΖΠ (Συνεδρίαση 118η /26-01-2023), σύμφωνα με το ν. 4957/2022 (Α' 141).

# Acknowledgements

This dissertation was elaborated in the "Laboratory of Anatomy and Physiology of Farm Animals, Department of Animal Science, Agricultural University of Athens". It was funded by E.U.'s H2020 SWINOSTICS project (G.A. ID 771649).

First and foremost, I would like to express my gratitude to my supervisor, Professor Ioannis Bossis, for trusting me with this project and for his continuous guidance and support throughout these years. I would also like to thank him for spending so much time instructing me on research methodology and laboratory techniques, for his research ideas and intuition, for providing Porcine Parvovirus (PPV1) and Porcine Reproductive and Respiratory Syndrome Virus (PRRSV) reference samples and finally for providing the financial support that allowed me to conclude this work.

I also thank the members of the advisory committee, Assistant Professor Athanasios Gelasakis and Assistant Professor Georgios Theodorou, for their support and understanding through this work and for their comments in improving this text.

I warmly thank the veterinarian Stelios Kouroupidis for instructing me in swine sample collection, Associate Professor Vasileios Papatsiros for sharing field samples, Afroditi Kalogianni for helping me in sample collection and the managers of swine farms for allowing me to collect samples.

I would also like to thank the SWINOSTICS consortium members Grzegorz Wozniakowski, member of the Polish National Reference Laboratory for African Swine Fever (ASF) and Classical Swine Fever (CSF), for providing deactivated ASF and CSF reference samples, Balka Gyula (University of Veterinary Medicine Budapest) for providing Porcine Circovirus and Swine Influenza A reference samples, Amadeu Griol (Universitat Politècnica de València) and Sergio Peransi (Lumensia Sensors) for supplying the Photonic Integrated Circuit sensors, Christos Mourouzis (Cyric Inc.) for developing the automated Python detection algorithm of the novel Point of Care device and Atanas Terziev (Cyric Inc.) for aiding in building the device and helping me optimize its mechanical functions.

Last but not least, I would like to thank my wife Evelina for her continuous support and patience throughout this project.

***Georgios Manesis***

# List of Publications

*The following publications are related to the work presented in this dissertation*

I. "**Manessis, G.,** A. I. Gelasakis, and I. Bossis. The challenge of introducing point of care diagnostics in farm animal health management. Biomedical Journal of Scientific & Technical Research 14 (2019). doi: 10.26717/BJSTR.2019.14.002601"

II. "**Manessis, G.;** Mourouzis, C.; Griol, A.; Zurita-Herranz, D.; Peransi, S.; Sanchez, C.; Giusti, A.; Gelasakis, A.I.; Bossis, I. "Integration of Microfluidics, Photonic Integrated Circuits and Data Acquisition and Analysis Methods in a Single Platform for the Detection of Swine Viral Diseases". *Animals* **2021**, *11*, 3193. doi: 10.3390/ani11113193 "

III. "Gómez-Gómez, M.; Sánchez, C.; Peransi, S.; Zurita, D.; Bellieres, L.; Recuero, S.; Rodrigo, M.; Simón, S.; Camarca, A.; Capo, A.; Staiano, M.; Varriale, A.; D'Auria, S.; **Manessis, G**.; Gelasakis, A.I.; Bossis, I.; Balka, G.; Dénes, L.; Frant, M.; Nannucci, L.; Bonasso, M.; Giusti, A.; Griol, A. Photonic Label-Free Biosensors for Fast and Multiplex Detection of Swine Viral Diseases. Sensors 2022, 22, 708. https://doi.org/10.3390/s22030708 "

IV. "**Manessis, G**.; Frant, M.; Wozniakowski, G.; Nannucci, L.; Benedetti, M.; Denes, L.; Gyula, B.; Gelasakis, A.I.; Squires, C.; Recuero, S.; Sanchez, C.; Griol, A.; Giusti, A.; Bossis, I. Point-of-Care and Label-Free Detection of Porcine Reproductive and Respiratory Syndrome and Swine Influenza Viruses Using a Microfluidic Device with Photonic Integrated Circuits. Viruses 2022, 14, 988. https://doi.org/10.3390/v14050988 "

V. "**Manessis, G**.; Gelasakis, A.I.; Bossis, I. Point-Of-Care Diagnostics for Farm Animal Diseases: From Biosensors to Integrated Lab-On-Chip Devices. Biosensors 2022, 12, 455. https://doi.org/10.3390/bios12070455 "

VI. "Capo, A.; Calabrese, A.; Frant, M.; Walczak, M.; Szczotka-Bochniarz, A.; **Manessis, G**.; Bossis, I.; Staiano, M.; D'Auria, S.; Varriale, A. SPR-Based Detection of ASF Virus in Cells. Int. J. Mol. Sci. 2022, 23, 7463. https://doi.org/10.3390/ijms23137463 "

# Table of contents

# List of figures

# List of tables

# Abbreviations

| | |
|---|---|
| **“PPV1”** | **“Porcine Parvovirus 1”** |
| **“PCV-2”** | **“Porcine Circovirus type 2”** |
| **“PRRSV”** | **“Porcine Reproductive and Respiratory Syndrome Virus”** |
| **“SIV”** | **“Swine Influenza A”** |
| **“ASFV”** | **“African Swine Fever Virus”** |
| **“CSFV”** | **“Classical Swine Fever Virus”** |
| **“ORF”** | **“Open Reading Frame”** |
| **“POS”** | **“Point Of Service”** |
| **“POC”** | **“Point Of Care”** |
| **“LFA”** | **“Lateral Flow Assays”** |
| **“µTAS”** | **“Microfluidic Total Analysis Systems”** |
| **“LOC”** | **“Lab On Chip”** |
| **“µPADs”** | **“Microfluidic Paper-Based Analytical Devices”** |
| **“PICs”** | **“Photonic Integrated Circuits”** |
| **“LOD”** | **“Limit Of Detection”** |
| **“ROC curve”** | **“Receiver Operating Characteristic curve”** |
| **“AUC”** | **“Area Under the Curve”** |
| **“TP”** | **“True Positives”** |
| **“FP”** | **“False Positives”** |
| **“TN”** | **“True Negatives”** |
| **“FN”** | **“False Negatives”** |
| **“95% CI”** | **“95% Confidence Interval”** |
| **“PPV”** | **“Positive Predictive Value”** |
| **“NPV”** | **“Negative Predictive Value”** |
| **“PLR”** | **“Postive Likelihood Ratio”** |
| **“NLR”** | **“Negative Likelihood Ratio”** |
| **“DOR”** | **“Diagnostic Odds Ratio”** |

# Chapter 1. Introduction

## 1.1 Swine Industry in Europe

In 2020, approximately 150 million pigs were reared within the EU, yielding 23.8 million tonnes of pork meat which accounted for nearly half of total EU meat production (Marie-Laure, 2020). EU is the second biggest producer of pork meat after China and the largest exporter of pork products (Bellini, 2021). Germany, Spain and France are the leading countries in pork production, representing nearly half of total EU production (Marie-Laure, 2020). The swine industry is highly diverse in terms of rearing methods and farm sizes across the EU Member States and ranges from small backyard farms and extensive/organic farms to industrial installations and intensive production systems (Bellini, 2021). In general, the EU pig production systems are not vertically integrated, at least not to the level that is seen in the poultry sector (Bellini, 2021). In contrast to the rest of the EU countries, the pig sector in Greece is vertically integrated to a much larger extent.

The swine industry in Europe is subjected to a number of legislative directives, including the Common Agricultural Policy (CAP), which regulates environmental protection, food safety and public health, organic production, animal health and welfare. The first CAP pillar, which focuses mainly to the common organization of markets, includes policies that protect pig production in Europe (e.g. import tariffs) and as well as general measures for mitigating animal diseases and loss of consumer confidence due to public, animal or plant health risks (Marie-Laure, 2020). Additionally, the EU seeks to strengthen innovation and research with its rural development policy (second CAP pillar), the agricultural European Innovation Partnership (EIP Agri) and the funding of the Horizon 2020 and the Horizon Europe (2021-2027) programs for international projects. It is worth mentioning that the environmental policies such as environmental permits (Annex I to Directive 2010/75/EU, active), the recently published Green Deal initiative and the Farm to Fork strategy, promote greener and more sustainable agriculture and food systems and are expected to reshape the legislation relevant to the pig sector, including animal health and welfare (Marie-Laure, 2020).

## 1.2. Swine Industry and Viral Diseases

The swine industry accounts for approximately 35% of global meat production (Maes *et al.*, 2020). To meet the surging demand for animal products and in parallel diminish production costs, modern farming systems are focused on intensification, increased inputs

and higher stocking density. However, increased stocking density can accelerate pathogen transmission, compromising animal health and welfare (VanderWaal and Deen, 2018). On top of that, extended, globalized trade networks and insufficient surveillance programs exacerbate disease outbreaks and the emergence of transboundary infectious agents (Perry, Grace and Sones, 2013; Morgan and Prakash, 2006). Porcine Parvovirus 1 (PPV1), Porcine Circovirus type 2 (PCV-2), Porcine Reproductive and Respiratory Syndrome Virus (PRRSV), Swine Influenza A (SIV), African Swine Fever Virus (ASFV) and Classical Swine Fever Virus (CSFV) are among the most important viral diseases affecting swine due to their economic impact, wide expansion and/or severity. As previous experiences with Swine Influenza A and African Swine Fever have demonstrated, viral diseases can be devastating to the swine sector due to (i) their transmission dynamics, (ii) the unavailability of effective treatments, (iii) the limited vaccine availability and efficiency and (iv) the lack of monitoring systems and coordinated preventive measures (Sun *et al.*, 2016; Dixon *et al.*, 2020; Fila and Woźniakowski, 2020; Kedkovid, Sirisereewan and Thanawongnuwech, 2020).

### 1.2.1. Porcine Parvovirus 1 (PPV1)

Porcine Parvovirus 1 (PPV1, *Ungulate parvovirus 1*) is a small, non-enveloped, negative single-stranded DNA virus of the *Parvoviridae* family (Mészáros *et al.*, 2017). The viral single stranded DNA size is about 5 kb and both its terminal sequences form complex palindromic hairpin structures of about 120-200 bases long. The PPV1 viral genome contains only two Open Reading Frames (ORFs) that encode, through differential RNA splicing and posttranslational modifications, six distinct proteins. The ORF1 encodes 3 nonstructural proteins, namely the NS1, NS2 and NS3 that are involved in DNA replication. The ORF2 encodes three structural proteins (VP1, VP2 and VP3). The VP1 RNA template produces also the VP2 protein by splicing and the two proteins differ only in their amino-terminus (Streck, Canal and Truyen, 2015). Protein VP3 is produced by the post-translational modification of VP2. The PPV1 icosahedral capsid consists of ~ 60 copies of a random mixture of VP1 and VP2. The VP3 protein is a minor component and it is found only in 1-3 copies. Both VP1 and VP2 are associated with viral infection and immunogenicity (Streck, Canal and Truyen, 2015). The unique N-terminal domain of VP1 is required for DNA packaging. The VP2 alone is able to self-assemble into virus-like particle. The VP2 protein is crucial in inducing PPV1-specific neutralizing antibodies and

protective immunity, contains a large number of epitopes and is a suitable target for diagnostic assays (Liu *et al.*, 2020).

Porcine Parvovirus 1 is associated with "reproductive failure in swine, and its clinical manifestation is described by the acronym SMEDI (stillbirth, mummification, embryonic death, and infertility)" (Streck, Canal and Truyen, 2015). However, in most cases PPV1 infection does not cause clinical symptoms in non-pregnant pigs (Mészáros *et al.*, 2017). In contrast, when susceptible pigs are infected with PPV1 during mating or gestation, embryos are infected via the transplacental route. The gestation stage during PPV1 infection plays an important role on the outcome of the disease. For example, infection prior to 35 days of gestation leads to fetus resorption and consequently a reduction of litter size or return to estrus. Infection between the $35^{th}$ and $70^{th}$ day of gestation is associated with embryonic death and mummification, whereas infections at a later gestation stage result in subclinical disease and immunocompetent piglets (Antonis *et al.*, 2006). Strain virulence is largely defined by the severity of the reproductive failure (Mészáros *et al.*, 2017). Consequently, highly virulent strains infecting susceptible herds can cause significant economic losses (Antonis *et al.*, 2006).

Natural exposure probably does not coincide with active immunity, as PPV1 remains a significant problem in endemic countries (Antonis *et al.*, 2006). In fact, PPV1 remains one of the leading causes of reproductive failure in swine. As there is no specific treatment for parvoviruses, maintaining a high health status, adopting a continuous vaccination strategy, and implementing hygiene and biosecurity measures are considered the most effective means to manage and control PPV1. Porcine Parvovirus 1 infections can be managed by herd or gilt immunization (depending on prevalence and previous herd immunity, e.g. herd immunization is preferred in cases of high prevalence and insufficient herd immunity) aiming to reduce the clinical symptoms and prevent reproductive failures. Proper cleaning and chemical disinfection of housing facilities also reduce the viral load in the environment and disrupt infections through fomites. Given that PPV1 is extremely stable in pig slurry[1] and that traditional vaccine strains may be ineffective against newly emerged, highly virulent strains, early diagnosis and herd screening can contribute to managing the disease (Mészáros *et al.*, 2017).

[1] PPV1 can stay infective for more than 40 weeks at 20 °C and requires exposure to temperatures of 50–55 °C for a week to be completely inactivated.

### 1.2.2. Porcine Circovirus type 2 (PCV-2)

Porcine Circovirus type 2 (PCV-2) is a small, icosahedral, single stranded DNA virus belonging to the genus *Circovirus* of the *Circoviridae* family. The 20.5 nm capsid contains the circular viral genome which is 1.7 kb in size (Trible *et al.*, 2012). Theoretically, the viral genome contains at least 11 ORFs, but in reality, 6 of them encode known proteins and only ORF1 and ORF2 are required for viral replication (Correa-Fiz *et al.*, 2020). ORF1 encodes two replicases, Rep and Rep' which are involved in the rolling circle amplification of the viral genome (Correa-Fiz *et al.*, 2020). ORF2 encodes the only structural protein of PCV-2 which is 233 or 234 amino acids long and forms the capsid (CP). The CP is crucial for the attachment and entry into cells, as well as for the translocation of the viral genome to the cell nucleus for replication (Trible *et al.*, 2012). Furthermore, CP is the main immunostimulatory protein and is responsible for the swine immunological response to PCV-2 infection (Correa-Fiz *et al.*, 2020). The ORF3 is incorporated in ORF1 and probably is involved in the regulation of cell apoptotic mechanisms, whereas ORFs 4 to 6 encode nonstructural proteins which are involved in viral replication and immune system evasion (Correa-Fiz *et al.*, 2020).

Viral infection has been associated with several syndromes, ranging from subclinical to acute, known as PCV-2 associated diseases (PCVAD). These syndromes are the following: i) Post-weaning Multisystemic Wasting Syndrome (PMWS), ii) porcine dermatitis and nephropathy syndrome (PDNS), iii) Proliferative and necrotizing pneumonia (PNP) and iv) acute pulmonary edema. The manifestation of PCVAD is affected by the presence of co-factors such as previous viral or bacterial infection or co-infections, immunization schemes and animal genetics (Trible *et al.*, 2012). Post-weaning Multisystemic Wasting Syndrome (PMWS) is the most common PCVAD and is characterized by gradual weight loss, dyspnea, tachypnea, anemia, diarrhea, enteritis, jaundice and lymphadenopathy with granulomatous inflammation and usually affects animals 5-15 weeks old (Segalés, 2012). Morbidity rates range between 4% and 30% (in some cases reaching 60%) and mortality rates range between 4% and 20% (Segalés, 2012). Another PCVAD, known as porcine dermatitis and nephropathy syndrome (PDNS) is characterized by irregular, purplish-red hemorrhagic spots, and necrotic spots and papules mainly on the hind legs and perineal area. Animals suffering from PDNS are anorexic, catatonic, recumbent or refusing to move and exhibit stiffness of limbs, with or without low fever (Drolet, 1999). Disease prevalence in PDNS-affected farms is approximately 1% and

mortality can be as high as 100% in pigs older than 3 months and 50% in younger pigs (Segalés, 2012). Proliferative and necrotizing pneumonia (PNP), a PCVAD syndrome, causes interstitial pneumonia, bronchitis and mild to acute necrotizing bronchiolitis with bronchial ulceration. The absence of lesions in the lymphatic organs allows the differential diagnosis from PMWS (Segalés, 2012). Porcine circovirus type 2 associated reproductive failure is characterized by abortions at the last stage of gestation, returns to estrus as well as the birth of stillborn or mummified piglets and is mostly relevant to immunologically naïve herds or gilts. However, this PCVAD is not common, as most gilts have been in contact with PCV-2 prior to gestation (Brunborg *et al.*, 2007). Finally, the last known PCVAD syndrome, acute pulmonary edema, was recorded in 2009 in the USA and is characterized with the sudden onset of respiratory disease and death in weaned and fattening piglets reaching mortality rates of 20% (Cino-Ozuna *et al.*, 2011).

The management of PCVAD relies on various vaccination schemes and general biosecurity measures, depending on disease prevalence and severity. In general, vaccination of piglets and fattening pigs is suggested in cases of high prevalence or intense symptoms, whereas in low prevalence settings only the vaccination of gilts is typically effective. Biosecurity measures include the use of PCV-2 free boars and proper cleaning and disinfection of the housing facilities. Vaccines can improve daily weight gain and reduce the implications of PCV-2 infection even in cases of subclinical disease (Young, Cunningham and Sanford, 2011). At this point, it is worth mentioning that isolated PCV-2 or PPV1 infections usually do not cause severe clinical disease and high mortality rates, but their importance is associated with the financial burden in terms of decreased weight gain (Krakowka *et al.*, 2001; Rovira *et al.*, 2002). Despite that, high levels of PPV1 and PCV-2 viral genome copies in oral fluids and serum ($>10^6$ viral genome copies/mL) can cause intense clinical symptoms (Olvera *et al.*, 2004; Miao *et al.*, 2009; Zhou *et al.*, 2016).

**Figure 1.** "Poor hygiene in a finisher unit. PPV1/PCV-2 co-infection was common among finishers, although clinical symptoms were mild. Retarded growth rate of weaned piglets was recorded in the same farm."

### 1.2.3. Porcine Reproductive and Respiratory Syndrome Virus (PRRSV)

The Porcine Reproductive and Respiratory Syndrome is caused by an enveloped, positive-strand RNA virus. The virus belongs to the *Arteriviridae* family. "It is comprised of two species, Betaarterivirus suid 1 and 2, formerly known as European Type 1 and North American Type 2" (Manessis *et al.,* 2022). Genomic PRRSV RNA contains 8 ORFs and is ~ 15 kb in length. The ORFs 1a and 1 b encode the RNA replicases and constitute 80% of the total PRRSV genome (Fang and Snijder, 2010). Furthermore, ORFs 2 to 5 encode the structural glycoproteins GP2 to GP5, respectively, whereas ORF6 and ORF7 encode the structural membrane protein M and the nucleocapsid protein N, respectively (Meulenberg, 2000). The M protein is the most conserved structural protein, reaching 78–81% amino acid identity between the North American and the European isolates. The most variable structural protein is GP5 with only 51–55% amino acid identity between the two clades. The PRRSV virion is largely constituted (20-40%) of the N protein. N protein is immunodominant and several B-cell epitopes are conserved in both the European and the North American isolates (Dokland, 2010), making anti-N protein antibodies suitable for diagnostic tests (Meulenberg, 2000).

The clinical manifestation of PRRSV infection includes respiratory distress and poor growth of suckling piglets, growing and finishing pigs as well as reproductive failure in pregnant sows including mummified, aborted and stillborn fetuses (Kappes and Faaberg,

2015). Apart from the acute clinical syndrome, PRRSV infection has been linked to life-long subclinical persistent disease at herd level (Chand, Trible and Rowland, 2012). On a global scale, PRRSV outbreaks are perpetuated by emerging (due to viral recombination and mutations) or re-emerging strains (Kappes and Faaberg, 2015) and amount to yearly damages of USD 664 million in the USA alone (Holtkamp *et al.*, 2013). Hygiene and biosecurity, including management practices such as pig flow, gilt acclimation, and vaccination, are the main strategies to control the disease at the farm level (Corzo *et al.*, 2010). General biosecurity measures include monitoring of incoming vehicles and visitors, insect and rodent control and personnel training. Again, PRRSV vaccination strategies focus on either mass vaccination to reduce the overall prevalence of PRRSV in the herd and promote herd-level immunity or gilt vaccination to reduce the risk of PRRSV transmission to their offspring. The eradication in farms can be achieved by animal culling (test and remove), whole herd depopulation and repopulation with certified PRRSV-free sows and boars, persistent monitoring of semen and long-term herd closure to achieve herd immunity. Despite these efforts and the applied biosecurity measures, virus re-introduction is common (Cho and Dee, 2006; Corzo *et al.*, 2010).

**Figure 2.** "Emaciated piglet with PPRSV type 1 infection, probably due to vaccine failure. Photo from personal archive."

## 1.2.4. Swine Influenza A Virus (SIV)

Influenza A is an enveloped, 80–120 nm in size, negative sense, segmented, single-stranded RNA virus belonging to the *Orthomyxoviridae* family (Olsen, 2002). Viral RNA consists of eight segments which vary in length (890–2341 nucleotides) and encodes 10 and in some cases up to 12 proteins (Vincent *et al.*, 2008). Segment 7 (Matrix, M) and segment 8 (Nonstructural, NS) encode two proteins, M1/M2 and NS1/NS2, respectively. The RNA segments are bound and protected by a conserved protein, the viral nucleoprotein (NP). The viral polymerase complex, the RNA, and the NP form a ribonucleoprotein (RNP) complex. SIV typing is based on the various combinations of two surface glycoproteins, haemagglutinin (HA) and neuraminidase (NA) (Vincent *et al.*, 2008). Currently, 18 HAs and 11 NAs have been identified in all animal reservoirs around the world.

HA of avian origin is capable of binding to the N-acetylneuraminic acid–2,3-galactose linkage of sialyloligosaccharides, whereas HA of mammalian origin binds to the N-acetylneuraminic acid–2,6-galactose linkage. Swine epithelial cells express both types of sialic acid linkages, enabling the co-infection of viruses of both avian and mammalian origin, thus mediating virus reassortment (Wang and Palese, 2009). Following adaptation to swine, Influenza viruses can be combined (in cases of co-infection) and exchange genes with viruses of both human and avian origin, a phenomenon also known as antigenic shift. Antigenic shifts produce triple reassortments such as the 2009 H1N1 pandemic virus (Wang and Palese, 2009). Point mutations, substitutions, deletions, and insertions are common due to the high error rate of the viral RNA polymerase during replication. When these point mutations are accumulated in the HA and NA encoding regions of the RNA, the antigenic properties of HA and NA are altered, causing antigenic drifts. Both antigenic shift and antigenic drift are facilitated by the fragmented nature of SIV RNA and occur frequently, leading to the emergence of novel reassortants/subtypes and strains and consequently, to annual epizootics (Kuntz-Simon and Madec, 2009). SIV outbreaks are characterized by a dramatic onset of disease, accompanied by high morbidity rates approaching 100%, and low mortality rates, typically less than 1%. Usually, the incubation period lasts 1-3 days and the symptoms include fever, lethargy, decreased food intake, respiratory distress, coughing, sneezing, conjunctivitis, and nasal discharge, followed by recovery within 4-7 days, although the severity of the disease can be affected by the viral strain (Vincent *et al.*, 2008). Cases of SIV reassortants breaking the species barrier and infecting humans have been well-documented. Control of SIV outbreaks in swine farms is based on hygiene, partial depopulation, segregation of weaned piglets, and all-in/all-out systems. Vaccination can reduce the incidence and the severity of the disease, however, SIV vaccines are not constantly updated due to costs and lack of global scale epidemiological surveillance and do not always provide complete or consistent protection. Effective control of the disease in European pig herds should include immunization against both H1 and H3 subtypes (Kothalawala, Toussaint and Gruys, 2006).

### 1.2.5. African Swine Fever Virus (ASFV)

African Swine Fever Virus (ASFV) is an enveloped, icosahedral DNA virus of the *Asfarviridae* family. ASFV genome consists of linear double stranded DNA, 170 to 193 kb in size and contains 151-167 ORFs, closely arranged and encoded in both DNA strands (Wang *et al.*, 2021). Base-paired hairpins covalently close genome termini. The icosahedral

ASFV particle is made of a multi-layered structure, with the outermost layer resembling an external envelope membrane that is not required for virus infectivity. Under this layer, the capsid layer is formed from 2800 hexagonal capsomers, having a maximum diameter of 250 nm. Under the capsid lays the inner membrane which consists of a single lipid bilayer derived from the cell host endoplasmic reticulum. The core shell and the inner core form the remaining layers of ASFV. The core shell is an independent domain of the virus, has a diameter of 180 nm and is formed by polyprotein 220 and polyprotein 62. The inner core consists of a genome-containing nucleoid layer which is surrounded by the thick protein layer of the core shell (Wang *et al.*, 2021). Of particular interest is the icosahedral capsid. It is synthesized by 8280 copies of protein p72 and several minor capsid proteins. Estimations suggest that p72 makes up 32% of the total weight of the viral particle. More importantly, p72 is the main antigen detected in naturally infected pigs, making it ideal for highly sensitive diagnostic assays (Wang *et al.*, 2021).

Typically, ASFV infection is characterized by acute hemorrhagic fever in naïve populations and chronic disease in endemic regions. The main symptoms include fever, abortion, hyperemic areas in the skin, and hemorrhages in several internal organs (Ungur *et al.*, 2021). Factors such as immune system status, route of infection, virulence, and dosage of virus impact the disease's clinical manifestation and its course. Highly virulent strains lead to hyperacute disease and sudden deaths. Severe and diffuse splenic enlargement with dark-black discoloration and increased friability of the parenchyma are the only gross features of this type of disease manifestation. On the contrary, the acute form of ASFV infection, which is the most common, is accompanied with mortality rates of 100%, emesis, nasal discharge, bloody diarrhea, apathy, abortion, and cutaneous hyperemia. Chronically infected pigs present multifocal necrosis in the skin, intermittent fever, respiratory distress, arthritis, loss of weight, stunted growth and deep ulcerations (Ungur *et al.*, 2021). The virus is persistent in both animal tissues and the environment, enabling transmission through swill feeding and fomites (Chang'a *et al.*, 2019).

ASFV hosts, apart from domestic swine, include wild suids, whereas ticks of the *Ornithodoros* genus are considered disease vectors. ASFV infection is asymptomatic in arthropod vectors that remain carriers throughout their life cycle. These vectors are capable of spreading the virus during mating (Wang *et al.*, 2021). Wild boars are also susceptible to the virus with symptoms similar to those of domestic pigs and are considered a route of disease spreading. Currently, antiviral drugs or vaccines are not available against the disease. Introduction of ASFV in an area leads to huge economic losses due to quarantine, animal

culling and the prohibition of either the commercialization or transportation of swine products. In addition, the efforts to control the disease include prophylactic depopulation of both domestic swine and wild boars in ASFV-affected areas to minimize the transmission risk.

### 1.2.6. Classical Swine Fever Virus (CSFV)

Classical Swine Fever Virus (CSFV) is an enveloped, icosahedral virus, 40-60 nm in diameter, which belongs to the genus *Pestivirus* of the *Flaviridae* family. The ssRNA genome is approximately 12.3 kb in length and consists of a single ORF which is positioned between two untranslated regions (UTRs), the 5' UTR carrying an internal ribosome entry site and the uridine-rich 3' UTR. The ORF encodes a large polyprotein. Polyprotein cleavage by viral and cellular proteases leads to the formation of 4 structural proteins, capsid protein C and envelope glycoproteins Erns, E1 and E2, and 8 eight nonstructural proteins (Npro, p7, NS2, NS3, NS4A, NS4B, NS5A and NS5B) (Ganges *et al.*, 2020). The non-structural proteins are crucial in the cytoplasmic viral replication with NS5B being an RNA-dependent RNA polymerase and NS3 a protease. The E2 structural protein is immunodominant and pigs recovering from CSFV infection produce neutralizing anti-E2 antibodies which persist lifelong (Blome *et al.*, 2017).

CSFV can be transmitted through the oronasal route, by direct or indirect contact with infected pigs and contaminated feed. Additionally, the virus can be transmitted vertically (transplacentally or direct contact) to piglets through infected sows. CSFV shedding from mucosal surfaces and the detection of the virus in semen indicate that insemination is another possible route of transmission. Moreover, cooled and frozen pork products can be reservoirs of the virus (Edwards *et al.*, 2000). CSFV can survive in excretions for several days at room temperature, with survival times being significantly reduced in temperatures over 35°C. CSFV initially infects the epithelial cells of tonsillar crypts, then is transferred to the lymphoid tissues and afterwards to the blood capillaries. The virus replicates in the bone marrow and secondary lymphoid organs, such as the spleen, lymph nodes and lymphoid structures surrounding the small intestine. At the last phase of viremia, the virus infects the parenchymatous organs (Ganges *et al.*, 2020).

CSFV infection usually has three distinct manifestations, the acute, the chronic and the persistent. The acute phase, within two weeks post-infection, is characterized by atypical clinical signs such as fever, anorexia, gastrointestinal symptoms, general weakness, and conjunctivitis. Two to four weeks post-infection, neurological signs occur including

incoordination, paresis, paralysis and convulsions and simultaneously typical symptoms such as skin hemorrhages or cyanosis appear on the ears, limbs, and ventral abdomen. These symptoms are followed by death. Mortality rates can be as high as 100% (Postel *et al.*, 2018). The chronic manifestation of CSFV includes non-specific clinical signs such as remittent fever, depression, wasting and diffuse dermatitis. Animals with chronic disease shed high amounts of the virus until their death, which usually occurs one month after the infection, whereas the produced antibodies are intermittently present and do not lead to the clearance of the virus from animal tissues and bodily fluids (Postel *et al.*, 2018). The persistent form of the disease is usually associated with mild clinical signs in sows during pregnancy. Depending on the stage of gestation, the persistent form leads to the absorption or mummification of the fetuses. Infection between the $50^{th}$ and $70^{th}$ day of pregnancy may lead to the birth of persistently infected piglets that despite looking healthy, shed large amounts of the virus until their inevitable death during the late onset of the disease (Blome *et al.*, 2017). In most countries, a legal framework exists for the control and surveillance of CSFV, whereas the disease is notifiable to the OIE. Disease control is based on reliable diagnosis, stamping out of infected herds, establishment of restriction zones, movement restrictions, and tracing of possible contacts. Prophylactic vaccination may or may not be implemented based on each country's policy and relevant epidemiological data (Blome *et al.*, 2017).

## 1.3. Point of Service (POS) Diagnostics

Considering that the time from disease onset to laboratory confirmation of the etiologic agent may vary from few days to up to a month, advanced laboratory technologies and biosensors are gradually integrated in Point Of Service (POS) diagnostic devices to provide timely diagnosis, optimize livestock biosecurity and tackle animal diseases. POS diagnostics are defined as analytical devices and other tests capable to provide rapid diagnosis on-site, without the need of core laboratories (Cummins, Ligler and Walker, 2016). The "World Health Organization (WHO)" has issued a set of criteria for ideal POS applications, under the acronym "ASSURED" which stands for: "1) affordable, (2) sensitive (minimum number of false negatives), (3) specific (minimum number of false positives), (4) user-friendly (simple to perform), (5) rapid and robust, (6) permanent equipment-free, and (7) deliverable to those who need them" (Drain *et al.*, 2014). Human medicine has largely contributed to the development of POS diagnostics targeting various health-relevant biomarkers and infectious diseases including emerging and re-emerging diseases, such as malaria and HIV.

Following these advances in human medicine, biosensors and POS applications for economically significant animal diseases and zoonoses are being developed. Despite that, POS applications for animal diseases have not yet been widely popularized. For example, "from a total of 14 diagnostic kits for 11 animal diseases that have been registered to OIE (https://www.woah.org/en/what-we-offer/veterinary-products/diagnostic-kits/the-register-of-diagnostic-kits/ accessed on 11 November 2022), only two of them are based on POS technologies" (Manessis, Gelasakis and Bossis, 2022). "In fact, most published articles on POS tests and devices are for animal pathogens that are either economically important (African swine fever, classical swine fever, porcine reproductive and respiratory syndrome, rinderpest, foot and mouth disease, and bluetongue disease) or are zoonotic (avian and swine influenza, *Salmonella spp*., *Brucella spp*., *Escherichia coli*, and *Campylobacter spp*.)" (Manessis, Gelasakis and Bossis, 2022). The available POS applications for animal diseases could be classified in two broad categories, paper-based diagnostics and microfluidic devices.

### 1.3.1. Paper-based POS Diagnostics

Cellulose is hydrophilic, fibrous, biodegradable, and insoluble in water and most organic solvents. Nitrocellulose is hydrophobic and is derived from the nitration of cellulose, a process which also strengthens porosity (Singh *et al.*, 2018). Both materials are extensively used in the fabrication of paper-based diagnostic tests (Sharma *et al.*, 2015). Porosity, surface chemistry, and optical properties are considered among the most important characteristics of paper-based diagnostics and obviously, are determined by the materials used in their assembly. Surface chemistry is crucial for the immobilization and absorption of molecules and in conjunction with porosity affects the paper fluidic properties. Paper optical properties are also crucial for the colorimetric and fluorescent signal readouts. To further improve or alter paper properties, polymeric additives are commonly used (Jie Hu *et al.*, 2014).

Chemical, electrochemical, electrochemiluminescence, and chemiluminescence technologies and image analysis have been employed for analyte detection in paper-based diagnostic tests. Precipitation, acid–alkali (pH indicators) and redox reactions, and molecular and enzymatic dyes are exploited to generate colour changes in the chemical detection mechanism. Antibodies, antigens, aptamers, or oligonucleotides are usually labeled with nanoparticles (gold, silver, latex, carbon dots, etc.) to enable the visual observation of biorecognition events.

Following a modified approach, redox indicators, combined with oxidases, peroxidases, and phosphatases are utilized in enzyme-mediated colorimetric detection. In this detection mechanism, the contrast between the reduced/oxidized forms of the substrate and the background colour of the paper material, both influence the colour produced by the redox indicators (Morbioli *et al.*, 2017). Semi-quantification of the analytes can be facilitated by colour-coded charts, however semi-quantification faces many challenges such as the uneven distribution of colour, the linearity of the response, and subjective colour assessment (Morbioli *et al.*, 2017).

In contrast, the electrochemical detection technologies (e.g., in glucose meters) exploit both redox reactions (electron transfer between, for example, enzymes and nanoparticles) and non-redox reactions that alter the electrical properties of the sample (impedance, resistance, conductance, and potential). Low-cost electrodes are used for signal transduction, allowing quantification and in some cases, enabling high sensitivity and selectivity (Jie Hu *et al.*, 2014). The major advantages of electrochemical detection are rapidity, sensitivity and independence from ambient light and colour deterioration due to the properties of paper. The main disadvantages are the reading equipment requirements and the increased cost and complexity of incorporating electrochemical detection in paper-based diagnostics.

The electrochemiluminescence method is based on readouts of light emissions produced by electronically excited intermediates during exergonic reactions. Typically, photomultipliers and cameras are used for signal amplification, detection, and quantification, but require dark conditions to avoid ambient-light interference (Yetisen, Akram and Lowe, 2013). Chemically generated luminescence through hydrogen peroxide-luminol/rhodamine systems is exploited for analyte detection in the chemiluminescence method. Despite the limited application of chemiluminescence in paper-based diagnostics, the method maintains significant advantages such as compatibility with microfabrication and suitability for the sensing of various biological analytes (cells, bacteria, and DNA/RNA) (Ge *et al.*, 2014). The introduction of smartphones allowed the combination of image analysis with the abovementioned detection mechanisms to provide better signal measurements (Vashist *et al.*, 2015).

Despite these advances in detection methods, robustness is not always guaranteed in paper-based diagnostics. To improve their performance, signal enhancement and increased colour intensity via enzymatic reactions or the accumulation of nanoparticles (gold, silver,

latex particles, quantum dots, up-converting phosphor reporters (UCP), carbon nanotubes and particles, platinum nanoparticles, lanthanide, SiO2 nanoparticles, super-paramagnetic nanoparticles, etc.) are commonly used (Mahato, Srivastava and Chandra, 2017; Morbioli *et al.*, 2017). Specifically, in the electrochemical detection method, the doping of paper with conductive polymers, nanocomposites, and graphene is used to transform it into a semiconductor or a conductor and to prevent paper-induced electrical signal inhibition (Mahato, Srivastava and Chandra, 2017; Quesada-González and Merkoçi, 2018).

With respect to the operation principle, paper-based POS devices can be classified to two major categories: dipstick and strip tests and lateral flow assays (LFAs).

#### *1.3.1.1. Dipstick and Strip Tests*

The most popular representative of this category is pH strips. Typically, dipstick and strip tests rely on colorimetric measurements. Analyte semi-quantification is usually facilitated with colour-coded charts. Strip and dipstick tests can be used for the detection of a wide range of analytes. These tests are mainly used in animal production for the assessment of physicochemical properties in biological fluids (e.g. milk, urine, blood). The detection of antibiotics in animal-derived food products and ketone bodies for the monitoring of diabetic pets or the diagnosis of ketosis in cattle are some examples of the adoption of dipstick tests in practice (Brady, Dennis and Wagner-Mann, 2003; Carrier *et al.*, 2004; Link, Weber and Fussenegger, 2007). Recently, dipstick tests for the detection of aflatoxin M1 in milk have also been popularized (Li *et al.*, 2021). The main advantages of these tests are rapidity, convenience, low-cost and simple operation, and execution by untrained personnel on-site. However, in many cases laboratory confirmation may be necessary to obtain valid results (Eltzov *et al.*, 2015).

#### *1.3.1.2. Lateral Flow Assays (LFAs)*

LFAs are qualitative or semi-quantitative diagnostic tests that rely on the lateral flow of analyte/buffer mixtures to predefined positions where the analysis takes place. The pregnancy test, the influenza HA test and the Covid-19 rapid test are the most well-known representatives of this category of paper-based diagnostics. The components of a typical LFA test are a sample application pad, a conjugate pad, a membrane for detection (commonly nitrocellulose), and an absorbent pad (Figure 3). Adjacent components are overlapping to coordinate the liquid lateral flow (Eltzov *et al.*, 2015). The pads are usually fabricated from different materials with nitrocellulose, glass-fiber paper, and fused silica being the most used. Protection from contamination, light and evaporation of reagents and

samples is provided by a plastic encapsulating cover (Yetisen, Akram and Lowe, 2013). The LFA operation principle is simple. Samples are pretreated with a buffer solution (on the sample pad or separately prior the application of the sample on the sample pad) to improve the performance of the assay reactants (Mohd Hanafiah *et al.*, 2017). The sample/buffer mixture flows through the conjugate pad carrying the preloaded conjugated (labeled) particles. Bioreceptors immobilized on the control and test zones of the membrane are capable to capture the conjugated particles, thus creating (visible) signals and enabling the analyte detection (Eltzov *et al.*, 2015, p. 201). The flow of the liquid samples is facilitated by the absorbent pad and the capillary forces that it generates.

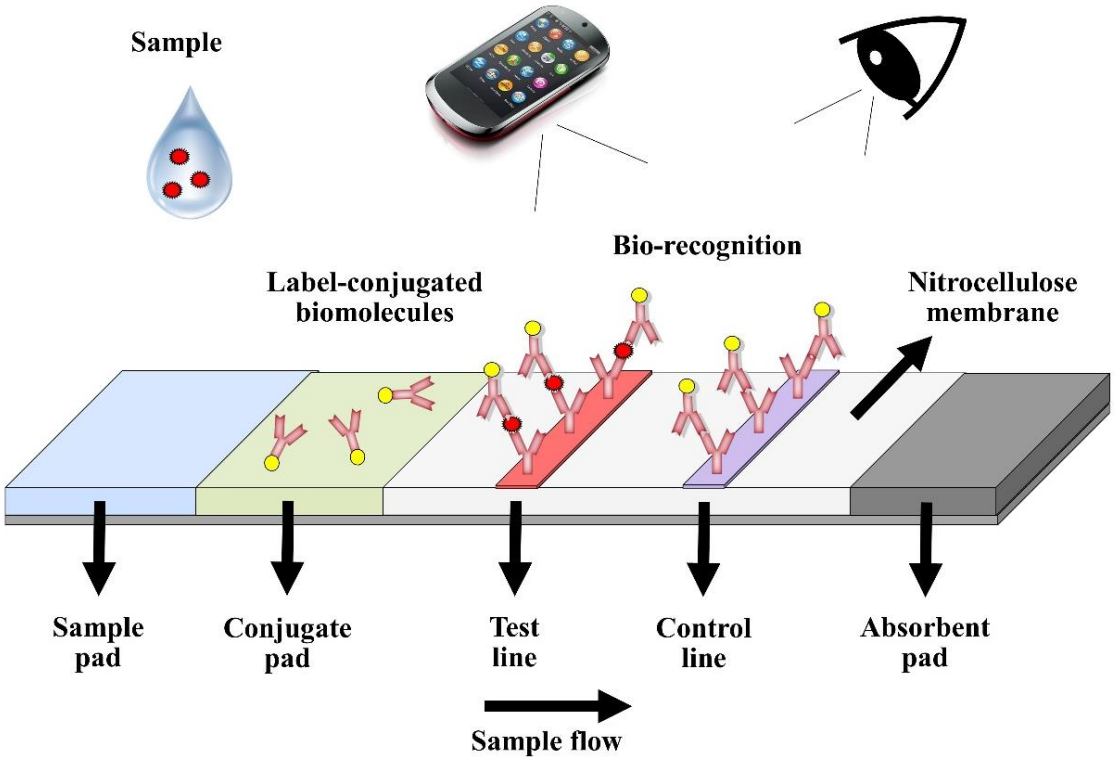


**Figure 3.** "Principle of LFA sandwich format (Manessis, Gelasakis and Bossis, 2022)".

Two main formats of LFA tests exist: the sandwich and the competitive formats. In the sandwich format, the analytes and the conjugated particles form complexes on the conjugate pad. As the sample/buffer mixture flows on the test membrane, the previously formed complexes are captured by immobilized molecular recognition elements (MREs, e.g., antibodies) on the test line via the remaining binding sites of the analyte. Excessive conjugated particles are capable to flow further and reach the control line. There, the conjugated particles are captured by other MREs forming the control line (Bahadır and Sezgintürk, 2016). On the contrary, the conjugated particles in the competitive format can react with MREs on both the control and test lines. The analytes are antagonizing the

conjugated particles for the binding sites of the capturing molecules (immobilized MREs) located on the test line. Consequently, conjugated particles do not accumulate on the test line in the presence of the analyte. Generally, sandwich formats are preferred for analytes with multiple binding sites (e.g., viruses, bacteria, etc.), while competitive formats are used for the detection of analytes with a single binding site (Bahadır and Sezgintürk, 2016).

The Covid-19 pandemic contributed to the popularization of LFAs and their simplicity and rapidity was exploited for on-site testing to minimize the risk of disease spreading due to long time intervals from infection to laboratory confirmation (Soin *et al.*, 2021). Similarly, LFA tests have been utilized for the rapid, on-site diagnosis of zoonotic diseases with significant economic impact that require immediate intervention such as the foot and mouth disease (FMD) and rinderpest (Yang *et al.*, 2010; Brüning-Richardson *et al.*, 2011). Additionally, LFAs have been an integral part of the food industry for the detection of food-borne pathogens and other unwanted and dangerous substances (e.g., mycotoxins) in food, animal products and even animal feed. Although promising, LFAs suffer from limitations such as inferior performance in comparison with laboratory tests, misuse when handled by untrained personnel, and qualitative or at best semi-quantitative measurements. It is worth mentioning that recent advancements in instrumentation have improved their quantitative capabilities to some extent (Busin *et al.*, 2016).

### 1.3.2. Microfluidic POS Devices

Microfluidic POS devices exploit microchannel networks for fluid delivery and analysis at the microliter or nanoliter scale. Analyte handling and detection is usually performed within specially designed microfluidic chambers or microfluidic channels. Liquid flow (laminar) in integrated devices is facilitated either passively with capillary forces or actively with pumping mechanisms (McDonald *et al.*, 2000). The recent advances in microfabrication have allowed the development of novel microfluidic devices and consequently new microfluidic POS devices (Teh *et al.*, 2008).

The microfluidic devices by definition require smaller sample and reagent volumes and smaller device apparatus size. These advantages make them easier to use and more cost-effective in comparison to laboratory testing. Additionally, fully integrated, all-in-one microfluidic devices require less specialized labor, are rapid and decrease the risk of human errors. This technology and approaches are currently applied in blood biochemical analysis, pathogen identification, and in the detection of environmental contaminants (Busin *et al.*, 2016). The main types of microfluidic devices are micro- total analysis systems (μTAS),

also known as “lab-on-a-chip” (LOC) devices, and microfluidic paper-based analytical devices (μPADs) (Manessis, Gelasakis and Bossis, 2022).

#### *1.3.2.1. Micro-total Analysis Systems (μTAS) & Lab on Chip (LOC) Devices*

LOC and μTAS devices are capable to perform a variety of assays (e.g., PCR, LAMP, RCA, etc.) by integrating all the necessary analytical steps into a single platform (Reyes *et al.*, 2002). The recent advances in the microelectronics industry have facilitated progress in developing this type of devices (Taberham *et al.*, 2008). The core of LOC and μTAS devices is the detection chip where the biorecognition/analysis takes place. The detection chips typically consist of glass, quartz, silicon, or polymeric materials. The unique mechanical, chemical and thermal properties of the polymeric materials have made them popular in the fabrication of these devices. Polytetrafluoroethylene (PTFE), photosensitive silicon, polymethylmethacrylate (PMMA), and biopolymers (such as cellulose acetate) are some examples of commonly used polymers in LOC device fabrication (Reyes *et al.*, 2002; Rossier, Reymond and Michel, 2002). Three main factors determine the efficiency of the detection chips: the microfluidics design, the format and the construction of the apparatus and the affinity and avidity of the main recognition elements on the chip. The recognition elements also affect the diagnostic performance of LOC devices. Detection chips are usually manufactured using soft lithography and 3D printing and are coupled with additional equipment for data extraction and signal processing and monitoring (Nasseri *et al.*, 2018). Signal detection methods include light detection, magneto-resistive sensors (GMR), electrochemical detection, acoustic sound-wave detection, mass spectroscopy (MS), and nuclear magnetic resonance (NMR) (Dittrich, Tachikawa and Manz, 2006). Figure 4 represents the concept of fully integrated LOC and μTAS devices.

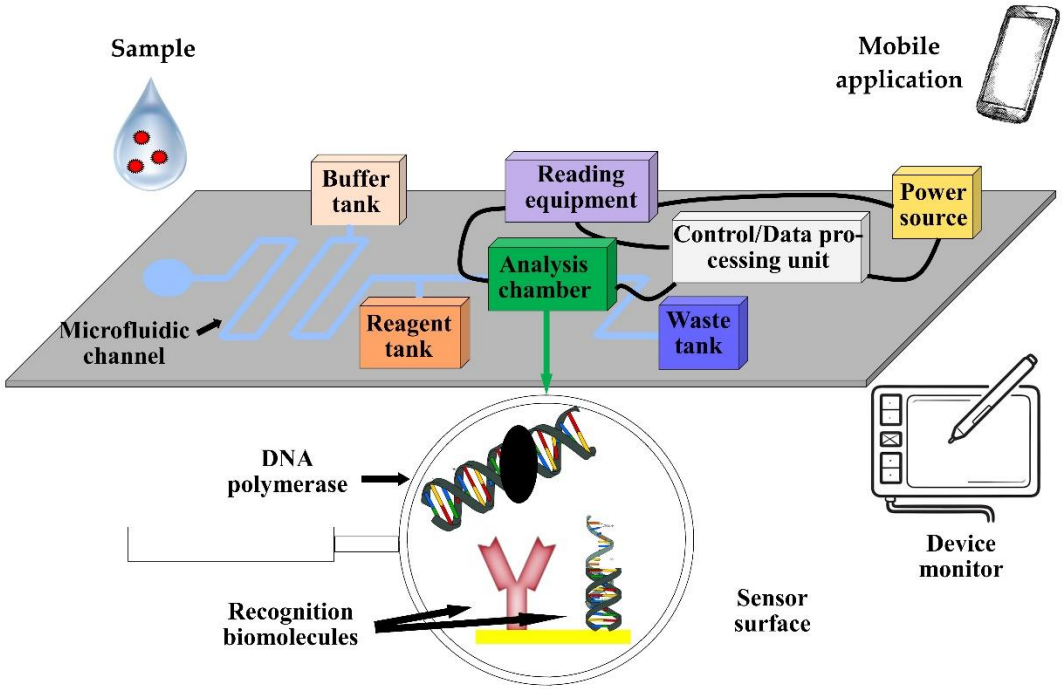


**Figure 4.** "Concept and main components of fully integrated LOC devices. The detection chip (gray parallelogram and analysis chamber) is magnified for demonstration purposes (Manessis, Gelasakis and Bossis, 2022)."

### *1.3.2.2. Microfluidic Paper-Based Analytical Devices (μPADs)*

The creation of μPADs can be traced back to the Whiteside group at Harvard University. Their development was an aftermath of research on paper strips for pH determination (Lisowski and Zarzycki, 2013). μPADs combine the properties of paper-based and microfluidic devices, maintaining "the benefits of microfluidics and utilizing low-cost materials (paper) and simple production processes" (Martinez *et al.*, 2010). μPADs, unlike LFAs and strip tests, allow the microfluidic handling (transportation, sorting, mixing, separation of liquids) thus facilitating the application of complex assays in paper-based diagnostics (Akyazi, Basabe-Desmonts and Benito-Lopez, 2018). Fluid movement is mediated by capillary forces, thus energy supply or mechanical valves and pumps are not required (Lisowski and Zarzycki, 2013). Additionally, μPADs can be manufactured on two or three dimensions (2D or 3D) and allow fluid movement both vertically and horizontally (Lisowski and Zarzycki, 2013). However, the complex fluid movement requires the creation of microfluidic channels and hydrophobic barriers (blocking of the paper pores). Hydrophobic patterning is crucial as it determines the length and width of the microfluidic channels and therefore the device's fluidic properties. Paper thickness determines the height of the microfluidic channels (Martinez *et al.*, 2010).

Hydrophobic patterning relies on several methods. Wax printing and dipping, movable type wax printing and wax screen-printing use wax printers to deposit solid wax for paper patterning. The wax is heated to its melting point and is absorbed by the paper sheets to create the hydrophobic barriers (Carrilho, Martinez and Whitesides, 2009). Wax-based methods are low-cost, non-toxic and offer disposable microfluidic devices, however the required equipment is costly, and the created microfluidic channels have relatively low resolution (Sher *et al.*, 2017). In contrast, inkjet printing requires a single piece of equipment to spray hydrophobic material such as SU-8 and PDMS on paper. This method is low-cost and rapid and is suitable for commercial production of paper-based microfluidic devices (Xia, Si and Li, 2016). On the contrary, inkjet etching relies on the spraying of solvent ink on the surface of polymeric material-covered paper. The solvent ink dissolves the polymeric material and creates hydrophilic microfluidic patterns on the exposed paper. Polydimethyl-siloxane (PDMS) ink is applied on paper for the creation of hydrophobic barriers in flexographic printing. This method is rapid, nevertheless it requires a multi-step procedure and modified commercial press printing equipment (Sher *et al.*, 2017). This procedure includes the creation of a photopolymer flexographic printing plate mold (FMold) through UV exposure and the transfer of the microfluidic pattern on an epoxy resin mold (ERMold), which is used for the deposition of PDMS on paper (Olmos *et al.*, 2019). Photolithography exploits low-cost and light sensitive photoresistants which are used to cover non-polymeric solid substrates (e.g. glass, silicon etc.). The covered non-polymeric substrates are then exposed to UV light through a high-resolution mask (plastic or glass). Depending on the targeted outcome, photolithography may range from a simple, rapid and user-friendly method with low equipment requirements (UV light and a heating plate) to a sophisticated method that requires expensive equipment, infrastructure (clean rooms) and trained staff (Xia, Si and Li, 2016). Following a different approach, $CO_2$ lasers emitting an infrared light beam for surface etching have been used for the patterning of paper, nitrocellulose and chromatography paper previously coated with hydrophobic materials. $CO_2$ laser cutting is simple but requires specialized equipment ($CO_2$ laser and 2 D graphics) (Singh *et al.*, 2018). Finally, the hydrophilic properties of paper can be reversed with the application of alkyl ketene dimer (AKD)-heptane. A heating step at 100ºC for 45 minutes is required to cure the AKD-heptane. The main drawback is the high cost of plasma treatment for the hydrophilic patterning (Sher *et al.*, 2017)).

In terms of detection mechanisms, μPADs are compatible with potentiometric, fluorometric, colorimetric and thermal (calorimetric) sensors, chemiluminescence,

electrochemiluminescence (ECL), fluorescent quantum dot nanoparticles and metal complexes and enzymatic readout methods (Figure 5) (Delaney *et al.*, 2011; Davaji and Lee, 2014; Caglayan *et al.*, 2016; Qi *et al.*, 2017; Jangid *et al.*, 2019; Yehia, Farag and Tantawy, 2020). A promising subcategory of μPADs, the paper-based electrochemical micro-fluidic devices (μPEDs), rely on redox reactions for the analyte detection and utilize electrodes fabricated from conducting carbon or metal inks through screen, inkjet printing or pencil-drawing (Fu and Wang, 2018). AuNP's carbon nanotubes, and graphene nanosheets are commonly used to modify the electrodes and increase the sensitivity of μPEDs (Jie Hu *et al.*, 2014).

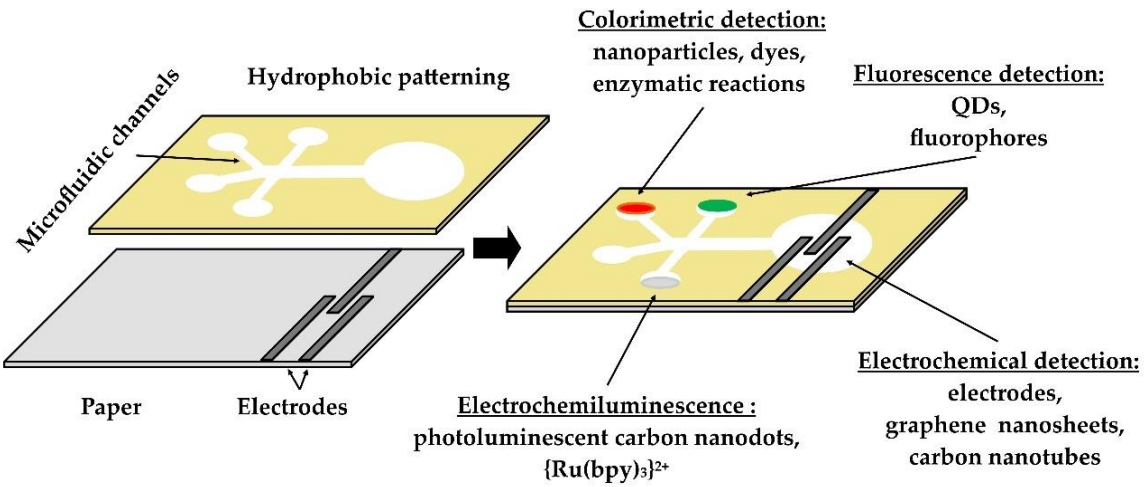


**Figure 5.** "Concept and popular detection methods of paper-based microfluidic devices. The hydrophobic patterning determines the fluidic properties of these devices ((Manessis, Gelasakis and Bossis, 2022)."

### *1.3.2.3 Applications of microfluidic technologies*

In general, microfluidic POS diagnostics can be categorized in three groups: nucleic acid-based, protein-based and cell-based devices. Conventional PCR is routinely used for nucleic acid amplification; however, it is laborious and requires trained staff and specialized equipment, including thermocyclers. As a result, "nucleic acid-based POS applications focus on alternative isothermal amplification technologies such as loop-mediated isothermal amplification (LAMP), nucleic-acid-sequence-based amplification (NASBA), helicase-dependent amplification (HDA), and recombinase polymerase amplification (RPA)" (Manessis, Gelasakis and Bossis, 2022). Amplicon detection is performed either visually or by smartphones and is usually facilitated by fluorescence, colorimetry and chemiluminescence in microfluidic devices. Up to date, some pathogens of veterinary importance such as *Cryptosporidium parvum*, *Escherichia coli*, *Salmonella typhimurium*, and suid Herpesviruses have been the targets of nucleic-based POS devices.

Protein-based POS devices are relative simpler and faster than nucleic acid-based applications, mainly because cell/viral lysis, nucleic acid purification, complex sample pretreatment and user interference are not required (W. Jung *et al.*, 2015; Manessis, Gelasakis and Bossis, 2022). For example, a microfluidic, magnetic beads-based device has been developed for the detection of antibodies against *Mycobacterium avium* subsp. *paratuberculosis* and the detection of Johne's disease in cattle (Wadhwa *et al.*, 2012). Finally, cell-based microfluidic devices have been successfully integrated in human healthcare such as the whole-blood microfluidic cell counters and CD4 counters for HIV-infected patients (W. Jung *et al.*, 2015). In animal diagnostics, milk analysis is of particular importance and some lab-on-chip devices for the detection of mastitis and milk neutrophil activity have been developed (Kimura *et al.*, 2012).

## 1.4. Study objectives

The main objectives of this thesis were the development of the analytical protocol and the validation of a novel, fully-integrated bench-top analyzer for the rapid and reliable detection of major swine viral pathogens in a POS setting. The state-of-the-art POS diagnostic system targeted 6 swine viruses namely Porcine Parvovirus (PPV1), Porcine Circovirus 2 (PCV-2), Swine Influenza (SIV), Porcine Reproductive and Respiratory Syndrome Virus (PRRSV), Classical Swine Fever Virus (CSFV), and African Swine Fever Virus (ASFV) and was developed in the framework of "European Union's H2020 SWINOSTICS (swine diseases field diagnostics toolbox) project". The system utilized microfluidics and Photonic Integrated Circuit (PIC) sensors for the label-free detection of viral antigens. This protein-based POS device exploited antibodies for the capturing and detection of the 6 viruses. Consequently, analyte detection coincided with the infection of animals. The optical biosensors (PICs) were selected to eliminate the complex handling required for the labelling of viral particles, thus allowing the usage of the device in field conditions.

# Chapter 2. Literature Review

## 2.1. Biosensors in Animal Production

Biosensors are defined as sensors with immobilized biomolecules on their surface which are capable to recognize specific analytes indicative of a microorganism or a condition. The recognition event is facilitated by the biomolecule elements, also known as bioreceptors. Common bioreceptors are monoclonal antibodies, RNA, DNA, glycans, lectins, enzymes, cofactors, tissues or whole cells (Wadhwa *et al.*, 2012). Depending on the bioreceptor used, biosensors are classified as immunosensors, genosensors, non-enzymatic receptor sensors, enzymatic sensors, and whole cell sensors. The biorecognition event is converted to measurable signals through transducers, allowing analyte detection and quantification (Su *et al.*, 2012). Biosensors should be capable to detect the targeted analytes robustly, regardless of the origin or complexity of the biological samples (Vidic *et al.*, 2017). Biosensors can be further classified to electrochemical, optical, piezoelectric, magnetic, thermal, radioactive, and mechanical sensors depending on the signal transduction method.

Despite that a staggering number of biosensors has been developed in the last years (Mohankumar *et al.*, 2021), only a small fraction of them are targeting analytes relevant to livestock biosecurity. The biosensors developed to optimize animal biosecurity are classified based on the employed signal transduction methods and they are presented below.

### 2.1.1. Electrochemical Biosensors

Electrochemical biosensors combine the selectivity of biomolecules with the sensitivity of electroanalytical methods. The biorecognition event is transduced to electrical signals, typically detected with electrodes. “Two major classes of electrochemical biosensors exist, biocatalytic devices and affinity sensors” (Ronkainen, Halsall and Heineman, 2010). Amperometry and electrochemical impedance spectroscopy are the most common transducing approaches. The development of nanomaterials such as graphene and carbon nanotubes have popularized electrochemical detection (Hammond *et al.*, 2016). The main advantages of electrochemical biosensors are low-cost, portability and ease of operation (Hammond *et al.*, 2016). In this text, electrochemical biosensors are classified to biocatalytic devices and affinity sensors (Figure 6).

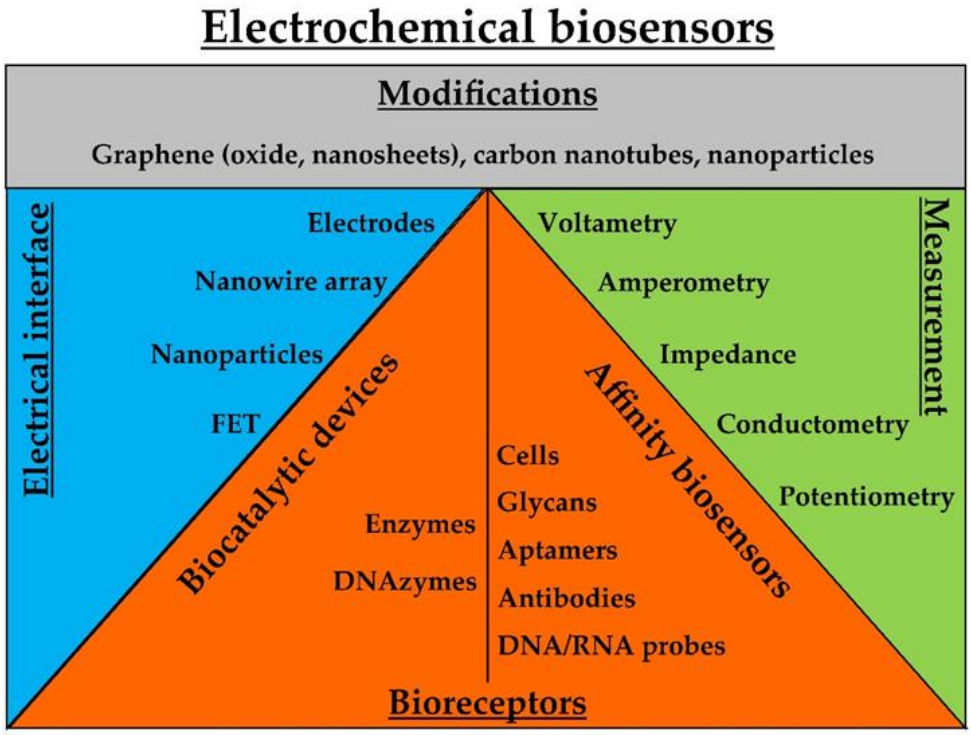


**Figure 6.** "The basic components of electrochemical biosensors. The interaction of the targeted analyte with the bioreceptors causes electrochemical changes transduced to measurable signals via the electrical interface. Nanomaterials and nanoparticles are used to improve the performance of the biosensors (Manessis, Gelasakis and Bossis, 2022)."

Biocatalytic electrochemical sensors exploit the selectivity and catalytic activity of enzymes for the transduction of the biorecognition event to electrical signals. In a typical setup, enzymes are immobilized on electrodes and catalyze the formation of electroactive products (Li *et al.*, 2009). Such an example is a superoxide dismutase-functionalized sensor which was used for the detection of neutrophil excreted $O_2^-$ radicals in mastitic milk (Kimura *et al.*, 2012). Beyond classic enzymatic reactions, peroxidase-mimicking DNAzymes were coupled with rolling circle amplification (RCA) for the detection of *Escherichia coli*. Anti-*E. coli* antibodies were immobilized on the surface of the electrodes to capture the bacterial cells. Anti-*E. coli* aptamers contained in probes and primer sequences complementary to other secondary circular probes with two G-quadruplex units were used to couple with the bacterial cells and initiate the RCA elongation. The DNAzyme and RCA resulted to the formation of G-quadruplex oligomers on the electrodes. The oligomers were then folded into G-quadruplex/hemin complexes in the presence of K+ and hemin. These complexes had a strong catalytic activity towards $H_2O_2$ and generated electrochemical signals. The biosensors showed a detection limit of 8 CFU/mL and a detection range of 5 orders of magnitude (Guo *et al.*, 2016). As it was previously mentioned, graphene and nanoparticles can modify the properties of transducers and improve their performance. In this context, ruthenium bi-pyridyl complex was coupled with graphene oxide nanosheets. The nanosheets

were functionalized with lipoxygenase for the detection of non-esterified fatty acids (NEFA) in serum samples. The sensor showed sensitivity of 40.5 μA/mM and signal linearity in a range of 0.1–1.0 mM (Veerapandian, Hunter and Neethirajan, 2016).

Affinity sensors follow a different, non-enzymatic approach for the detection of the targeted analytes and rely on changes of the electrical properties of the sensor after the biorecognition event. For example, an aptamer-based impedance biosensor using gold interdigitated microelectrodes was developed for the detection of H5N1 avian influenza virus. Signal amplification was achieved with gold nanoparticles and the Limit of Detection (LOD) was 0.25 HAU units for purified virus samples and 1 HAU unit for tracheal swabs (Karash *et al.*, 2016). Apart from aptamers, single stranded nucleic acid probes can be used as Molecular Recognition Elements (MREs) on electrochemical biosensors which are known as genosensors. For example, a genosensor for the detection of *Escherichia coli* genomic DNA and cells within 14 minutes showed LOD values of 0.01 ng/μL and 11 cells/mL, respectively (Arora *et al.*, 2007). In another study, DNA probes were initially immobilized on palladium nanoparticles for signal enhancement, and then were electrodeposited on a gold electrode for the detection of *Brucella* DNA. The sensitivity was 0.02 μA $dm^3$/mol and the LOD was $2.7 \times 10^{-20}$ mol $dm^{-3}$ (Rahi, Sattarahmady and Heli, 2016).

Field Effect Transistor (FET) devices are capable to manipulate the electrical current flow and have high input impedance. FET characteristics were exploited for the creation of a potentiometric biosensor. The biosensor was based on an extended-gate FET setup for the serological diagnosis of Bovine Herpes Virus-1 (BHV-1) using the viral protein gE. The assay could be completed within 10 minutes and the performance was similar to that of ELISA. Additionally, the chip was integrated into a microfluidic chip (Tarasov *et al.*, 2016). Similarly, a FET biosensor was functionalized with α2,3- and α2,6-sialic acid-containing oligosaccharides (glycans) for the detection of H1 and H5 influenza A hemagglutinin, respectively. The small Debye length of the selected MREs allowed the efficient detection of H1 and H5. The LOD was 60 H5 hemagglutinin molecules and 6000 H1 hemagglutinin molecules in 20 μL samples (Hideshima *et al.*, 2013).

The unique properties of graphene and carbon nanotubes have been exploited for the coating of electrodes or nanoparticles to enhance detection signals in electrochemical biosensing (Wang, 2005; Shao *et al.*, 2010). For example, electro-reduced graphene oxide was used to coat dual screen-printed electrode sensors for the detection of non-esterified

fatty acids (NEFA) and beta hydroxyl-butyrate (βHBA) in milk. Antibodies were used as MREs. The non-conducting behavior of the captured biomolecules resulted in reduced electrochemical sensor responses. Sensor responses showed a good correlation ($R^2$ 0.99) to analyte concentration to a range from 0.1 mM to 10 mM (Tuteja and Neethirajan, 2018). In another study, carbon nanotube biosensors were assembled on gold electrodes using a layer-by-layer technique and were functionalized with antibodies against avian metapneumovirus (Newcastle Disease Virus-NDV). The biorecognition event resulted in changes in the conductance of the sensor. LOD was $10^2$ $TCID_{50}$/ml (Bhattacharya *et al.*, 2011).

Nanoparticles of various compositions have been exploited for signal enhancement in electrochemical biosensors. For example, polyethylene glycol-coated and hyaluronic acid modified $Fe_3O$/Au nanoparticles were used for electrode modification of an anti-fouling immunosensor. The brucella outer membrane protein OMP31 was used as an MRE for the detection anti-Brucella antibodies in serum. The targeted analyte could be quantified in a range of $10^{-15}$ g/ml to $10^{-11}$ g/ml. The LOD was 0.36 fg/ml (Lv *et al.*, 2018). In another study, a sandwich immunoassay was developed for the detection of *Salmonella pullorum*. Antibody-functionalized silica coated magnetic beads and secondary antibody-functionalized reduced graphene oxide coated with gold nanoparticles (electro-chemical label) were used to form an immunocomplex in the presence of the bacterial cells. The immunocomplex was detected with a four-channel screen-printed carbon electrode using differential pulse voltammetry in the presence of 0.2 M HCl. Linear responses were recorded in the range from $10^2$ to $10^6$ CFU/mL, the LOD was 89 CFU/mL and the assay could be completed within 90 minutes (Fei, Dou and Zhao, 2016).

Magnetic nanoparticles have been used for the magnetic separation of the targeted analytes and the subsequent electrochemical detection (Haun *et al.*, 2010). A biosensor based on diagnostic magnetic resonance was developed for the detection of Gram (-) bacteria. Magnetic nanoparticles functionalized with anti-LPS antibodies were used for cell separation. The real-time detection was based on conductometry (Jaffrezic-Renault *et al.*, 2007).

### 2.1.2. Optical Biosensors

Optical biosensors rely on novel technologies and materials such as surface plasmon resonance (SPR), optical waveguides and resonators, photonic crystals and optic fibers for analyte detection (Chen and Wang, 2020). Absorbance, reflectance, fluorescence, refractive index and chemiluminescence are some of the most common detection methods in optical

biosensors (Figure 7). Extended reviews on optical biosensors have been published previously (Borisov and Wolfbeis, 2008; Chen and Wang, 2020).

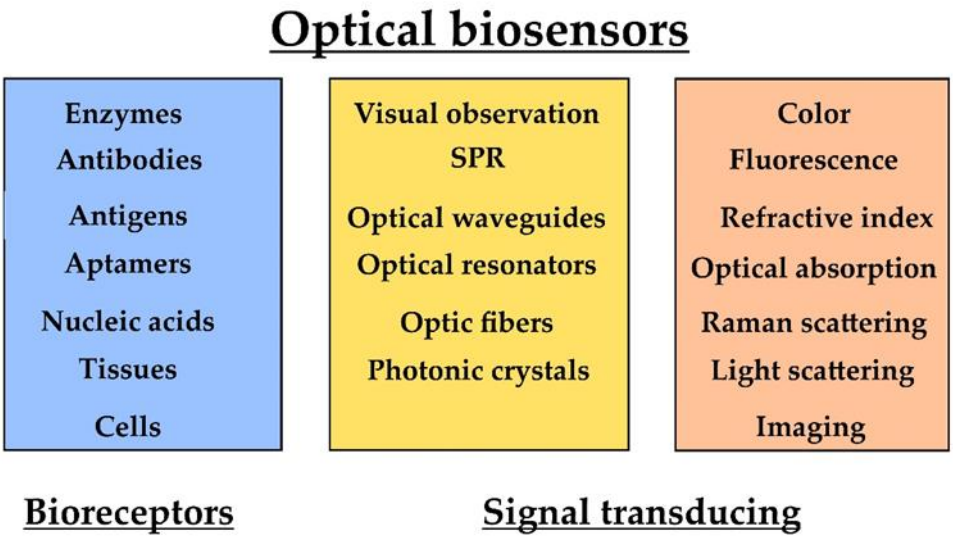


**Figure 7.** "The basic components of optical biosensors. The interaction of the targeted analyte with the bioreceptors changes the optical properties of the transducers (Manessis, Gelasakis and Bossis, 2022)."

Various combinations of MREs and labels have been exploited for analyte detection in optical biosensors. Gold nanoparticles have been extensively used in LFA applications where they facilitate simple visual observations (Petrakova *et al.*, 2019). For example, an aptamer-mediated isothermal strand displacement amplification coupled with an LFA test was developed for the detection of *Salmonella enteritidis*. A secondary, biotin-conjugated aptamer was used for the magnetic separation of amplicons with streptavidin-modified magnetic nanoparticles. Amplicons were detected with an LFA test utilizing Au-nanoparticle probes. The LOD was 10 CFU/mL and the results could be semi-quantified with a strip reader (Fang *et al.*, 2014). In another study, unmodified gold nanoparticles and a peptide nucleic acid (PNA) were used for the detection of Avian Influenza viral RNA. In the presence of viral RNA complementary to the PNA, PNA-induced gold nanoparticle agglomeration was prevented, and the absorbance (recorded with a spectrophotometer) was reduced. The assay could be completed within 15 minutes, had LOD values of 2.3 ng and showed specificity of 96.46% (95% CI = 93.8 to 98.2) and sensitivity of 82.41% (95% CI = 73.9 to 89.1) (Kumar *et al.*, 2020).

Apart from gold nanoparticles, fluorescent labels and dyes are also frequently used in optical biosensors. DNAzymes were conjugated with fluorescent dyes for the detection of bacterial lysates. The DNAzymes were allosterically converted into active forms in the presence of the lysates, thus resulting in the cleavage of fluorescent substrates. The assay

was performed on paper-based sensors and could selectively detect *Escherichia coli* in spiked milk, apple juice and water samples within 5 minutes. The LOD value was 100 cells/mL (Ali *et al.*, 2017). In another study, the Fc fragments of purified human IgG antibodies were used to functionalize Sephadex renewable micro-columns. *Staphylococcus aureus* bacteria were captured on the micro-columns via the Fc/protein-A interaction. The Texas Red fluorescence marker was conjugated with anti-protein A goat polyclonal antibodies which were used for the capturing of the previously formed complexes, facilitating optical detection. Measurements were carried out with a FIALab 3500B system and an Ocean Optics USB 2000 instrument with a spectrophotometer. The LOD was 200 CFU/mL in milk samples and linear responses were recorded in the range from $4\times10^2$ to $4\times10^7$ CFU/mL. The assay could be completed within 17 minutes (Peedel and Rinken, 2014).

The dielectrophoresis (DEP) force is generated by non-uniform electric fields and is capable to manipulate dielectric particles based on their size. Antibodies immobilized on the surface of golden tungsten microwires were used to create a DEP force-based microwire sensor for the detection of *Escherichia coli* cells. Fluorescein-conjugated secondary antibodies were used to detect and quantify the bacteria captured on the sensor's surface (Lu and Jun, 2012).

Quantum dots (QDs) are semiconducting nanoparticles of various chemical substances, increasingly used during the last years in biomedical applications and optical biosensors (Wagner *et al.*, 2019). QDs quenched through modification with nicotinamide adenine dinucleotide (NAD+) were used for the detection of β-hydroxybutyrate (βHBA), a key biomarker of subclinical ketosis. The NAD+ enzymatically reacted with βHBA forming NADH and eliminating NAD+ quenching of the QDs. The reaction could be performed in a microfluidic chip with an integrated low-cost optical detection unit. LOD values in serum and milk were 34.8 μM and 40.3 μM, respectively (Weng *et al.*, 2015).

Carbon nanotubes stand at the crossroads of electrochemical and optical biosensing. Carbon nanotubes were used to produce a near–infrared electrochemiluminesence sandwich immunosensor for the detection of Porcine Reproductive and Respiratory Syndrome virus (PRRSV). Glassy carbon electrodes were modified in sequence with carbon nanotubes, CdTe/CdS quantum dots, chitosan, Au nanoparticles and anti-PRRSV antibodies, whereas porous PtAu bimetallic nanotubes were used as near infrared electrochemiluminesence catalysts. To recognize the previously captured viral antigens on the glassy carbon electrodes

and form sandwich immunocomplexes, PtAu nanotubes were modified with β-cyclodextrin and adamantine/anti-PRRSV antibody conjugates The LOD was 10.8 pg of viral antigens per mL (Shao *et al.*, 2017).

The recent development of Surface Plasmon Resonance (SPR) technologies has promoted an increase in fabrication of optical biosensors in the fields of life science, clinical diagnosis and food safety. For example, single-strand DNA probes with locked nucleic acid nucleotides (LNA) substitutions were used for the SPR-based detection of the VP72 gene of African Swine Fever virus (ASFV). The LOD and the Limit of Quantification (LOQ) were 178 and 245 copies/μL of genomic viral DNA, respectively. The assay could quantify the genomic ASFV DNA in the range from 373 to 1058 copies/μL and could be completed within 5 minutes. In another study, an SPR-based biosensor was used for the detection of haptoglobin, a predictor of mastitis. Haptoglobin interacts with hemoglobin. Exploiting this phenomenon, milk samples were mixed with bovine hemoglobin and then applied on the haptoglobin-modified sensor. The sensor followed a competitive format setup and in the presence of haptoglobin in milk samples the artificially added hemoglobin could not interact with the sensor. The LOD was 1.1 mg/L (Åkerstedt *et al.*, 2006).

Label-free optical biosensors based on refractive index measurements are in general compatible with transducing platforms such as ring resonators, waveguides, surface plasmon resonance, fiber gratings and photonic crystals (Fan *et al.*, 2008). For example, the label-free detection of Porcine Circovirus type 2 (PCV-2) was enabled using excessively tilted fiber grating (Ex-TFG) inscribed in standard single mode fiber. Protein A was immobilized on the sensor's surface for the binding of anti-PCV-2 monoclonal antibodies. The captured viral antigens caused changes in the refractive index upon laser excitation which were recorded with a fiber optic grating demodulation system. The LOD was ~9.371 $TCID_{50}$/mL (Luo *et al.*, 2016).

Finally, the label-free detection of avian influenza virus H5N1 was achieved using a biosensor integrated in a microfluidic reactor array system. The biosensor was based on high spatial resolution imaging ellipsometry. Protein A was immobilized on the sensor surface and coupled with anti-H5N1 virus 4A4 monoclonal antibody. The biosensor's silicon wafers were analyzed with imaging ellipsometry after the biorecognition event. The assay could be completed in 10 minutes and the LOD was $2.56 \times 10^{-3}$ $TCID_{50}$/ml (Qi *et al.*, 2010). Table 1 summarizes the currently available electrochemical and optical biosensors for the detection of important animal diseases and mastitis.

**Table 1.** "Available electrochemical and optical biosensors for the detection of mastitis and animal diseases (Manessis, Gelasakis and Bossis, 2022)."

| **"Targeted Analyte"** | **"Recognition Element"** | **"Materials"** | **"Detection Technique"** | **"Detection Matrix"** | **"Performance"** | **"Reference"** |
|---|---|---|---|---|---|---|
| | | | ***"Electrochemical biosensors"*** | | | |
| Haptoglobin | Goat anti-bovine Hp polyclonal antibody (Abcam) | Functionalized gold electrode | Amperometric detection | Skimmed milk | LOD [1] of 0.63 ng/mL. Linear response range: 15 - 100 mg/L. Detection in 5 minutes | (Tan *et al.*, 2012) |
| Haptoglobin | Anti-Hp antibody | Functionalized liquid-exfoliated two-dimensional phosphorene (Ph) nanosheets electrodeposited on screen-printed electrode | Differential pulse voltammetry | Spiked serum samples | LOD of 11 ng/mL. Linear response range: 10 – $10 \times 10^3$ ng/mL. Detection in 60 seconds | (Tuteja and Neethirajan, 2018) |
| Influenza A virus | Mouse polyclonal anti-M1 antibodies | Functionalized gold electrodes | Electrochemical impedance spectroscopy | PBS[2] buffer | LOD of $2 \times 10^{-2}$ ng/mL. Detection in 30 minutes | (Nidzworski *et al.*, 2014) |
| Avian Influenza A H5N1 virus | Monoclonal antibodies (produced in mouse myeloma cells) | Protein A-modified interdigitated array microelectrode | Electrochemical impedance spectroscopy | Tracheal and cloacal swabs | LOD of $2^{-1}$ HAU[3]/50 µl. Linear response range: $2^{-1}$ - $2^4$ HAU/50 µl. Detection in 1 hour | (Lin *et al.*, 2015) |
| Avian Influenza A H5N1 virus | H5N1-specific aptamer | Aptamer-modified magnetic beads, concanavalin A-glucose oxidase-Au nanoparticle complexes, glucose solution, screen- | Electrochemical impedance spectroscopy | PBS buffer | LOD of $8 \times 10^{-4}$ HAU in 200 µL | (Fu *et al.*, 2014) |

| | | | | | | |
|---|---|---|---|---|---|---|
| | | printed interdigitated array electrode | | | | |
| Avian Influenza A H7N1 virus | Rabbit anti-H7N1 polyclonal antibodies (affinity chromatography-purified) | Functionalized gold electrodes | Electrochemical impedance spectroscopy | Antigen extracted from vaccine diluted in buffer | LOD of $5 \times 10^3$ ng/mL | (Diouani *et al.*, 2008) |
| Avian influenza A H7N9 single-stranded (ss)DNA | DNA tetrahedral probe | Biotinylated-ssDNA oligonucleotide (detection probe), avidin-horseradish peroxidase (HRP) | Amperometric detection | ssDNA (PCR product in buffer) | Sensitivity of $10^{-7}$ μM. Detection in under 80 minutes | (Dong *et al.*, 2015) |
| Quantum dot-modified Influenza hemagglutinin | Biotinylated glycans | Streptavidin-modified magnetic particles, glassy carbon microelectrode, 3D microfluidic chip | Differential pulse voltammetry | Vaccine hemagglutinin buffer | Accuracy 80%. Linear response range: 60 – 500 μM. Detection in 45 minutes. | (Krejcova *et al.*, 2014) |
| Bovine Viral Diarrhea (BVD) antibodies | BVD virus | Functionalized nanowire sensor integrated on chip | Electrochemical impedance spectroscopy, Cyclic voltammetry | Serum | Detection of $10^3$ ng/mL. Detection in 20 min | (Montrose *et al.*, 2015) |
| BVD virus, anti-BVD antibodies | BVDV-1 monoclonal antibody (RAE0823), recombinant purified BVDV-1 Erns protein (BVDR16-R-10) | Six gold nanoband electrodes, silicon chip-based biosensor platform | Electrochemical impedance spectroscopy | Serum | Detection in 20 minutes | (Creedon *et al.*, 2018) |
| Fowl adenovirus-9 | Anti-Adenovirus, Group II | Functionalized graphene quantum dots, | Voltammetry, local electric signal enhancement by light– | Serum | LOD of 10 $PFU^4$/mL in | (Ahmed *et al.*, 2018) |

| | | | | | | |
|---|---|---|---|---|---|---|
| | polyclonal antibody | functionalized gold nanobundles, carbon electrodes, UV–visible light irradiation | matter interation (graphene mediated) | | buffer and 50 PFU/mL | |
| Protective antigen (Anthrax biomarker) | Short chain peptide | Functionalized gold electrodes | Square wave voltammetry | Antigen diluted in PBS + BSA[5] | LOD of $5.2 \times 10^{-6}$ μM. Detection in 60-100 minutes | (Huan *et al.*, 2009) |
| *Streptococcus suis* serotype 2 | Antibodies (sandwich immunoassay) | Antibodies immobilized on gold nanoparticles electrodeposited on a glassy carbon electrode, l-cysteine/ hollow PtPd nanochains /Glucose Oxidase/antibody bioconjugates (HRP-mimicking), d-glucose solution | Peroxydisulfate electrochemiluminescence | Antigen diluted in serum | LOD of $33 \times 10^{-6}$ ng/mL. Linear response range: 0.0001 - 100 ng/mL. Detection in 40 minutes | (Wang *et al.*, 2013) |
| Gram-negative bacteria | Anti-LPS antibodies (mouse monoclonal and goat polyclonal, Abcam) | Functionalized magnetic nanoparticles, interdigitated microelectrodes | Conductometry | 1% serum in PBS | Detection range: $10–10^3$ CFU[6]/mL | (El Ichi *et al.*, 2014) |
| *Salmonella spp.* | Anti-salmonella magnetic beads (Prod. Nº 710.02, Dynal Biotech). Anti-Salmonella-HRP (rabbit polyclonal, Prod. Nº ab20771, abcam) | Antibody-functionalized magnetic particle, polyclonal anti-Salmonella-HRP antibody, graphite-epoxy composite magneto-sensor | Amperometric detection | Skimmed milk | LOD of $7.5 \times 10^3$ CFU/mL. Detection in 50 minutes | (Liébana *et al.*, 2009) |

| | | | | | | |
|---|---|---|---|---|---|---|
| *Brucella melitensis* | Anti-brucella antibodies | Gold nanoparticle-modified screen-printed carbon electrodes | Cyclic voltammetry, electrochemical impedance spectroscopy | Milk | LOD of $4\times10^5$ CFU/mL. Linear response range: $4\times10^4$ - $4\times10^6$ CFU/mL. Detection in 90 minutes. | (Wu *et al.*, 2013) |
| *Brucella abortus* | Anti-lipopolysaccharide antibody (Abcam 3535) | Screen-printed gold-plated electrodes, copper doped nickel and zirconium oxide nanoparticles. | Cyclic voltammetry, electrochemical impedance spectroscopy | Phosphate buffer | Detection range: $10^3$ CFU/mL – $2\times10^6$ CFU/mL | (Khan *et al.*, 2018) |
| *Babesia bovis* circulating antibodies | Recombinant version of the C-terminal portion of RAP-1 (Portuguese *B. bovis* Santarém strain) | Functionalized gold electrodes | Electrochemical impedance spectroscopy | Serum | Detection range: 16.7 - 500 μM | (Silva *et al.*, 2008) |
| | | ***"Optical biosensors"*** | | | | |
| Influenza A H1N1 virus | FAM-labeled aptamers | Aptamer-modified magnetic beads for magnetic separation, fully integrated microfluidic chip, optical detection unit | Fluorescent measurements | PBS | LOD of 0.032 HAU units. Detection in 30 minutes | (Tseng *et al.*, 2016) |
| Swine-origin influenza A H1N1 virus | Anti-H1 antibody (ProSci, Poway, CA) | SPR chip (BK7 glass slide coated with a laminated Ag/Au 37/8 nm, metal layer), paired surface | Surface Plasmon Resonance (SPR) | Mimic solution (human mucosa in PBS) | Theoretical LOD of 30 PFU/mL, $1.8\times10^2$ PFU/mL . Detection in 20 minutes | (Su *et al.*, 2012) |

| | | | | | | |
|---|---|---|---|---|---|---|
| | | plasma waves biosensor | | | | |
| Avian influenza A H5N1 virus | Anti-H5N1 hemagglutinin antibody 2B7 (ab135382), anti-H5N1 neuraminidase polyclonal antibody (Cat. PA5-34949) | Anti-H5N1 hemagglutinin antibody functionalized chiral gold nanohybrids, anti-H5N1 neuraminidase functionalized Quantum Dots | Circular dichroism spectra | Serum | LOD of $10^{-3}$ ng/mL | (Ahmed, Nagy and Neethirajan, 2017) |
| Infectious Bronchitis Virus (IBV) | Anti-IBV antibodies | Alexa Fluor 488 labeled anti-IBV antibody, anti-IBV antibody conjugated with molybdenum disulfide(quencher) and immobilized on a cotton thread-based microfluidic platform | Fluorescence Resonance Energy Transfer (FRET) | Serum | LOD of 4.6 × 10 2 $EID_{50}^{7}$/mL. Linear response range: $10^{2}$ -$10^{6}$ $EID_{50}$/mL | (Weng and Neethirajan, 2018) |
| Muscovy duck parvovirus | ssDNA aptamer | Unmodified gold nanoparticles | Spectrophotometry or visual observation | Allantoic fluids | LOD of 1.5 $EID_{50}$ for spectrophotometry or 3 $EID_{50}$ for visual observation. Detection in 70 minutes | (Lu *et al.*, 2018) |
| PRRSV [9] | Anti-PRRSV monoclonal antibody (SDOW17) | Fluorescent (Alexa Fluor 546) labeled antibody/Protein A/Gold nanoparticles or Quantum dots | Fluorescence Resonance Energy Transfer (FRET) | PBS | Detection limit of 3 viral particles/µl | (Stringer *et al.*, 2008) |

| | | | | | | |
|---|---|---|---|---|---|---|
| | | (Catskill green) complexes | | | | |
| PRRSV | Anti-PRRSV antibody (lgG2b isotype) | CdTe:$Zn2^{+}$ quantum dots, antibody modified platinum nanotubes (quencher) | Fluorescence | Serum diluted in PBS | LOD of 2.4 ng/mL. Linear response range: 5.6 ng/mL - 66.6 ng/mL | (Chen *et al.*, 2015) |
| Bovine Viral Diarrhea (BVD) virus | Anti-BVD virus monoclonal antibodies (9021 Jeno Biotech or 244-FA National Veterinary Service Laboratories-USA | Functionalized highly carboxylated polystyrene microparticles, y-channel microfluidic chip with optical fibers | Static forward light scattering | Tissue culture media and fetal calf serum diluted in PBS | LOD of 10 $TCID_{50}{}^{8}$/mL | (Heinze *et al.*, 2009) |
| Foot and Mouth Disease (FMD) antibodies | FMD antigen (O, A and Asia-1 serotypes from commercial vaccine) | Anti-bovine IgG functionalized gold nanoparticles, nitrocellulose or nylon membrane | Dot-blot assay, visual observation | Serum | $10^{-4}$ dilution of serum samples | (Jain *et al.*, 2018) |
| Vesicular stomatitis virus (VSV) | Anti-VSV-G (monoclonal 8G5, monoclonal 1E9), anti-VSV-M (monoclonal 23H12), anti-VSV-N (monoclonal 10G4) | Interferometric Reflectance Imaging Sensor (IRIS), thermally grown SiO2 on Si, CCD camera | Spectral reflectance imaging | Cell lysate | $3.5 \times 10^{5}$ PFU/mL | (Lopez *et al.*, 2011) |
| *Brucella* DNA | Nucleotide probe | Ionic self-assembled multilayer, long-period grating optical fiber | Optical spectrum analysis of the refractive index | Culture and tissue lysates | LOD of 100 cells/ml. Detection in 30 minutes | (McCutcheon *et al.*, 2019) |

| | | | | | |
|---|---|---|---|---|---|
| *Salmonella typhimurium* | Goat anti-Salmonella antibodies (Kirkegaard & Perry Laboratories) | Labeled (donor Alexa Fluor 546) anti-Salmonella antibodies, labeled (acceptor Alexa Fluor 594) protein G, fiber optic biosensor | Fluorescence Resonance Energy Transfer (FRET) | Ground pork | LOD of $10^5$ CFU/g of ground pork. Detection in 5 minutes | (Ko and Grant, 2006) |

[1] LOD: Limit of detection, [2] PBS: phosphate buffered saline, [3] HAU: haemagglutination units, [4] PFU: plaque-forming units, [5] BSA: bovine serum albumin, [6] CFU: colony forming units, [7] $EID_{50}$: 50% egg infection dose, [8] $TCID_{50}$: median tissue culture infectious dose, [9] PRRSV: Porcine Reproductive and Respiratory Syndrome Virus

### 2.1.3. Piezoelectric Biosensors

Quartz crystal microbalance (QCM) sensors are piezoelectric disk-shaped crystals that oscillate when excited by electric current. This produces shear waves that propagate perpendicularly to the crystal surface. The oscillation's resonant frequency is proportional to the mass attached on the crystal surface. This phenomenon can be exploited to detect mass changes on the sensor's surface (Chen, Penn and Xi, 2018). A QCM immunosensor coupled with a flow injection system and an oscillator/frequency counter was developed for the detection of Influenza A and B viruses. Anti-influenza M1 antibodies were oriented and immobilized on the sensor's surface with protein A. The LOD was $10^4$ PFU/mL. The conjugation of the detection antibody with 13 nm gold nanoparticles reduced the LOD to $10^3$ PFU/mL. The assay could be completed within an hour (Peduru Hewa *et al.*, 2009). Under the same concept a nano-well structure (nano-porous gold film on a gold electrode) was used to modify a QCM sensor for the detection of H5N1 avian influenza virus. Aptamers were used as MREs. The detection range was from $2^{-4}$ to $2^4$ hemagglutination units (HAUs)/50 μL (Wang *et al.*, 2017). QCM sensors functionalized with aptamers have also been developed for the detection of *Brucella melitensis* in milk samples. The assay included the magnetic separation and pre-concentration of the bacteria from liquid solutions using aptamer-modified magnetic particles ($Fe_3O_4$). The magnetic particles could be recovered up to 8 times. The LOD was 100 CFU/mL and the assay showed linear responses in the range from $10^2$ to $10^7$ CFU/mL (Bayramoglu *et al.*, 2019).

### 2.1.4. Magnetic Biosensors

Apart from magnetic separation, magnetic nanoparticles can be used as signal transducers. For example, resonant coil magnetometers can quantify paramagnetic particles

(PMPs). This has been exploited for the development of a competitive immunoassay for the detection of anti-PRRSV antibodies in serum. A polystyrene surface was functionalized with recombinant His-tagged ORF 7 proteins through mouse anti-His antibodies. Anti-ORF 7 protein antibodies (SDOW17A) were used to functionalize PMPs. Serum samples containing anti-PRRSV antibodies antagonized the coupling between the functionalized PMPs and the sensor's surface resulting in dose-dependent signal reductions. The assay had sensitivity and specificity values of 73% and 100%, respectively, and could be completed within 5 minutes (Barnett *et al.*, 2020).

Following a different approach, anti-NP influenza antibodies (MAB8800; EMD Millipore Corporation) were used to functionalize giant magnetoresistance (GMR) sensors for the detection of both human and swine origin Influenza A. Biotinylated monoclonal detection antibodies (MAB8257B, EMD Millipore Corporation) were coupled with streptavidin-labeled magnetic nanoparticles through the biotin-streptavidin interaction. The presence of viral particles resulted in the formation of GMR sensor/virus/magnetic nanoparticles complexes, thus altering the magnetization of the GMR sensors. The LOD was $1.5 \times 10^2$ $TCID_{50}$/mL and the saturation point was $1.0 \times 10^5$ $TCID_{50}$/mL (Krishna *et al.*, 2016).

For the detection of *Salmonella typhimurium* on eggshells wireless magnetoelastic (ME) biosensors were modified with E2 phages. Signal were transduced using a ME resonator. The mass-sensitive biosensors can be wirelessly actuated into mechanical resonance with an externally applied time-varying magnetic field. The additional captured mass due to phage/bacteria interaction resulted in a proportional decrease of the resonant frequency. The assay required the incubation of the biosensors on the eggshells for 20 minutes in a humidity-controlled chamber (95% humidity). The LOD was $1.6 \times 10^2$ $CFU/cm^2$ of eggshell surface (Chai *et al.*, 2012).

### 2.1.5. Other Approaches in Signal Transduction

Cantilever sensors are based on the detection of mechanical stresses caused by the binding of molecules on the sensor's surface. These stresses lead to the bending of the sensors following Hooke's law. Sensor deflection is proportional to the applied force and the cantilever spring constant. Consequently, the spring constant determines the sensitivity and specificity of cantilever sensors. Cantilever sensitivity can be exploited only when reliable readout methods such as beam deflection or optical lever are involved. Captured

mass causes a reduction of the resonance frequency of oscillating cantilevers, enabling the detection of the targeted analyte (Fritz, 2008).

Acoustic wave biosensors offer simplicity and good real-time monitoring capabilities. Biorecognition events are monitored through changes either of the resonant frequency or the motional resistance. An acoustic immunosensor following these principles was developed for the detection of the herbicide atrazine (Kun Jia, Toury and Ionescu, 2012). Acoustic waves have also been used for the elimination of lipid particles from raw milk through acoustophoresis. This was performed in a microfluidic chip for the label-free somatic cell cytometry without the need of solvents, cell labelling and centrifugation. Cytometry was performed with a Coulter counter or direct light microscopy (Grenvall *et al.*, 2012).

The development of smartphones and their unique characteristics (user-friendliness, computational power, data sharing, wide adoption) have led to their adoption in biomedical applications. Smartphones can be used as parts of both optical (colorimetric, fluorescence, luminescence, surface plasmon resonance, spectroscopy, light scattering and microscopy), and electrochemical biosensors. Modules such as collimating lenses and optic fibers have been used on smartphones to address issues in optical detection caused by the uncontrolled or uneven light interference. Moreover, algorithms and computational methods can be exploited to reduce cost and overcome platform limitations (Zarei, 2017).

## 2.2. POS Tests and Devices for Animal Diseases

Successful POS tests and devices should be low-cost, sensitive and selective, user-friendly, portable capable to operate with small volumes of complex samples and enable multiplexing (Zarei, 2017). LFA testing has been popularized through the pregnancy and Covid-19 rapid tests. Additionally, standard laboratory assays such as PCR, ELISA and LAMP have been translated to POS devices with varying levels of success. Although promising, some of the proposed methodologies do not meet the necessary standards for POS testing. For example, some assays require complex sample pretreatment and off-chip handling (isolation of nucleic acids, labeling etc.) or specialized reading equipment which is unavailable at the POS setting.

### 2.2.1. LFAs

As it was previously mentioned, gold nanoparticles are widely used in LFA applications due to ease of modification and simple visual test interpretation. Commercially

available LFA tests offering three test lines spotted with anti-rhodamine, anti-fluorescein antibodies and biotin-binding proteins, respectively, were used for the detection of Foot and Mouth Disease virus (FMDV) serotypes O, A and Asia 1. Serotype-specific antibodies were conjugated with either rhodamine/fluorescein or streptavidin for the immobilization of each serotype to its respective test line. For the visualization of positive tests, secondary, non-specific serotype, anti-FMDV antibodies were conjugated with colloidal gold. The assay could be completed within 15 minutes and the positive detection rates in lesion swabs of experimentally infected sheep were 38% for serotype O and 50% for serotype A (Yang *et al.*, 2015). In another study, a pan-serotype anti-FMDV monoclonal antibody and a universal capture ligand (recombinant bovine integrin αvβ6 - RBIαvβ6) were used for the detection of FMDV. Colloidal gold was used to label the mouse anti-FMDV, pan-serotype antibody and biotin to label the RBIαvβ6. Positive samples resulted in RBIαvβ6/FMDV/Antibody sandwich immunocomplexes. The immunocomplexes were captured at the test line by an anti-biotin antibody, whereas excessive gold-labeled antibodies were captured at the control line by an anti-mouse IgG antibody. The assay could be completed within 30 minutes, showed 100% specificity, sensitivity similar to commercial ELISAs and LOD between 3.7 and 5.4 $\log_{10}$ $TCID_{50}$/0.1 mL (depending on the serotype) (M. Yang *et al.*, 2022).

Some LFA tests have been also used for the serological diagnosis of *Mycobacterium avium* subspecies *paratuberculosis* in bovine sera. Protein A and the recombinant protein MAP2963 (44 kDa) were immobilized on the control and test lines, respectively. Gold-functionalized guinea pig anti-bovine IgG antibodies were used to capture bovine antibodies in serum. The test's selectivity against *M. avium* subsp. *paratuberculosis* was ensured by spotting of the recombinant protein MAP2963 on the test line. Excessive gold-functionalized guinea pig antibodies were captured at the control line via Protein A-guinea pig antibody interactions. The assay could be completed within 10 minutes and showed sensitivity of 84.2%, specificity of 83.3%, positive predictive value (PPV) of 88.89%, and LOD of 1.98 μg/mL when tested with 31 non-hemolyzed serum samples (Agrawal *et al.*, 2020).

Apart from antibodies, other bioreceptors such as aptamers have been labeled with gold nanoparticles for analyte detection in LFA tests. For example, aptamers J3APT and JH4APT can recognize H5N2 avian influenza virus and form sandwich complexes. JH4APT aptamer was labeled with gold nanoparticles and J3APT aptamer was used to spot the test line. In the presence of the viral particles, gold-labeled sandwich complexes were formed on the test line facilitating detection. The LOD was $6 \times 10^5$ $EID_{50}$/mL in buffer and $1.2 \times 10^6$

$EID_{50}$/mL in duck fecal samples. Image analysis (ImageJ software) reduced LOD values to $1.27 \times 10^5$ $EID_{50}$/mL and $2.09 \times 10_5$ $EID_{50}$/mL in buffer and fecal samples, respectively (Kim *et al.*, 2019).

Gold nanoparticles have also been used with QDs in LFA testing. In a study, a typical LFA test relying on gold-labeled antibodies for the detection of avian influenza A was treated with HCl–$Br_2$ on the test line to release the gold ions captured on the test line. The gold ions were collected in a 96-well plate and CdTe QDs were subsequently added. In the presence of gold ions (i.e., in positive tests), QD fluorescence was reduced due to the quenching capabilities of the aforementioned ions. Fluorescence was recorded with a plate microreader. The assay had LOD of 0.09 ng/mL and showed sensitivity of 100%, specificity of 88.2% and detection efficiency of 90% when tested with clinical samples (Li *et al.*, 2012).

In another approach, QD-functionalized monoclonal antibodies were used in an LFA assay for the detection of Influenza A virus subtype H5 or H9. The QD/antibody/influenza complexes were captured at two distinct tests lines (one for H5 and the other for H9) forming sandwich immunocomplexes. A low-cost test strip scanner was used to record fluorescence upon 365 nm UV excitation, allowing quantification. This approach was tested with both serum and cloacal swab samples. The assay could be completed within 15 minutes and achieved LOD values of 0.016 HAU for subtype H5 and 0.25 HAU for subtype H9 (Wu *et al.*, 2016).

Latex particle agglomeration can be exploited for the visualization of results in LFAs. For example, a commercial, rapid immunochromatographic method was developed for the detection of Bluetongue virus-specific antibodies in animal sera. The VP7 protein was immobilized on the test line and VP7-functionalized red latex microspheres were used for the detection of anti VP7 specific antibodies, forming sandwich immunocomplexes. Biotin-conjugated blue latex particles were used for the formation of the control line. The assay had specificity of 95.2% (95% C.I. [76.2–99.9]) and sensitivity of 100% (95% C.I. [90.5–100]). Repeatability (accordance) and reproducibility (concordance) for seropositive samples were 100%, whereas for seronegative samples were 45% and 89%, respectively. Cohen's kappa values was 0.79 (95% CI [0.62–0.95]) in comparison with a commercial ELISA assay (Hanon *et al.*, 2016).

The development and subsequent popularization of smartphones has led to their exploitation in LFA testing. A competitive LFA format was combined with a smartphone-based optical detection method for the detection of porcine pseudorabies virus (PRV) anti-

gE protein antibodies. The LFA's test and control lines were spotted with anti-gE antibodies and chicken IgY antibodies, respectively. Latex beads were coated with either PRV or goat anti-chicken IgY antibodies which were immobilized on the test and control lines, respectively. In the presence of anti-gE antibodies, the capturing of the PRV-coated latex beads on the test line was inhibited, resulting in reductions in the optical transmittance. Measurements were performed with the smartphone's ambient light sensor and a LED light incorporated in a 3D printed reader and the captured images were analyzed with ImajeJ software. The assay can be used to differentiate vaccinated from naturally infected animals as the commercial anti-PRV vaccines are gE-deleted. Sensitivity and specificity were 100% and 97.2%, respectively. The assay could be completed within 15 minutes and had 98% agreement with a commercial ELISA kit (Huang *et al.*, 2021).

Lateral Flow Assays have also been utilized for the detection of nucleic acid amplicons. A LAMP assay was coupled with an amplicon detecting LFA for the detection of ASFV DNA in blood and tissue samples. The LAMP amplicons were labeled with both biotin and fluorescein and bound with latex beads to facilitate LFA detection. The assay did not require specialized equipment and showed LOD values of 330 genome copies (James *et al.*, 2010). In a similar study, Fast Technology Analysis (FTA) cards and glass fiber were used for nucleic acid extraction and LAMP-based amplification of *E. coli* DNA. A portable, battery-powered heater was used for the isothermal amplification to allow the use of the assay in the POS setting. An oligonucleotide detector probe coupled with gold nanoparticles was used for amplicon detection and the results were quantified with a smartphone. The LOD was 10-1000 CFU/mL in complex sample matrices and the assay could be completed within 1 hour (Choi *et al.*, 2016).

In another study, a recombinase polymerase amplification (RPA) and an LFA test utilizing streptavidin-coated gold nanoparticles were used for the detection of *Salmonella enteritidis*. DNA extraction included boiling and centrifugation and was followed by the RPA. Amplicons were coupled with both biotin and digoxin, enabling the coupling with the streptavidin-modified gold nanoparticles. The formed complexes were captured on the test line via digoxin-recognizing antibodies. Anti-streptavidin antibodies on the control line were used to capture excessive gold nanoparticles. Results were analyzed with a smartphone and a laptop was used for further analysis and quantification. The assay was completed within 40 minutes and the LOD was 91.4 CFU/mL (Fu *et al.*, 2021).

Following a vertical setup, a stacked flow LFA was developed for the detection of *E. coli*. Sample application resulted in its vertical (upwards) migration to a conjugate pad containing HRP-labeled anti-*E. coli* antibodies forming immunocomplexes in the presence of *E. coli* cells. The immunocomplexes and excessive HRP-labeled antibodies flowed further into a blocking pad containing immobilized *E. coli* cells for the immobilization of excessive HRP-conjugated antibodies. The immunocomplexes were able to reach the upper substrate pad which contained $H_2O_2$ and luminol, thus leading to enzymatic light production. The assay was completed within 5 minutes and showed LOD values of 100 CFU/mL in water samples (Eltzov and Marks, 2016). The substitution of luminol with TMB did not affect LOD values (Eltzov and Marks, 2017). Table 2 summarizes the available LFA tests for the detection of animal pathogens.

**Table 2.** "Available LFA tests for the detection of animal pathogens (Manessis, Gelasakis and Bossis, 2022)."

| Targeted analyte | Materials and methods | Equipment | Samples and handling | Performance | Reference |
|---|---|---|---|---|---|
| Pseudorabies virus (PRV) | Fluorescent immunochromatographic strip, anti-PRV gB monoclonal antibodies, 3D-printed customized pocket fluorescence observation instrument | None | Homogenized pig tissues | LOD of 0.13 ng/mL. Detection within 13 minutes | (Shen *et al.*, 2018) |
| Porcine Epidemic Diarrhea virus (PEDV) | LFA test, antibody-functionalized gold nanoparticles, 3D-printed transmittance reader, image analysis | Smartphone | PEDV solution | LOD of 55 ng/mL. Linear detection range: 78–20 × $10^3$ ng/mL | (Xiao *et al.*, 2018) |
| Bovine Ephemeral Fever virus (BEFV) | RPA [1], FAM [2] and biotin labeled amplicons, LFA | TwistAmp NFO kit for RPA amplification, heat block | RNA isolation from clinical samples and reverse transcription | LOD of 8 genomic copies per reaction. Coincidence rate with real-time PCR of 96.09%. | (Hou *et al.*, 2018) |

| | | | | | |
|---|---|---|---|---|---|
| | | | | Detection in 25 minutes | |
| BVDV | Immunochromato-graphic test strip, anti-NS3 monoclonal antibody 46/1-conjugated gold nanoparticles | None | Leukocyte extracts | Sensitivity and specificity of 100% and 97.2%, respectively. Detection in 15 minutes | (Kameyama *et al.*, 2006) |
| FMDV | LFA test, gold nanoparticles, monoclonal anti-FMDV antibody 1F10 or 2H6 | None | Homogenized epithelial suspensions | Sensitivity of 84% for 1F10 and 88% for 2H6. Specificity of 99% for both antibodies | (Ferris *et al.*, 2009, 2010) |
| FMDV viral RNA | RT-LAMP, FIP [3] and BIP [4] labeling at the 5′ terminus with fluorescein and biotin, LFA test | Water bath | RNA, epithelial suspensions spiked with FMD virus, epithelial samples, air samples, RNA isolation | LOD of 10 viral genome copies | (Waters *et al.*, 2014) |
| FMDV viral RNA | RT-RPA, FAM and biotin labelled amplicons, LFA | TwistAmp NFO kit for RPA amplification, water bath | cDNA, reverse transcription, RNA isolation | LOD of 10 copies (plasmid DNA), 98.6% concordance with real-time PCR | (Wang *et al.*, 2018) |
| ASFV DNA | RPA, FITC [5] and biotin labeled amplicons, LFA | TwistAmp NFO kit for RPA amplification, thermocycler | DNA isolated with a magnetic | Positive agreement of 100% with PCR. | (Miao *et al.*, 2019) |

| | | | | | |
|---|---|---|---|---|---|
| | | | bead-based kit | Detection in 15 minutes | |
| Classical Swine Fever (CSFV) | Fluorescent microsphere (FM)-based LFA, monoclonal antibody-functionalized FMs | Fluorescent immunochromatographic strip reader, fluorescent camera | Tissue extracts | LOD of 5.28 ng/mL, positive coincidence rate, negative coincidence rate, and total coincidence rate of 95.8%, 100%, and 98%, respectively. Detection within 15minutes | (Xie *et al.*, 2021) |
| CSFV RNA | RT-LAMP, DIG [6] and FITC labelled amplicons, LFA | Thermocycler | Cell culture supernatants, serum, RNA isolation | LOD of 100 copies per reaction. Detection in 70 minutes | (Chowdry *et al.*, 2014) |
| PCV-2 antibodies | Immunochromatographic test strip, recombinant Cap protein-labelled colloidal gold | None | Serum samples | Agreement of 94% with commercial ELISA. Sensitivity and specificity of 93.14% and 98.70%, respectively. Detection in 5 minutes | (Jin *et al.*, 2012) |
| PRRSV antibodies | Immunochromatographic test strip, PRRSV recombinant membrane and nucleocapsid | None | Serum samples | Sensitivity of 98.6%, specificity of 97.8%, | (Cui *et al.*, 2008) |

| | | | | | |
|---|---|---|---|---|---|
| | proteins, Protein G-conjugated gold nanoparticles | | | accuracy of 98.3% | |
| *Salmonella hilA* gene | LAMP, FITC and biotin labeled amplicons, LFA test | Heating block | DNA isolated with commercial kit | LOD values of $13.5 \times 10^{-3}$ ng/mL of genomic DNA and 6.7 CFU/mL. Detection in 40 minutes. | (Mei *et al.*, 2019) |
| *Salmonella* Typhimurium DNA | RPA, DIG and FAM labeled amplicons, LFA | TwistAmp RPA reaction kit. Thermostatic water bath | DNA isolated with commercial kit | LOD of $10^{-6}$ ng (genomic DNA) and 1.95 CFU/mL in milk samples. Detection in less than 20 minutes | (Hu *et al.*, 2019) |
| *Brucella* spp | Multiple cross displacement amplification, FITC and biotin-labeling of amplicons, LFA utilizing dye streptavidin coated polymer nanoparticles | Water bath or heat block | Human and goat serum samples, DNA extraction | LOD of $10^{-5}$ ng of templates (pure cultures). Detection in 70 minutes | (Li *et al.*, 2019) |
| *Campylobacter jejuni* and *Campylobacter coli* | LFA test, gold nanoparticles, monoclonal mouse anti–Campylobacter A and/or B | None | Chicken feces, dilution with saline, filtration, sedimentation for 10 minutes | LOD of 6.7 log CFU/g for *Campylobacter jejuni* or 7.1 log CFU/g for *Campylobacter coli* of Detection in 20 minutes. | (Wadl *et al.*, 2009) |

| | | | | | |
|---|---|---|---|---|---|
| *Mycobacterium avium subsp. paratuberculosis* | RPA, labelled amplicons, LFA | TwistAmp RPA reaction kit, thermostatic water tank | DNA extracted with commercial kit | LOD of 8 copies per reaction. Sensitivity and specificity of 100% and 97.63%, respectively. Detection in 35 minutes | (Zhao *et al.*, 2018) |
| *Mycoplasma ovipneumoniae* DNA | LAMP, DIG and biotin labeled amplicons, LFA | Water bath | Lung tissue sample, DNA extraction | LOD of 100 CFU/mL. Sensitivity of 86% in clinical samples, Detection in 70 minutes | (Zhang *et al.*, 2019) |

[1] RPA: Recombinase Polymerase Amplification, [2] FAM: Fluorescein Amidite, [3] FIP: Forward Inner Primer, [4] BIP: Backward Inner Primer, [5] FITC: Fluorescein Isothiocyanate, [6] DIG: Digoxigenin

### 2.2.2. LOC devices

Ideally, LOC devices should be able to perform the whole analytical procedure into a single device and provide results that allow evidence-based decision making. In general, LOC devices are capable of detecting various analytes including cells, nucleic acids and proteins. In animal production, cell-based LOC devices are mainly used for the assessment of somatic and bacterial cell counts in milk. Such an example is the development of a portable microfluidic sedimentation cytometer for the assessment of somatic cell counts and milk fat content. The device consisted of a rotating plastic compact disc with twelve flattened funnel structures. Due to rotation, somatic cells were driven into a microfluidic channel whereas fat globules were accumulated in the center of the disc forming a fat zone. The cell pellet and the fat band were assessed with two low-cost microscopes. The device required 150 μL of milk and could accurately estimate cell counts in the range of 50,000–3,000,000 cells/mL (Garcia-Cordero *et al.*, 2010).

In another study, a microfluidic cell counter based on fluorescent detection was developed. Sample treatment, including the application of the fluorescent cell dye, was integrated in a chip. A miniaturized hand-held fluorescence detection device was used for

the quantification of somatic cells. A custom software and a detection algorithm were used for image analysis. The accuracy of the assay was 98.2% within the range of 100,000 to 300,000 cells/mL (Kim *et al.*, 2017). Using a similar approach, a fluorescence-based cell counter using disposable plastic microchips and ethidium bromide to stain somatic cells was developed. A CCD camera and a microscope were used to record fluorescence and images were analyzed with a computer software. The correlation coefficient $R^2$ in comparison with other commercial cell counters ranged from 0.935 to 0.964 (Moon *et al.*, 2007).

Lab On Chip devices have also been developed for the detection of milk bacteria. Superparamagnetic nanoparticles functionalized with antibodies and a microfluidic magnetoresistive cytometer were integrated in a LOC device for the detection of *Streptococcus agalactiae* (Group B streptococci) and *Streptococcus uberis* in raw milk samples. The LOD was 100 CFU/mL. The method showed sensitivity of 73% and 41%, specificity of 25% and 57% and Positive Predictive Values (PPV) of 35% and 54% with the anti-S. agalactiae and anti-GB antibodies, respectively (Fernandes *et al.*, 2014; Duarte *et al.*, 2016).

LOC devices targeting nucleic acids have received increased research interest due to their high sensitivity and the development of isothermal amplification techniques. For example, a portable real-time RT-PCR (RAPID® 7200) assay using dried reagents was developed and validated with field and spiked samples for the surveillance of avian influenza in wild birds. The assay required data analysis using a laptop, sample pretreatment for nucleic acid isolation and could be performed by trained personnel. Sensitivity and specificity were 98% and 100%, respectively, in field conditions (Takekawa *et al.*, 2010).

In an elaborate study, a polycarbonate disc was used for the implementation of a reverse transcription LAMP for influenza A detection. Centrifugal fluidic handling and segregation of analytical steps was performed with microfluidic channels and chambers incorporated in the disc. A heat plate was used for the isothermal amplification and a miniaturized fluorescence detector was used for signal detection. A calcein/magnesium ions system was used to generate fluorescence. Viral lysates were analyzed within 47 minutes and the recorded LOD was 10 copies of viral RNA (J. H. Jung *et al.*, 2015). In another study, optic fibers and sensors were integrated in a microfluidic chip for the LAMP-based detection of pseudorabies virus (PRV). However, DNA extraction was performed in the laboratory using a commercial kit. The microfluidic chip was incubated in a water bath at 63°C for 1

hour. Detection was performed either by absorbance or visual observation of turbidity. The LOD was 10 fg and required 0.4 µL of sample (Fang *et al.*, 2010).

Recombinase polymerase amplification (RPA) requires low amplification temperatures (theoretically even at room temperature) allowing easier handling at the POS setting. A portable laboratory named "Diagnostics-in-a-Suitcase" was developed for the RT-RPA-based detection of avian influenza H7N9. The RNA extraction was performed with magnetic beads within 30 minutes, whereas RT-RPA was performed using TwistAmp™ RT exo kit within 15 minutes. A fluorescence tube scanner (Twista) was used for amplicon detection. The LOD was 10 and 100 RNA copies for H7 and N9, respectively. The device could be operated by a solar battery and the reagent shelf-life in ambient temperature was 3 months (Abd El Wahed, Weidmann and Hufert, 2015). Using the same amplification technique, DNA extraction, RPA and detection of amplicons were integrated in a disc-based centrifugal microfluidic device for the detection of Salmonella. Wireless control of valve actuation, cell lysis and noncontact heating were facilitated by a single laser. Antibody-functionalized magnetic beads and magnetic separation were used for sample enrichment. Amplicons were detected in the final step with a simple LFA assay. The LOD was 10 CFU/mL in PBS and 100 CFU/mL in milk (Kim *et al.*, 2014).

A circular fluorescent probe-mediated, isothermal nucleic acid amplification (CFPA) assay was integrated in a portable system for the detection of ASFV. The assay relies on the Bst DNA polymerase and the structure-specific endonuclease 1 (FEN1) enzymes for amplification and fluorescence mediated by cleavage for detection. Microbeads, a metal bath and a microcentrifuge were used for DNA extraction, whereas an in-house fabricated hand-held fluorescence detection device was used for amplicon quantification. The system was encased in a lithium-powered suitcase and a cloud-based platform was used for uploading results and facilitating real-time monitoring of pigs. The LOD was 10 copies/µL, sensitivity was 92.73%, specificity was 100% and the assay could be completed within 10-30 minutes (Ye *et al.*, 2019).

A cutting-edge molecular tool, CRISPR-Cas12a, was performed in microfluidic cartridges and was used for the detection of ASFV DNA. The CRISPR-Cas12a programming was performed with a CRISPR RNA (crRNA). In the presence of ASFV DNA, a Cas12a/crRNA/ASFV DNA complex was formed which was capable to cleave a fluorescent single stranded DNA (ssDNA) reporter. A portable custom designed fluorometer was used to record fluorescence. The LOD was 1 pM in 2 hours. The complex was stable

and could remain active for 24 hours allowing the detection of up to 100 fM ASFV DNA. The detection was performed using DNA templates in binding buffer (He *et al.*, 2020).

Lab On Chip devices relevant to animal production target mainly disease markers such as enzymes and antigens. Protein-based LOC devices do not include an amplification step, simplifying sample pretreatment. Such an example is the development of a simple volumetric chip for the detection and quantification of bovine catalase. The $H_2O_2$ and catalase-spiked milk samples were mixed and then loaded in the chip. A preloaded ink bar advanced due to the produced $O_2$ allowing the quantification of catalase via smartphone imaging. The LOD was 20mg/mL and the assay was completed within 20 minutes. Microfluidic chips cost $0.2 each and could be fabricated within 3 minutes (Cui *et al.*, 2016). Another LOC device fabricated on PDMS was used to monitor milk pH and to detect *E. coli*, *Streptococcus agalactiae*, penicillin G, dihydrostreptomycin and neutrophils. FITC-labeled antibodies were used to detect analytes via fluorescence microscopy and SNARF-dextran was used as a pH indicator. The assay could be completed within 2 hours (Choi *et al.*, 2006).

To eliminate sample contamination and minimize complex sample handling such as labeling, protein-based LOC devices have utilized advanced sensors relying on refractive index measurements. Multiple high-precision planar Bragg gratings were integrated in a microfluidic optical chip for the detection of Foot and Mouth Disease virus (FMDV). The sensors were functionalized with BF8 monoclonal antibodies against FMDV type O1 Manisa. The assay was integrated in a single portable device. Simple yes or no answers and semi-quantitative information could be provided within minutes (Bhatta *et al.*, 2012).

Surface Plasmon Resonance (SPR) assay's sensitivity and rapidity has been exploited in POS devices. More specifically, a bioanalyzer based on SPR was developed for the detection of bursal disease virus. The system consisted of a micro-flow cell, a temperature regulator, an integrated biosensor (TSPR1k23), an optical platform, an electronic control unit incorporated into a photoelectric conversion device and a universal serial bus (USB) interface circuit board. Monoclonal antibodies were used to capture the antigen. The LOD was 2.5 nm/mL of purified viral samples diluted in PBS. The assay was completed within 20 minutes (Hu *et al.*, 2012). Under the same concept, the analyzer was used for the detection of CP PCV-2 antigen in buffer solutions with a theoretical LOD of 0.04 μg/mL (Jiandong Hu *et al.*, 2014).

## 2.3. Legislative Regulations of POS Tests for Animal Diseases

Exhaustive reviews have been published on novel biosensors and POS devices however the relevant regulations and legislation rarely receive the necessary attention. A review on current regulations related to POS devices has been published on the official OIE webpage (Potockova, Dohnal and Thome-Kromer, 2020). Regulatory surveillance of POS devices entering the market may vary between regions. For example, regulations for POS devices do not exist at the European Union level, but rather on individual member level.

In contrast, Japan implements strict regulations for POS devices for animal diseases, similar to that of human in vitro diagnostics (Potockova, Dohnal and Thome-Kromer, 2020). In Japan, the Ministry of Agriculture, Forestry and Fisheries supervises POS tests under the Pharmaceutical and Medical Devices Act. Prior to marketing of POS devices, the manufacturer must be registered in the local prefecture or for foreign manufacturers to the ministry, a marketing authorization holder must be appointed, and each marketed device should be approved. Compliance is verified every five years by on-site visits of competent authorities (Potockova, Dohnal and Thome-Kromer, 2020).

In the European Union, veterinary POS devices should comply with general directives for products marketed within the union. These are “Directive 85/374/EEC on product liability” and “Directive 2001/95/EC on product safety”. Especially for devices powered by electricity (e.g. benchtop analyzers), compliance with “Directives 2014/30/EU and 2014/35/EU on electromagnetic compatibility and low voltage instruments”, respectively, should be guaranteed (Potockova, Dohnal and Thome-Kromer, 2020). However, the European market lacks legislation for the safety, quality and performance of veterinary POS diagnostics.

In the USA, the “Federal Food, Drug and Cosmetic Act, paragraph 321h” defines veterinary POS diagnostics. Marketing of veterinary POS diagnostics does not require specific clearance but requires the device and protocol validation. In fact, a POS test can reach the US market after the cross-laboratory validation of its sensitivity, specificity and reproducibility. Additionally, the FDA oversees such products and can withdraw from the market misbranded or adulterated products, whereas end-users are encouraged to report adverse events associated with these devices. The “Center of Veterinary Biologics” of the “United States Department of Agriculture” holds jurisdiction over POS devices and tests as defined in the “Virus-Serum-Toxin Act, Title 9, Code of Federal Regulation, Parts 101-104” (Morgan, 1998; Potockova, Dohnal and Thome-Kromer, 2020). As a result, POS tests used by official authorities for disease control and eradication must undergo secondary evaluation with large, well-defined animal populations. A registry of adverse events related to POS tests is mandatory kept by license holders since 2018.

# Chapter 3. Materials and Methods

## 3.1. Samples

Reference samples were collected from various sources. The PPV1 vaccine strain NADL-2 was used as reference sample and was provided by Professor I. Bossis (University of Maryland, College Park, MD, USA). The PCV-2 reference samples (R15 strain) were provided by the University of Veterinary Medicine Budapest (UVMB, Budapest, Hungary). For PRRSV type 1, the Lelystad strain was used as a reference sample and was provided by Professor I. Bossis (University of Maryland, College Park, MD, USA). Moreover, swine influenza H1N1 and H3N2 field isolates (laboratory confirmation and isolation was conducted at the "Department of Pathology, University of Veterinary Medicine, Budapest") were used in the study as reference samples. Reference, heat inactivated ASF samples were received from the National Veterinary Research Institute of Poland (PIWET). The same organization (PIWET) provided heat inactivated CSF reference samples (strain Alfort 187) ass well. More details on reference samples are provided in the Appendix.

Six swine farms located in Central and Southern Greece were used to retrieve samples for the device validation. Farms were classified into three categories, small farms (less than 250 sows), medium size farms (251 to 1000 sows) and large farms (more than 1000 sows). The first small farm did not implement any vaccination schemes against the six targeted diseases and the hygiene status was poor, mainly in terms of dirty housing and equipment. All PPV1 positive samples and some PCV-2 samples originated from that farm. The second small farm implemented vaccinations against PPV1, PCV-2 and PRRSV (in piglets, that were then used for reproduction under a "closed farm" system) and the hygiene status was high (clean housing, equipment and animals). All samples collected from this farm were negative for the targeted diseases in this study. The first medium size farm implemented vaccination against PPV1 and PRRSV (PPV1 in gilts and PRRSV in piglets), but not against PCV-2. The hygiene status was high. The rest of the PCV-2 positive samples originated from this farm, The second medium size farm vaccinated against PPV1, PCV-1, PRRSV and SIV (gilts and for SIV sows as well) and the hygiene status was high. All samples from this farm were negative for the targeted diseases. The first large farm vaccinated against PPV1 (gilts), PCV-2 (gilts) and PRRSV (piglets) and the hygiene status was high. Only a couple of samples (one serum sample and one sample of oral fluids) tested positive for PRRSV. The second large farm vaccinated gilts against PPV1 and PCV-2 but did not implement any vaccination against PRRSV. The hygiene status was medium, mainly

in terms of not allowing sufficient time between cleaning and animal introduction in the pens for proper drying. Most PRRSV positive samples originated from this farm.

Three sample types were collected form the farms, oral fluids and fecal samples (non-intrusive) and sera. Oral fluids were collected by placing a cotton rope for 10 to 20 minutes (depending on the interest shown by the pigs) in each pen (pooled samples) for the pigs to chew and play with (Figure 8). Oral fluids were extracted from the rope through squeezing in a sterilized plastic bag. Fresh fecal samples were collected from the pen floor from different locations in a sterilized 50 ml conical tube (Figure 9). Serum samples were collected only by trained veterinarians and as part of standard disease monitoring practices (Figure 10). After sample collection an aliquot was received for testing the new device.

**Figure 8. "**Oral fluid sample collection from a swine farm in Greece using cotton ropes. Sampling is non-intrusive and does not compromise animal welfare."

**Figure 9. "**Collection of fecal samples for testing with the novel device. Fecal samples are non-intrusive and stress-free, as shown in the photo."

**Figure 10. "**Serum sample collection in a Greek farm, performed by a trained veterinarian as part of the yearly swine health monitoring activities. Serum sample collection is laborious, time consuming and requires animal restraint."

For PPV1 and PCV-2, oral fluid and fecal samples were retrieved at pen level from the previously mentioned swine farms. Samples were transported to the laboratory at 4 – 6 °C and processed within 24 h. After a freeze–thaw cycle, oral fluids were centrifuged at 12,000×g for 10 min, and supernatants were stored at -80 °C. Feces were incubated for 30 min in 20% w/v sucrose in PBS solution at 1:3 ratio. Afterwards, they were centrifuged at 3000×g for 20 min, and supernatants were collected and stored at -80 °C. The PPV1 functionalized PIC sensors were tested with 36 negative samples and 32 positive oral fluid samples (16 spiked and 16 clinical samples) for the assessment of the novel POS system. Six serial 3-fold dilutions of the reference PPV1 sample in oral fluids were used for the

estimation of the LOD of the sensors. The PCV-2 functionalized sensors were tested with 32 negative and 36 positive oral fluid samples (16 spiked and 20 clinical samples) for their evaluation. Six serial 3-fold dilutions of the PCV-2 reference sample were used for the estimation of the LOD.

For the evaluation of PRRSV and SIV functionalized sensors, oral fluid samples were retrieved from four countries: Greece, Italy, Hungary, and Poland. Samples were treated and stored as previously described. PRRSV functionalized sensors were tested with 37 negative and 38 PRRS positive oral fluid samples (17 spiked and 21 clinical positive samples originating from all four countries) for the assessment of the performance of the device. Six serial 3-fold dilutions of the reference PRRSV type 1 sample in oral fluids were used for the estimation of the limit of detection (LOD) of the sensors. SIV functionalized sensors were tested with 17 negative and 17 SIV positive oral fluid samples (15 spiked and 2 clinical positive samples from Hungary). For the estimation of the limit of detection (LOD), six serial 3-fold dilutions of the reference SIV sample in the oral fluids were used.

For ASF and CSF, oral fluid samples were retrieved from Poland and Hungary. Additionally, serum samples were collected as part of standard health monitoring practices that are implemented to commercial swine farms. All samples were transported to the laboratory at 4 – 6 °C and processed within 24 hours. Oral fluids were treated and stored as previously described. Serum samples were centrifuged at 3000×g for 10 minutes and supernatants were also stored at -80 °C. ASF functionalized sensors were tested with 9 negative (clinical) and 18 positive (11 spiked and 7 clinical) oral fluid samples. These studies were performed at PIWET in Poland during regular visits and a second SWINOSTICS device build later in the project after initial validation of the original prototype at AUA. Additionally, ASF functionalized sensors were tested with 36 positive serum samples (22 spiked and 14 clinical). To estimate the limit of detection (LOD) of the ASF functionalized sensors, six serial 3-fold dilutions of the reference ASF sample in serum and oral fluids were used. CSF functionalized sensors were tested with 47 negative and 33 positive (31 spiked and 2 clinical) oral fluid samples. Six serial 3-fold dilutions of the CSF reference sample in oral fluids were used for the estimation of the LOD of CSF functionalized sensors.

All samples were serially filtered with 5 and 0.45 μm pore size filters prior to testing with the prototype. The status (negative, positive) of all samples was confirmed in the laboratory using conventional and real-time PCR for DNA viruses and reverse transcription conventional and real-time PCR for RNA viruses.


**Figure 11.** "Sample filtering using 5.0 µm filter and syringe prior to testing with the novel diagnostic device."

## 3.2 Conventional PCR Assays

Viral PPV1, PCV-2 and ASF DNA were isolated using the "PureLink™ Viral RNA/DNA Mini Kit (Invitrogen, Carlsbad, CA, USA)". The DNA isolation protocol was performed according to the manufacturer's instructions using a standard volume of 200 µL per sample. Nucleic acids from each sample were eluted in 20 µL of elution buffer and stored at -20 °C. Viral PRRSV, SIV and CSF RNA were isolated using the same kit and sample/buffer volumes. Nucleic acids from each sample were eluted in 20 µL of elution buffer and stored at -80 °C. Reverse transcription of total RNA to cDNA was performed with random primers using the "High-Capacity cDNA Reverse Transcription Kit with RNase Inhibitor (Applied Biosystems™, Vilnius, Lithuania)" and standard reaction volumes of 20 µL (10 µL sample and 10 µL kit reagents), according to the manufacturer's instructions. The cDNA was stored at -20 °C.

The PPV1 DNA was detected with conventional PCR using 3 different primer sets located within the NS and NS1 gene regions (Table 3). The PCV-2 DNA was detected with 3 different primer sets located within the capsid protein gene, rep gene, and open reading frame 1 (ORF1) regions. The PRRSV cDNA was detected with conventional PCR using three primer sets targeting the ORF1b and ORF7 (Table 1). The SIV cDNA was detected with two primer sets (SIV_Set_1–2, Table 1) targeting the M and NP genes, respectively. Swine influenza was typed using seven additional primer sets. The ASF DNA was detected with conventional PCR using a primer set (ASF_Set_1) targeting the VP72 gene. The CSF RNA was detected with nested conventional PCR using four primer sets targeting the E2 gene and 5' NTR. The primer sets and products of PPV1, PCV-2, PRRSV, SIV, CSF and ASF amplification are presented in Table 3.

All conventional PCR assays were performed in a total volume of 25 µL consisting of 22.5 µL PCR 1.1 × SuperMix (Invitrogen, Carlsbad, CA, USA), 0.5 µL of 10 µM forward

primer solution, 0.5 µL of 10 µM reverse primer solution, and 1.5 µL of template DNA or cDNA. Cycling conditions were as follows: pre-denaturation at 95 °C for 2 minutes, followed by 32 cycles of denaturation at 94 °C for 20 seconds, annealing for 30 seconds, extension at 72 °C and final extension at 72 °C for 1 minute. Optimized annealing temperatures and extension times for each primer set are presented in Table 3. PCR products were analyzed in 2% agarose gel and stained with ethidium bromide. A 100 bp ladder (Thermoscientific, Vilnius, Lithuania) was used to assess amplicon length.

**Table 3.** "Primer sets used in conventional PCR for the detection of PPV1, PCV-2, PRRSV, SIV, ASF, CSF and optimized annealing temperatures and extension times (Manessis et al., 2021, 2022)."

| Primer set | Target region | Primer sequence (5'-3') | Amplicon length (bp) | Reference | "Annealing for 30 s at" | "Extension at 72 °C" |
|---|---|---|---|---|---|---|
| "PPV1_Set_1" | "NS1 gene" | Forward: "TTGGTAATGTTGGTTGCTACAATGC"<br>Reverse: "ACCTGAACATATGGCTTTGAATTGG" | 127 | (Soares *et al.*, 1999) | "62 °C" | "30 s" |
| "PPV1_Set_2" | "NS1 gene" | Forward: "AGCCAAAAATGCAAACCCCAATA"<br>Reverse: "CTCCACGGCTCCAAGGCTAAAG" | 142 | (Huang *et al.*, 2004) | "59 °C" | "30 s" |
| "PPV1_Set_3" | "NS1 gene" | Forward: "ATACAATTCTATTTCATGGGCCAGC"<br>Reverse: "TATGTTCTGGTCTTTCCTCGCATC" | 330 | (Soares *et al.*, 1999) | "62 °C" | "30 s" |
| "PCV2_Set_1" | "PCV-2 Capsid protein gene" | Forward: "TAGGTTAGGGCTGTGGCCTT"<br>Reverse: "CCGCACCTTCGGATATACTG" | 263 | (Larochelle *et al.*, 2000) | "60 °C" | "30 s" |
| "PCV2_Set_2" | "PCV-2 Rep gene" | Forward: "CACATCGAGAAAGCGAAAGGAAC"<br>Reverse: "TGCGGGCCAAAAAAGGTACAGTT" | 505 | (Yang *et al.*, 2019) | "62 °C" | "40 s" |
| "PCV2-Set_3" | "PCV-2 ORF1" | Forward: "GCCAGTTCGTCACCCTTTC"<br>Reverse: "CTCCCGCACCTTCGGATAT" | 657 | (Rincón Monroy *et al.*, 2014) | "59 °C" | "40 s" |

| | | | | | | |
|---|---|---|---|---|---|---|
| “PRRS_Set_1” | “ORF1b” | Forward: “CCTCCTGTATGAACTTGC” Reverse: “AGGTCCTCGAACTTGAGCTG” | Type 1 & Type 2 255 bp | (Gilbert *et al.*, 1997) | “59 °C” | “40 s” |
| “PRRS_Set_2” | “ORF7” | Forward: “CCAGCCAGTCAATCARCTGTG” Reverse: “GCGAATCAGGCGCACWGTATG” | Type 1 & Type 2 300 bp | (Donadeu, 1999) | “62 °C” | “40 s” |
| “PRRS_Set_3” | “ORF7” | Forward: “TGGCCAGCCAGTCAATCA” Reverse: “TCGCCCTAATTGAATAGGTGA” | Type 1 398 bp Type 2 433 bp (Discriminative primer set) | (Choi *et al.*, 2012) | “57 °C” | “45 s” |
| “SIV_Set_1” | “M gene (pan-influenza A)” | Forward: “GACCRATCCTGTCACCTCTGAC” Reverse: “AGGGCATTYTGGACAAAKCGTCTA” | 106 | (de-Paris *et al.*, 2012) | “63 °C” | “30 s” |
| “SIV_Set_2” | “NP gene (swine influenza)” | Forward: “GCACGGTCAGCACTTATYCTRAG” Reverse: “GTGRGCTGGGTTTTCATTTGGTC” | 200 | (Klungthong *et al.*, 2010) | “63 °C” | “40 s” |
| “SIV_Set_3” | “H1 swine type hemagglutinin” | Forward: “GTGCTATAAACACCAGCCTYCCA” Reverse: “CGGGATATTCCTTAATCCTGTRGC” | 116 | (Klungthong *et al.*, 2010) | “63 °C” | “30 s” |
| “SIV_Set_4” | “H3 swine type hemagglutinin” | Forward: “CTTGATGGRGMAAAYTGCACA” Reverse: “GGCACATCATAWGGGTAACA” | 133 | (Bonin *et al.*, 2018) | “56 °C” | “30 s” |
| “SIV_Set_5” | “H1 avian type hemagglutinin” | Forward: “GAAGGRGGATGGACAGGAATGA” Reverse: “CAATTAHTGARTTCACTTTGTTGC” | 139 | (Bonin *et al.*, 2018) | “57 °C” | “30 s” |

| | | | | | | |
|---|---|---|---|---|---|---|
| “SIV_Set_6” | “H1 pandemic hemagglutinin (Pandemic 2009) ” | Forward: “GGGCATTCACCATCCATCTACT” Reverse: “CCTCACTTTGGGTCTTATTGCTATTT” | 133 | (Bonin *et al.*, 2018) | “62 °C” | “30 s” |
| “SIV_Set_7” | “N1 swine type neuraminidase” | Forward: “AGRCCTTGYTTCTGGGTTGA” Reverse: ACCGTCTGGCCAAGACCA” | 126 | (Bonin *et al.*, 2018) | “57 °C” | “30 s” |
| “SIV_Set_8” | “N2 swine type neuraminidase” | Forward: “AGTCTGGTGGACYTCAAAYAG” Reverse: “TTGCGAAAGCTTATATAGVCATGA” | 116 | (Bonin *et al.*, 2018) | “58 °C” | “30 s” |
| “SIV_Set_9” | “N1 pandemic hemagglutinin (Pandemic 2009) ” | Forward: “GGGACAGACAATAACTTCTCAATAAAGC” Reverse: “TTCAGCATCCAGAACTAACAGGGT” | 100 | (Bonin *et al.*, 2018) | “64 °C” | “30 s” |
| “ASF_Set_1” | “VP72 gene” | Forward: “GGTTGGTATTCCTCCCGTG” Reverse: “GATTGGCACAAGTTCGGAC” | 326 | (Luo *et al.*, 2017) | “58 °C” | “40 s” |
| “CSF_Set_1_Nested1” | “E2 gene” | Forward: “AGRCCAGACTGGTGGCCNTAYGA” Reverse: “TTYACCACTTCTGTTCTCA” | 671 | (Barman *et al.*, 2010) | “52 °C” | “50 s” |
| “CSF_Set_1_Nested2” | “E2 gene” | Forward: “TCRWCAACCAAYGAGATAGGG” Reverse: “CACAGYCCRAAYCCRAAGTCATC” | 272 | (Barman *et al.*, 2010) | “58 °C” | “40 s” |

| | | | | | | |
|---|---|---|---|---|---|---|
| “CSF_Set_2_Nested1” | “5’ NTR region” | Forward: “CTAGCCATGCCCWYAGTAGG” Reverse: “CAGCTTCARYGTTGATTGT” | 421 | (Barman *et al.*, 2010) | “52 °C” | “50 s” |
| “CSF_Set_2_Nested2” | “5’ NTR region” | Forward: “AGCTCCCTGGGTGGTCTA” Reverse: “TGTTTGCTTGTGTTGTATA” | 272 | (Barman *et al.*, 2010) | “50 °C” | “40 s” |

## 3.3. Real-time PCR Assays

Real-time PCR for the quantification of viral DNA and cDNA isolated from clinical and spiked samples was performed in triplicate using SYBR Green chemistry. The primer sets used were "PPV1_Set_2 (NS1 gene)", "PCV2_Set_1 (Cap gene)", "PRRS_Set_1 (ORF1b gene)", "SIV_Set_1 (M gene)", "ASF_Set_1 (VP72 gene)" and "CSF_Set_1_Nested_2" (E2 gene) for PPV1, PCV-2, PRRSV, SIV, ASF and CSF, respectively. The reactions were performed in a total volume of 20 μL, consisting of 10 μL "2 × PowerUp™ SYBR™ Green Master Mix with 500 nm ROX" (Applied Biosystems, Vilnius, Lithuania), 0.5 μL of 10 μM forward primer solution, 0.5 μL of 10 μM reverse primer solution, 1 μL of template viral DNA or cDNA, and 8 μL $H_2O$. Cycling conditions were as follows: Initial activation of UDG for 2 min at 50 °C, activation of the Dual-Lock polymerase for 2 min at 95 °C, 40 cycles of denaturation at 95 °C for 15 seconds and annealing and extension at 60 °C for 1 min. Data were collected with a "7500 Real Time PCR System" and analyzed with 7500 software, v.2.0.6 (Applied Biosystems).

The quantification of the viral load was performed with standard curves generated from known amounts of DNA, ranging from $10^{10}$ ($10^9$ for PCV-2 and ASF) to $10^3$ viral genome copies per PCR reaction, in duplicate. The DNA used for the creation of the standard curves originated from purified PCR products after gel electrophoresis. To calculate DNA content, all samples were quantified with photometry (Quawell Q5000, San Jose, CA, USA). The copy number was calculated using the DNA content, the average molecular weight of deoxyribonucleotides, the number of deoxyribonucleotide bases for each DNA product and Avogadro's number. Viral concentrations were expressed as the viral copy number per ml of sample.

## 3.4. Novel POS Device

The novel POS device was built in the framework of EU's H2020 SWINOSTICS program. The device followed a modular approach to efficiently integrate its components into a single, portable diagnostic platform weighing around 45 kg, with a size of about 40×50×60 cm (Figure 12). "The platform was powered by a single plug (connected to 220 V socket). The new diagnostic device can be divided into three functional subsystems. The first one is the mechanics/microfluidics subsystem which consists of (i) a syringe system that delivers the sample and the buffers to the sensors (Figure 13), (ii) motors that move the syringe system on the x- and z- axes, (iii) a microfluidics channel, (iv) a waste tank, and (v) a Peltier element as the temperature control module (Figure 12)" (Manessis *et al.* 2021).

"The optics subsystem consists of (i) a tunable laser module (model PPCL200, Pure Photonics, Milpitas, CA, USA), operating at a wavelength range of 1549.3150 to 1550.9180 nm with a central sweeping point of 1550.1161 nm, (ii) optic fibers, and (iii) a fiber pigtailed InGaAs photodiode (75 μm, 9/125 SMF, FC/PC connector, 1 m, model PDINP0751FCA-0-0-01, Huntingdon, UK). The optics subsystem also utilizes the sensors, the Photonic Integrated Circuits (PICs) on silicon nitride, coupled with the tunable laser and the photodiode. Finally, the firmware subsystem consists of (i) the microcontroller and its software, (ii) the arduino data logger, and (iii) an SD card. The microcontroller utilizes Bluetooth Low Energy technology to communicate with a tablet through an Android application for the operation of the device. Experimental data are uploaded to a cloud platform via the tablet, generating in real-time simple yes/no results" (Manessis *et al.* 2022). "The cloud platform also enables real-time data sharing with authorized personnel and veterinarians. In the absence of an Internet connection, the results can be stored and uploaded later in the cloud platform. Features such as system operation, analysis progress, data collection/storage, and results are monitored via an android application in the tablet. The assay could be completed within 60 min. Minimal handling and training was required for the operation of the device. End-users must only add pipette tips and the samples in the device. The device allows for multiplexing, as a sample can be tested simultaneously for the panel of six swine viral diseases using 3 out of the 4 sampling slots. The device underwent limited, initial field testing at commercial swine farms in Greece, Italy, and Hungary for proof of concept experiments" (Manessis *et al.* 2022).

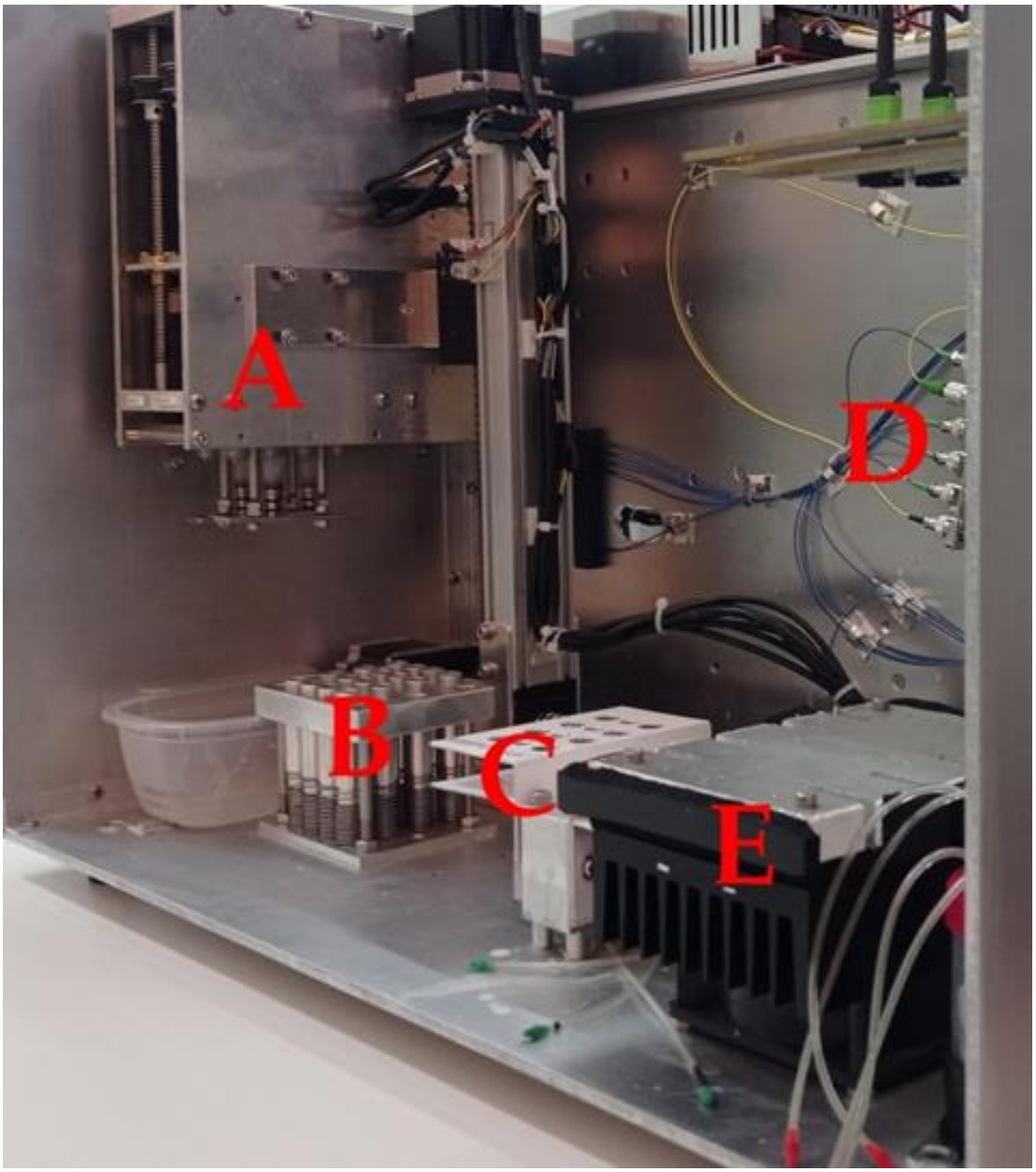


**Figure 12.** "The novel POS system: (A) syringe system, (B): pipette tip holder, (C) buffer/sample holder, (D) optic fibers and optical splitter, (E) temperature control (Peltier surface) module."

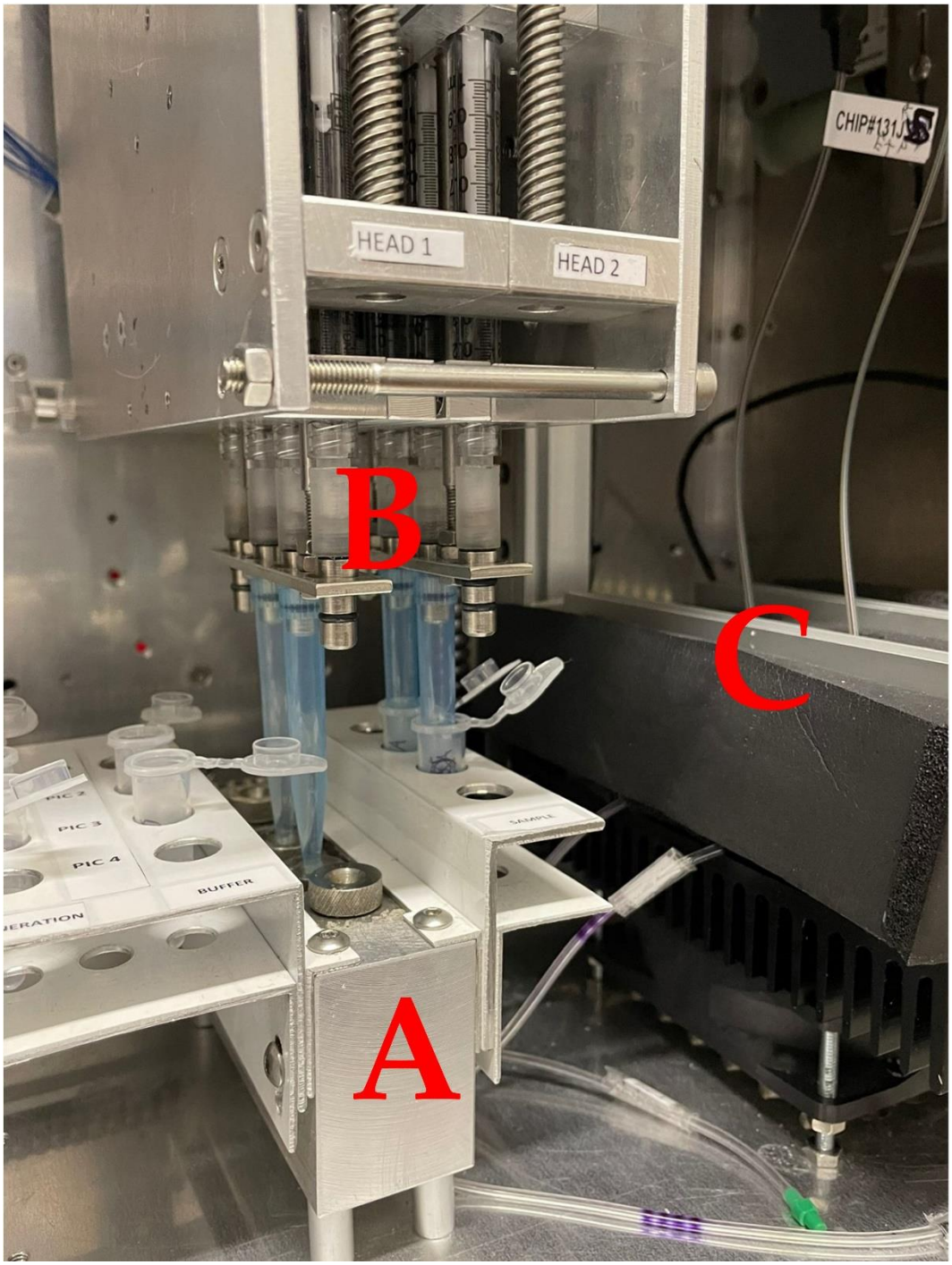


**Figure 13.** "The novel POS system: (A) Sample and buffer holder. Pipette tips are pressed against the microfluidic inlet (circular button on the top area of the holder) to propel the fluids to the sensors, (B): Syringe system that draws and propels fluids, (C) Insulating material. Underneath lie the sensors on a Peltier surface that keeps the temperature steady at 25 °C. The optic fibers (tagged cables) of the PICs exit the insulating material through ports."

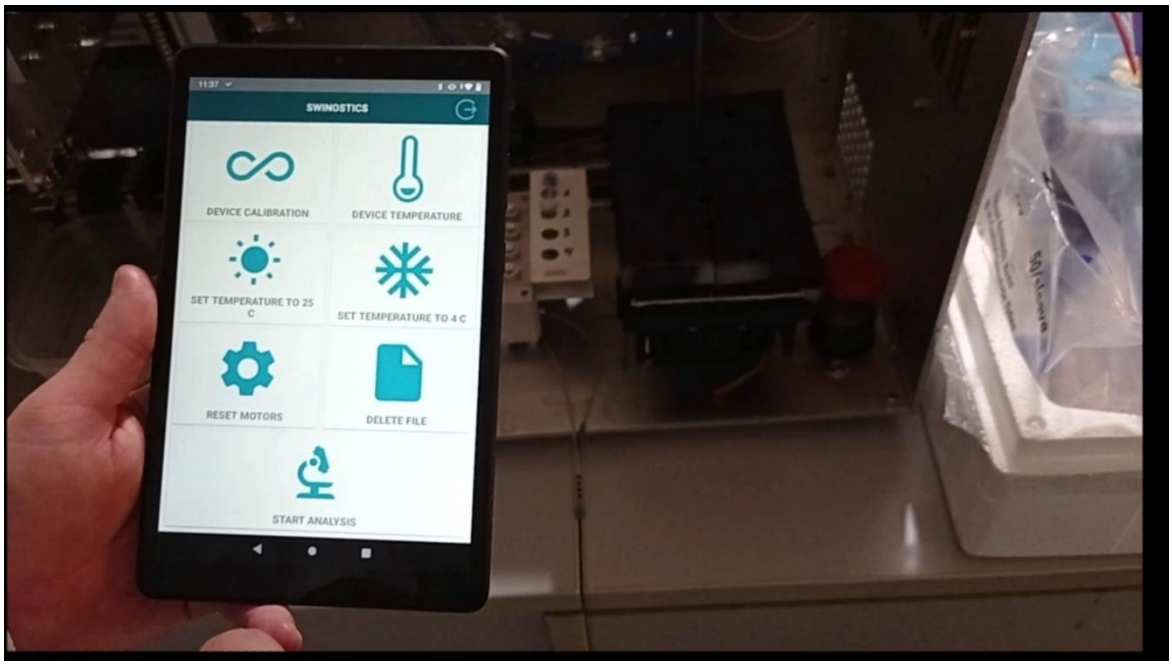


**Figure 14.** "Using the android application and the tablet to operate the novel POS device in field conditions."

## 3.5. Sensors & Antibodies

At the core of the POS device are its sensors. Photonic Integrated Circuits (PICs) utilize 8 ring resonators with immobilized antibodies (MREs) on their surfaces for the capturing of the viral particles. The eight ring resonators of PICs are split into two blocks, consisting of four rings each. In each block, three rings are functionalized with immobilized antibodies for a given disease (e.g., PPV1 or PCV-2, PRRS or CSF, SIV or ASF) whereas the surface of one ring is blocked with fish gelatin and serves as the reference ring (Figure 15). Following laser excitation at a continuous wavelength (laser sweeping) in the range of approximately 1.5 nm, each ring resonates at a specific wavelength, trapping that particular wavelength in the ring and preventing it from reaching the photodiode. This results in a measurable minimum in the wavelength spectrum, which can be detected by the photodiode. The capture of viral antigens via the antibodies results in a localized change in the refractive index which extends beyond the sensor's surface (Mudumba *et al.*, 2017). This change in the refractive index modifies the resonant wavelength of the rings, causing a signal shift that is detected by the photodiode.

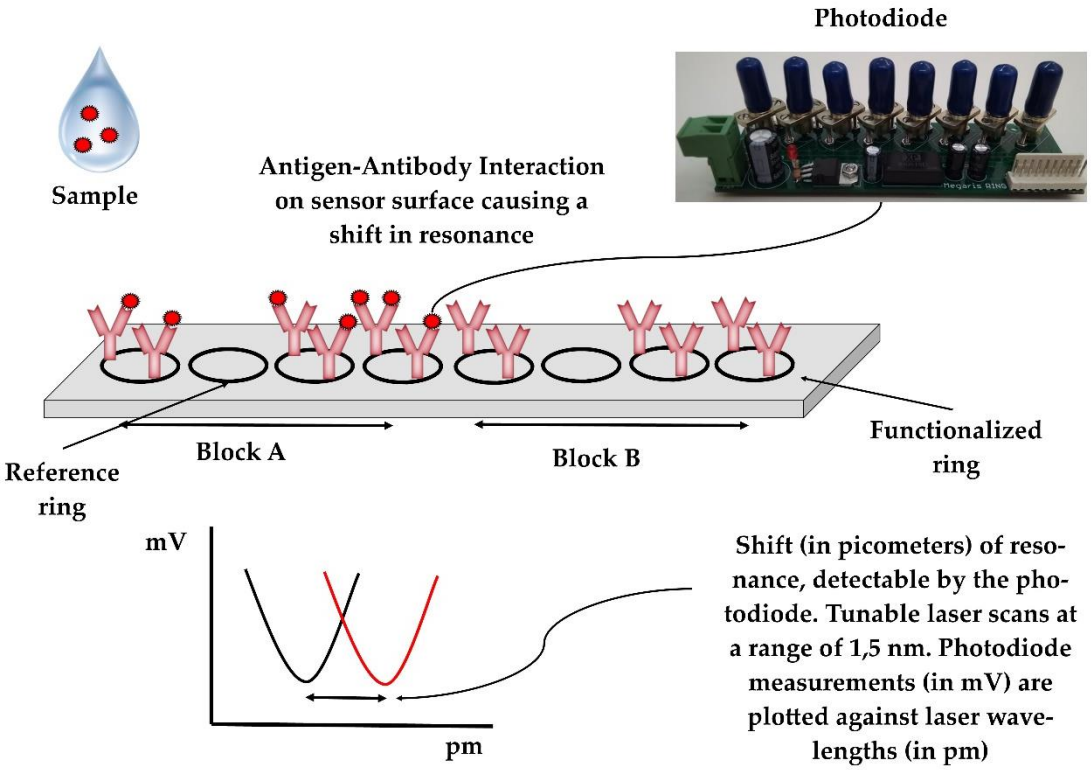


**Figure 15.** "Sensors and the principle of viral detection. Upon laser excitation, a minimum in the laser's sweeping spectrum is detected. The value (in nm) of the recorded minimum in the wavelength spectrum is affected by the sensor's refractive index. To calculate the shift (in pm) which is attributable to the captured antigen, the shift of the reference ring is subtracted from the shift of each functionalized ring."

PICs were provided by Universitat Politècnica de València Nanophotonics and Technology Center and Lumensia Sensors S.L. and were fabricated and functionalized as previously described by (Griol *et al.*, 2019). The dimensions of the microfluidic board of PICs were 7 × 3 cm, and the board was fabricated in cyclic olefin polymer (COP). The diameter of the microfluidic channels was 500 μm (Figure 16). Each PIC was functionalized with two types of antibodies for the simultaneous detection of two viruses in each sample, as previously described (Gómez-Gómez *et al.*, 2022). The PPV1/PCV-2 sensors were functionalized with polyclonal anti-PPV1 VP2 antisera antibodies (Cat. No. PPVVP21-S, Alpha Diagnostic, San Antonio, Texas, USA) in the first sensor block, and with polyclonal anti-PCV-2 anti-CP (capsid protein) antibodies (Cat. No. PA5-34969, Invitro-gen, Carlsbad, California, USA) in the second block. Under the same concept, PRRSV/CSF sensors were functionalized with polyclonal anti-PRRS type 1 nucleocapsid protein antibody pAb PRSNP11-S (Alpha Diagnostic, San Antonio, TX, USA) and with polyclonal anti-CSF E2 envelope protein antibody (CSFE21-S, Alpha Diagnostic, San Antonio, TX, USA). Similarly, SIV/ASF sensors were functionalized with anti-SIV influenza A virus nucleoprotein monoclonal antibody MA5-17101 (Thermo Fisher Scientific, Waltham, MA, USA), and with anti-ASF VP72 protein monoclonal antibody (M.11.PPA.I1BC11, Ingenasa,

Madrid, Spain). More information on the selection of anti SIV and anti-ASF antibodies are provided in the Appendix. All antibodies were selected to recognize conserved regions to facilitate the detection of a wide range of circulating viral strains.

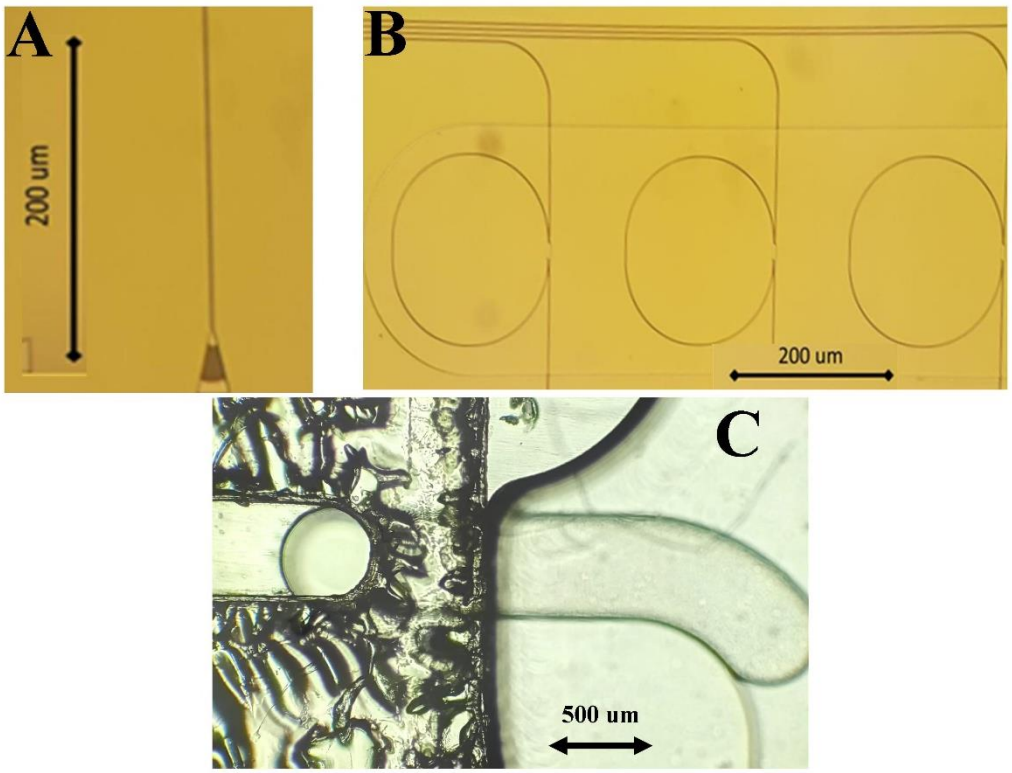


**Figure 16.** "Microscopic images of PICs: (A) grating coupler, (B) ring resonators of PICs, and (C) buffer drop entering the PIC surface."

## 3.6. Shift Calculation

The analysis protocol of the novel POS device included five consecutive steps: i) the buffer step, ii) the sample step, iii) the washing step, iv) the regeneration step and v) the final washing step. Data analysis was performed using a case-specific algorithm and a novel software for PC, written in Python. This shift calculation algorithm was also accessible through the android application (in the tablet) and the online platform.

To calculate the signal shifts in pm, photodiode responses in mV were plotted against their respective wavelength values in nm (the laser was sweeping in a wavelength range of approximately 1.5 nm). Minimum values of mV (notches, Figure 15) corresponded to specific wavelength values in nm. For both functionalized ($R_{functionalized}$) and reference rings ($R_{reference}$), the minimum wavelength values (in nm) were selected at two steps of the analysis, the buffer step (Step 1—S1) and the washing step (Step 3—S3). Shifts of both functionalized and reference rings were calculated as the differences between the minimum

wavelength values in steps 1 and 3 for each ring type ($D_{functionalized}$ and $D_{reference}$, respectively). Relevant shifts caused by virus–antibody interactions were calculated by subtracting the absolute values of the two differences ($|D_{functionalized}| - |D_{reference}|$) (Manessis *et al.*, 2021).

Positive relevant shifts corresponded to viral antigen detection, while negative relevant shifts corresponded to negative results. Relevant shifts were calculated for all functionalized rings, as rings operated independently (Manessis *et al.*, 2021).

## 3.7. Optimization of the Novel POS Device

Prior to the initiation of the validation experiments presented in the following sections, non-functionalized (i.e. "blank" PICs) and PPV1/PCV-2 functionalized PICs were used to optimize the device and finalize the analysis protocol and the new data analysis software. These experiments were crucial for further development of the sensors/device to successfully initiate testing with complex field samples, such as oral fluids and blood serum, where the analyte of interest is a minor fraction of the overall protein content. The optimization of the novel POS device was a significant part of the research activities in the current study. To avoid text fragmentation and provide the necessary supporting evidence for the following chapters, the optimization of the POS device along with relevant results will be presented herein.

### 3.7.1 Microfluidics and sample pretreatment

The microfluidics subsystem consists of polymeric materials (Tygon ® 2375) which are resistant to chemicals, low/high pH and cleaning solutions used during sanitization. Additionally, the microfluidic tubes are suitable for food and beverage applications. This indicated that the microfluidic subsystem did not interact with samples. The modular concept of the microfluidic subsystem and the facile replacement of the tubes made it ideal for POS applications.

In this stage, complex biological matrices (oral fluids, blood, feces and swabs) were tested with the POS device as well. Samples were pre-treated to prevent the blocking of the mirofluidic subsystem by large particulate matter. Samples were initially centrifuged according to the protocol described in section "3.1. Samples". The samples were then consecutively filtered with 5 μm and 0.45 μm filters for the removal of large agglomerates. The filtering process was also implemented during the limited field testing of the device. In field conditions, centrifugation was not required, and the filtering allowed the operation of the device without the need of special equipment (centrifuges).

A series of tests with hemolyzed serum were first performed to assure the proper delivery of fluids to the PICs. During these experiments, it was observed that the wash buffer (after sample introduction to the PICs) was contaminated with traces of serum. The traces of sample affect the photonic measurements on the washing step. To address this issue, additional washing time was integrated in the analysis protocol. Further experiments with hemolyzed serum were performed to synchronize the laser scanning timing with the introduction of clean wash buffer to the PICs.

### 3.7.2. Device calibration

Calibration of the POS device was always performed for all the rings of each PIC, both functionalized and reference rings, before the commencement of the assay. Calibration could be performed with or without liquids in the sensor chamber. As expected, calibration of new PICs was performed on a dry state without the presence of liquids in the sensor. Calibration of used and regenerated PICs was performed with liquids in the sensor. Photonic measurements required manual calibration of laser light intensity using a polarization controller (Figure 17). The calibration was performed by observing ring signal responses via the android application.

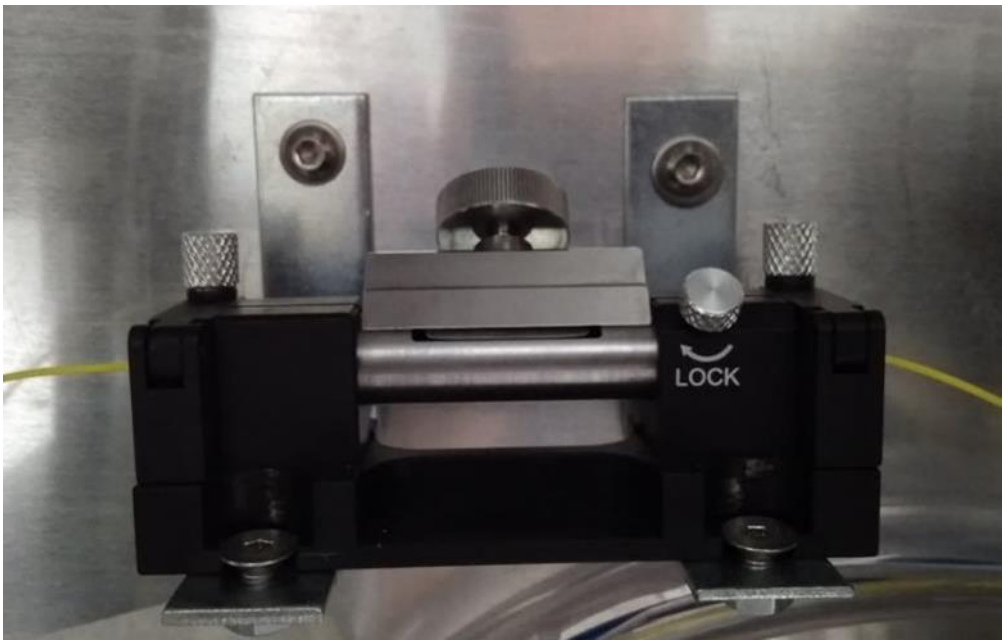


**Figure 17.** "The polarization controller used for the manual calibration of the POS device."

Calibration prior to each analysis was necessary to acquire the appropriate signal (distinct notches in the microvolt curve) for the estimation of signal shifts. Initially, the variation between ring responses on the same PIC made calibration a challenging task. In

fact, light intensity calibration could not be performed simultaneously for all of the rings on a PIC, resulting on cropped notches in some cases (Figure 18).

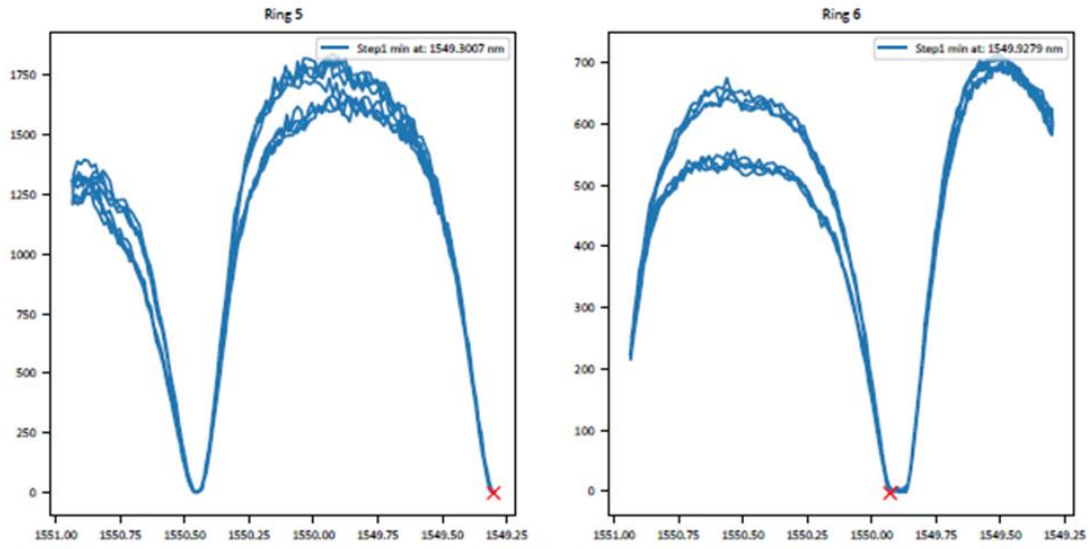


**Figure 18.** "Calibration data showing a "normal" notch on the left and a "cropped" notch on the right. Plots were generated with the android application."

The cropped notches did not allow the estimation of the "true" minimum, affecting the shift measurements in some instances. The issue was addressed by replacing the photodiode. The new photodiode was programmed to collect the cropped data, and therefore facilitated the calibration of the device and the collection of data (Figure 19).

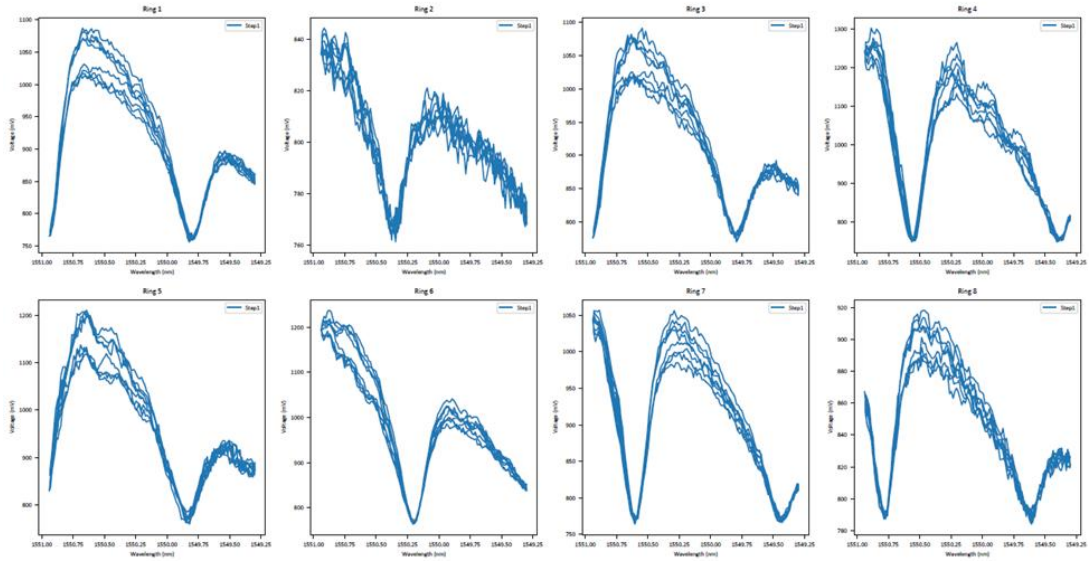

**Figure 19.** "Calibration data acquired with the new photodiode showing notches (minimums) in all of the 8 rings of one PIC."

### 3.7.3. Laser frequency scanning range

The laser sweeping of the SWINOSTICS device was set to a range of 150 GHz, which was interpolated to a wavelength range of approximately 1 nm. In some cases, this range was not sufficient to capture a notch (minimum), and therefore the estimation of the signal shifts could not be performed (Figure 20).

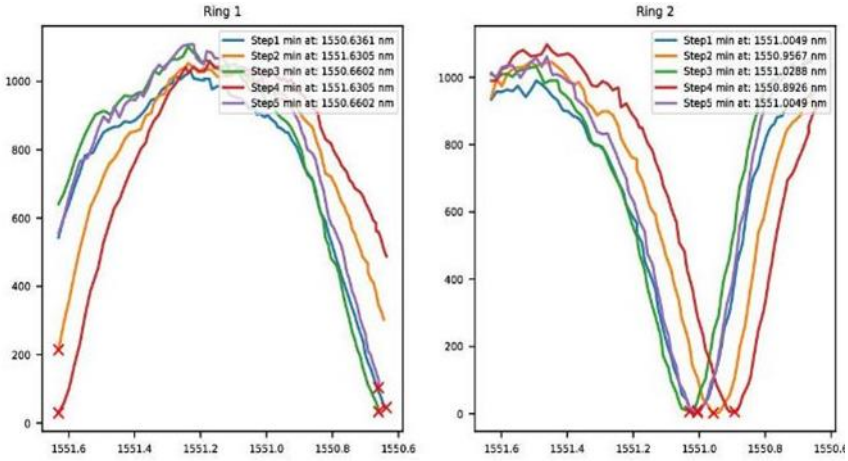


**Figure 20.** "A clear notch (minimum) is not captured in Ring 1, thus not allowing the reliable estimation of the shifts. On the contrary, in Ring 2 clear notches are detected."

To reassure the successful capturing of the notches, the laser software was updated and the laser frequency scanning range was set to 200 GHz, which corresponds roughly to a wavelength range of 1,5 nm. The use of laser calibration factors (provided by the manufacturer) for the proper functioning of the laser were required. The extension of the laser sweeping range allowed the detection of notches in Ring 1, as shown in the image below.

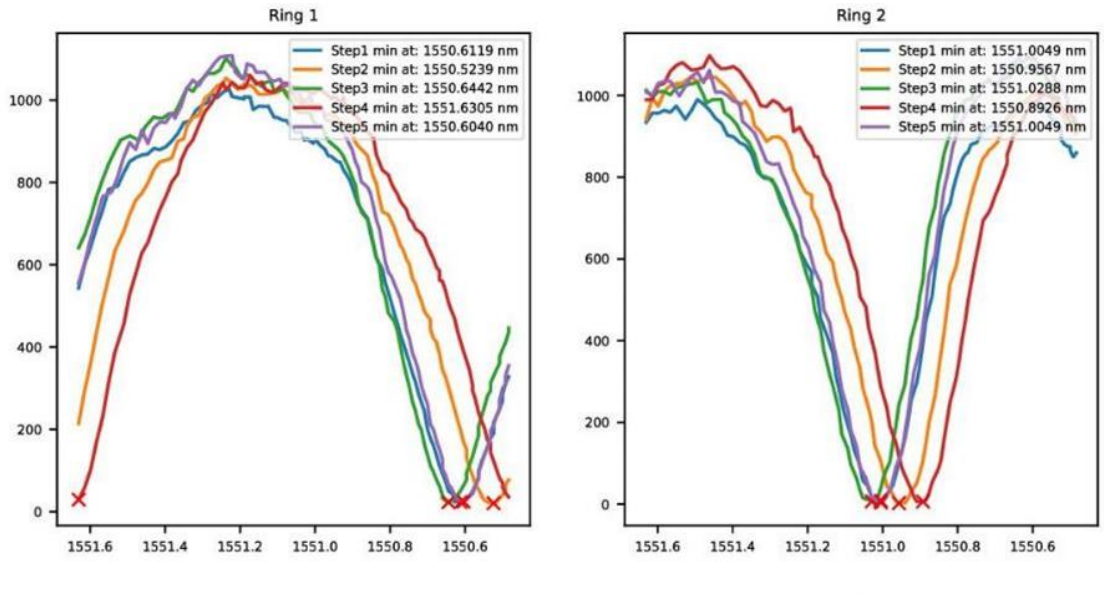


**Figure 21.** "The extension of the laser frequency scanning range allowed the capture of notches in Ring 1."

### 3.7.4. The effect of complex biological samples on reference rings

The introduction of complex biological samples (high in protein, lipid, carbohydrate content etc.) was expected to have a significant impact on the photonic measurements, in terms of signal shift and background. A series of experiments with oral fluids, blood serum, feces and nasal swabs were performed to evaluate the behavior of blank (reference) rings in terms of signal shifts and consequently optimize the analysis protocol and PIC fabrication.

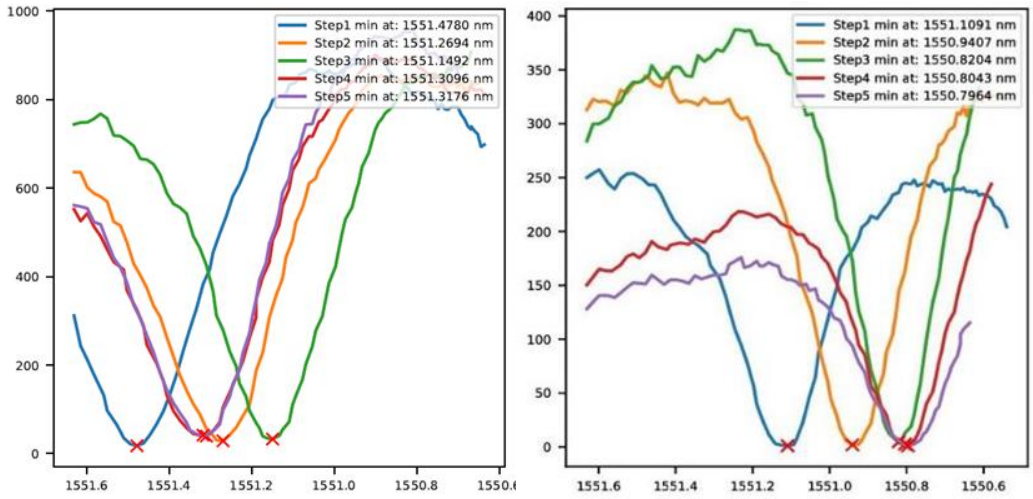


**Figure 22.** "Measurements showing the shift caused by oral fluids on the left and serum on the right. The introduction of complex samples causes significant shifts in blank rings."

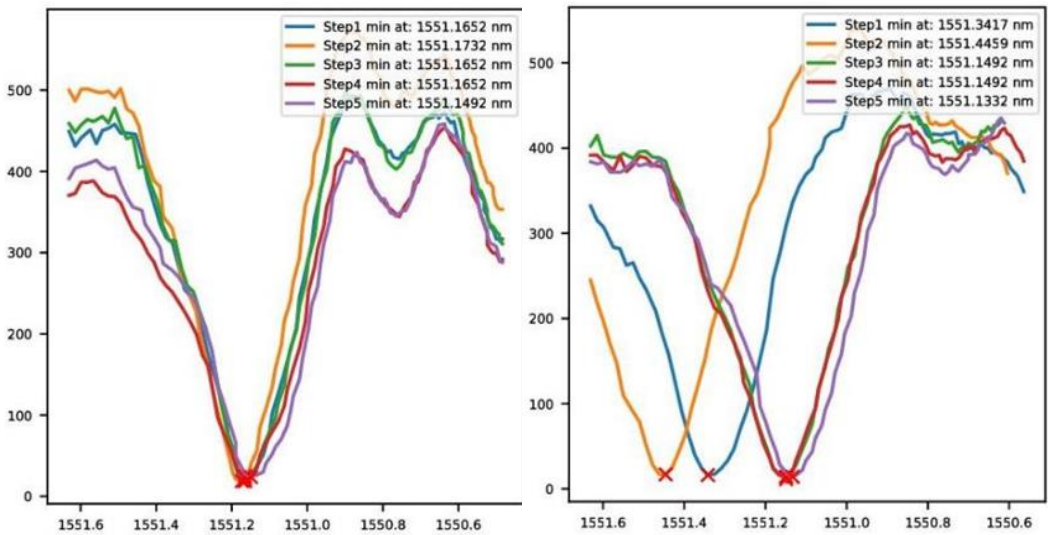


**Figure 23.** "Measurements showing the shift caused by nasal swabs on the left and processed fecal samples on the right The introduction of nasal swabs did not cause significant shifts in blank rings, whereas the opposite was observed for fecal samples."

As it is clearly demonstrated from the images above, the most suitable sample matrix was nasal swabs. However, not all of the six investigated viruses are found in sufficiently high concentrations in nasal swabs. Consequently, oral fluids, which are appropriate for the detection of all of the investigated viruses, were selected as the sample of choice. Due to the

lack of blocking proteins or antibodies immobilized on blank rings, the high protein content of complex biological samples induced large shifts. As the shift caused by captured viral particles is corrected with regard to the blank (reference) rings, this phenomenon could lead to false negatives. As a result, the surface of the reference rings was fully blocked with proteins (e.g. fish gelatin) to reduce the noise caused by samples with high protein content.

### 3.7.5. Signal stabilization/Establishing a baseline in functionalized rings

The initial trials with functionalized PICs indicated that the signal of functionalized rings was unstable during the first five minutes of buffer introduction (Figure 24). As a result, the true minimum value could not be detected or in other words, the signal baseline could not be established. In contrast, reference rings showed that within the first five minutes of buffer introduction the signal was much more stable (Figure 24).

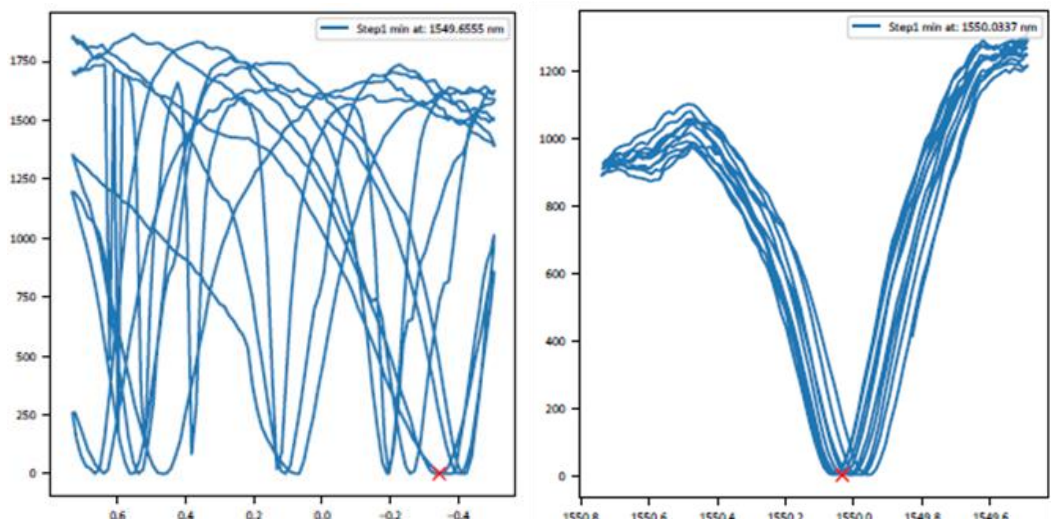


**Figure 24.** "On the left, the signal of a functionalized ring is not stabilized within the first 5 minutes of buffer introduction. On the contrary, the reference ring (right) showed a stable signal."

These observations led to the assumption that the antibodies require more time to be electrically stabilized in an ionic solution (buffer) and that an extension of the buffer step (step 1) from 5 to 15 minutes could eliminate the previously described phenomenon in functionalized PICs. To validate this assumption, a series of experiments using functionalized PICs and extending the buffer step were performed. Data analysis showed that the extension of the buffer introduction stabilized the signal allowing the establishment of the baseline (Figure 25).

The same issue, signal destabilization, was observed after the introduction of complex samples in functionalized rings and during the subsequent washing step. Again, increasing the washing time (after sample introduction) from 5 min to 15 min did not only

reduce sample contaminants but also led to signal stabilization in functionalized rings, thus allowing accurate shift calculation (Figure 25).

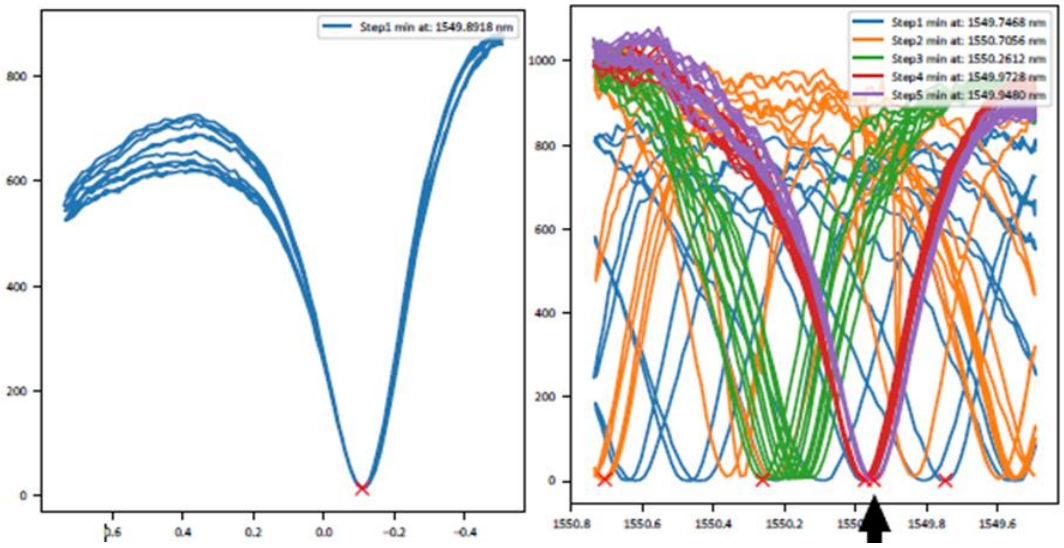


**Figure 25.** "On the left, signal stabilization in functionalized rings was achieved after the extension of the buffer step from 5 to 15 minutes. On the right, signal stabilization (black arrow) was achieved after the extension of the washing step from 5 to 15 minutes in functionalized rings."

## 3.7.6. The effect of Bovine Serum Albumin (BSA) on photonic measurements

As it was previously mentioned, sample proteins have a significant effect on photonic measurements introducing signal noises, especially in non-functionalized rings. Reference rings showed large shift variations when complex biological fluids were introduced in the sensors. To solve this issue and to acquire the relative shifts truly attributed to the virus-antibody interaction (i.e., calculate the differences between reference and functionalized rings) it was decided that the buffer should imitate the protein content of biological fluids. To this end, Bovine Serum Albumin (BSA) was added to the buffer solution to a final concentration of 1 % w/v.

Experimental data suggested that this approach could reduce the protein-induced background. The images below (Figure 26 and Figure 27) present a complete diagram of shifts with the addition of buffer and sample in sequence. In Figure 26, no BSA was added in the buffer and a significant shift was observed after the addition of the sample in reference rings, thus obstructing the establishment of a signal baseline. In Figure 26, BSA was added in the buffer and the introduction of negative (for PPV1 and other diseases) oral fluid samples did not cause a shift in both PPV1-functionalized and reference rings. In fact, minimums of the buffer step (step 3-green line) were aligned with the minimums of the sample step (step 4-red line) on both rings. The similar behavior of the different ring types

(functionalized and reference) allowed the establishment of the signal baseline. In addition, it was also observed that it takes about 12 min prior to signal stabilization after the introduction of buffer (blue curves).

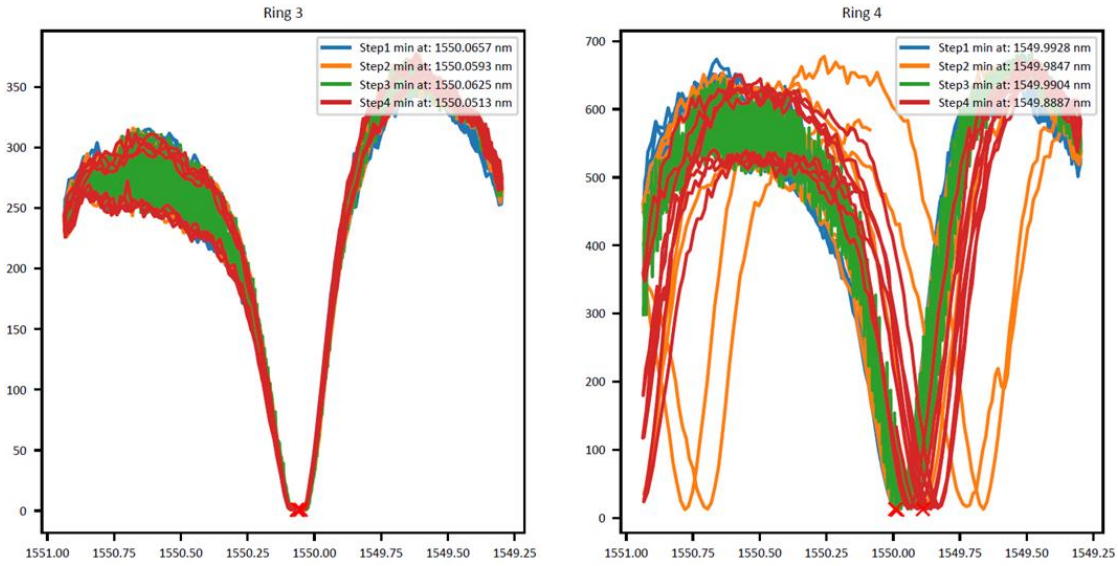


**Figure 26.** "The notch of Step 3 (buffer - green line) is aligned with the notch of Step 4 (oral fluids – red line) in the PPV1-functionalized ring (Ring 3). On the contrary, the notches are not aligned in the reference ring (Ring 4), obstructing the establishment of the signal baseline."

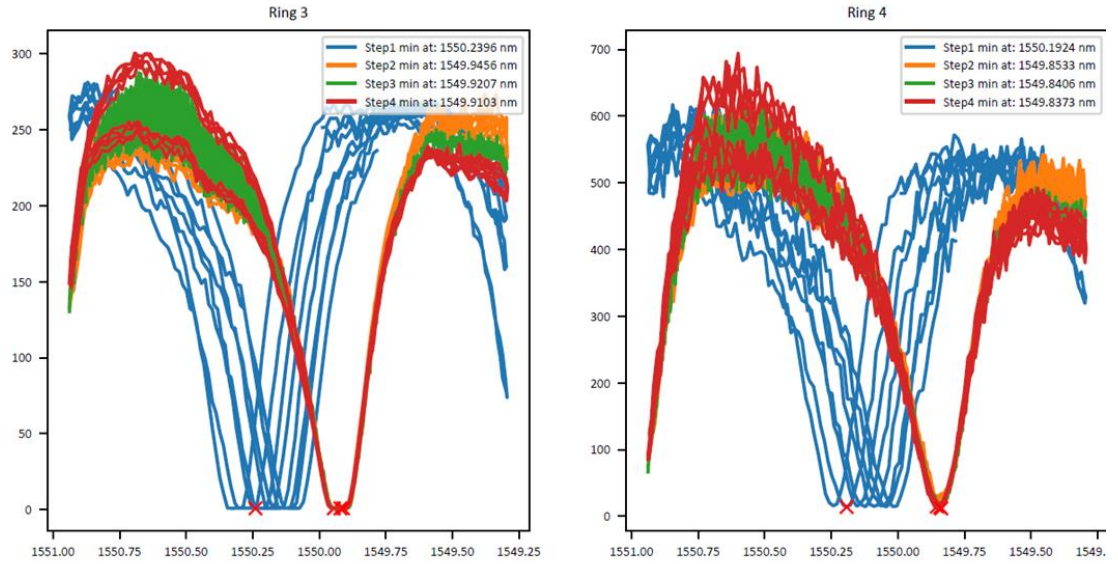


**Figure 27.** "The notch of Step 3 (buffer - green line) is aligned with the notch of Step 4 (oral fluids – red line) in both the PPV1-functionalized ring (Ring 3) and the reference ring (Ring 4) after the introduction of 1% BSA in the buffer solution."

These observations were integrated in the analysis protocol for the optimization of the photonic measurements.

## 3.8. Analysis Protocol

Based on the observations above (section 3.7), the analysis protocol was optimized for the detection of the studied viruses in complex biological matrices (oral fluids and sera). Two main buffers, phosphate buffered saline (PBS) and 2-(N-morpholino) ethanesulfonic acid (MES) were selected for viral detection, based on preliminary data using a commercial laboratory photonic setup. The analysis protocol for the detection of each virus is presented in Table 5.

**Table 4.** "Description of the analysis protocol for the detection of each virus. The purpose, timing and buffers at each step are presented."

| **"Analysis Step"** | **"Purpose"** | **"Time"** | **"Buffer for PPV1, PCV-2, SIV and ASF detection"** | **"Buffer for PRRSV and CSFV detection"** |
|---|---|---|---|---|
| *"Buffer Step"* | "Photonic signal stabilization and baseline establishment" | "15 minutes" | "PBS + 0.05% v/v Tween 20 + 1% w/v BSA, pH = 7.4" | "MES 0.1 M + 1% w/v BSA, pH = 6" |
| *"Sample Step"* | "Testing. Binding of the targeted analytes on functionalized PIC surfaces" | "10 minutes" | "Sample (300 µL) was diluted at a ratio of 1:1 with PBS + 0.05% v/v Tween 20 + 1% w/v BSA, pH = 7.4" | "Sample (300 µL) was diluted at a ratio of 1:1 with MES 0.1 M + 1% w/v BSA, pH = 6" |
| *"Washing Step"* | "Removal of unbound viral particles and sample residues" | "15 minutes" | "PBS + 0.05% v/v Tween 20 + 1% w/v BSA, pH = 7.4" | "MES 0.1 M + 1% w/v BSA, pH = 6" |
| *"PIC surface regeneration step"* | "PIC surface regeneration and release of captured antigens" | "5 minutes" | "50 mM Glycine + 50% v/v ethylene glycol, pH = 3" | "50 mM Glycine + 50% v/v ethylene glycol, pH = 3" |
| *"Final washing step"* | "BSA was excluded from the washing buffer to prevent protein accumulation in the microfluidic channels of the sensors" | "5 minutes" | "PBS + 0.05% v/v Tween 20, pH = 7.4" | "MES 0.1 M, pH = 6" |

For PIC surface regeneration, i.e. the release of captured viral particles from the sensors, the typical acidic glycine buffer used in SPR was supplemented with 50% ethylene

glycol to reassure analyte/antibody decoupling without compromising the structural and biochemical properties of antibodies. A simple proof-of-concept experiment for PIC regeneration is presented in the Appendix. Outflows were delivered to a waste tank for UV sterilization. Information on the sanitization protocol for the novel device are provided in the Appendix.

## 3.9. Data Fitting

The automated shift calculation software incorporated the LOWESS (Locally Weighted Scatterplot Smoothing) algorithm. The LOWESS was developed to enhance the visual information of scatterplots (such a scatterplot represents the data generated by the novel POS device). This algorithm smoothens a scatterplot, $(x_i, y_i)$, i = 1, . . . , n, in which the fitted value at $x_k$ is a polynomial fit to the data using the weighted least squares method, where the weight for $(x_i, y_i)$ is large if $x_i$ is close to $x_k$ and small if it is not. A robust fitting procedure is used to prevent the distortion of smooth points by deviant points (Cleveland, 1979). Supposing that the input data has N points, the algorithm works by estimating the smoothed $y_i$ by taking the frac*N closest points to $(x_i, y_i)$ based on their $x_i$ values and estimating $y_i$ by using a weighted linear regression. This indicates that the $x_i$ values (in our case the minimum in nanometers) are not distorted by the algorithm. Therefore, the estimation of the shifts (estimated by the differences in $x_i$ values of different analysis steps) is not affected by the implementation of the LOWESS algorithm (Manessis *et al.*, 2021).

## 3.10. Limit of Detection Experiments

Reference samples for the targeted viruses were quantified using the qPCR assays described earlier. For the estimation of the LOD for each functionalization type (PPV1, PCV-2 etc.), six serial 3-fold dilutions of the reference samples were used starting from $10^8$ viral genome copies/mL for PPV1, PCV-2, PPRSV and CSF and from $10^7$ viral genome copies/mL for SIV and CSF. Six PICs for each PPV1, PCV-2, PPRSV and CSF functionalization types were used in the LOD experiments. Four ASF functionalized and two SIV functionalized sensors were used in the respective experiments. Additionally, the LOD of ASF functionalized sensors in sera was tested with 4 sensors, by using six serial 3-fold dilutions (range of $10^7 – 3.3 \times 10^4$ viral genome copies/mL). Positive shift values were considered indicative of viral antigen detection.

## 3.11. Validation and System Performance

Due to the fact that LOD shift values (presented in detail in Chapter 4) could not fit into a linear model, a qualitative system with a binary response variable (positive, negative)

was adopted for the interpretation of results. Sensitivity, specificity, accuracy, precision, positive likelihood ratio (PLR), negative likelihood ratio (NLR), and diagnostic odds ratio (DOR) for each virus were calculated for the assessment of the diagnostic performance of the device. Calibrators (samples) were classified into three categories as previously suggested (Rabenau *et al.*, 2007) for the estimation of True Positives (TP), True Negatives (TN), False Positives (FP), and False Negatives (FN). Negative calibrators were considered as the samples that tested negative with conventional and real-time PCR methods. Positives (P) were considered samples that had Ct values lower than 30 in real-time PCR, whereas Low Positives (LP, samples up to a dilution factor of three over the lower limit of detection of the test) were considered as samples with Ct values equal or higher than 30. All of the three calibrator categories were included in the estimation of sensitivity (TP/(TP + FN)), specificity (TN/(FP + TN)), accuracy ((TP + TN)/(TP + TN + FP + FN)), precision (TP/(TP + FP)), PLR (sensitivity/(1 - specificity)), and NLR ((1 - sensitivity)/specificity) as well as their 95% confidence intervals (95% CI). The calculations were performed with MedCalc online software (https://www.medcalc.org/calc/diagnostic_test.php, accessed on 12 February 2023). The need for a global estimator of the discriminative power of the diagnostic device that allows comparisons between different diagnostic tests regardless of disease prevalence in the studied sample led to the calculation of DOR ((TP/FP)/(FN/TN)) (Glas *et al.*, 2003). DOR is defined as the ratio of the odds of positivity in the positive group, relative to the odds of positivity in the negative group. The positive and negative groups are defined by the golden standard method (quantitative PCR). The 95% CI of DOR was calculated using the formula Log(DOR) ± 1.96SE(Log(DOR)),where SE(Log(DOR)) = √(1/TP + 1/TN+ 1/FP + 1/FN) (Glas *et al.*, 2003).

PPV1 and PCV-2 samples were tested with a total of 12 PPV1/PCV-2 functionalized sensors, PRRSV and CSF samples were tested with 20 PRRSV/CSFV functionalized PICs, SIV samples were tested with 11 SIV functionalized PICs and ASF samples were tested with 17 PICs. The PICs were used up to six times and additional experiments were not attempted due to the structural deterioration of the sensors after excessive use. Each PIC had three functionalized rings for each disease and provided multiple independent measurements for a single sample. PPV1 functionalized rings provided 191 valid results, PCV-2 functionalized rings 193, PRRSV functionalized rings 277, CSF functionalized rings 272, SIV-functionalized rings 100, and ASF functionalized rings 177 valid results. The difference between the number of valid results obtained between the different viruses can be explained by the different number of PICs used in the study, as well as some deteriorated ring

resonators. Considering that each ring resonator functions independently, the validation of the POC device was conducted at the ring level.

## 3.12. Statistical analysis

Mean shift values from the LOD experiments were plotted against their respective viral concentrations (in log10 (Viral genome copies/mL)). Receiver operating characteristic (ROC) curves were drawn and the area under the curve (AUC) and the respective 95% confidence intervals (95% CI) for all studied viruses were calculated. Test outcomes (TP, TN, FP, and FN) were calculated for each virus using the optimal threshold of the ROC curve analysis. Afterwards the diagnostic performance of the PICs was estimated. The statistical analysis was performed with SPSS v23 software (IBM Corp., Armonk, NY, USA).

# Chapter 4. Results

## 4.1 Conventional and real-time PCR results

Samples were screened with the previously mentioned conventional and real-time PCR assays. All samples included in this study met the following qualification criteria: i) negative samples for a specific disease should test negative with all available primers for this disease. Specifically for SIV, negatives were considered the samples that tested negative when using SIV_set_1 and SIV_set_2 primer sets, ii) positive samples should test positive with all available primer sets for these diseases. Specifically for SIV, positive samples should test positive with both the SIV_set_1 and SIV_set_2 primer sets and additionally be successfully typed (SIV_set_3-9). For the device validation, the included PRRSV samples belonged to type 1 and were distinguished from type 2 using the primer set PRRSV_set_3. The SIV positive samples used in this study belonged to commonly circulating H1N1 or H3N2 subtypes. Positive clinical and reference samples, as well as those used in the LOD experiments, were quantified using the SYBR Green, real-time PCR assays and the standard curves presented below.

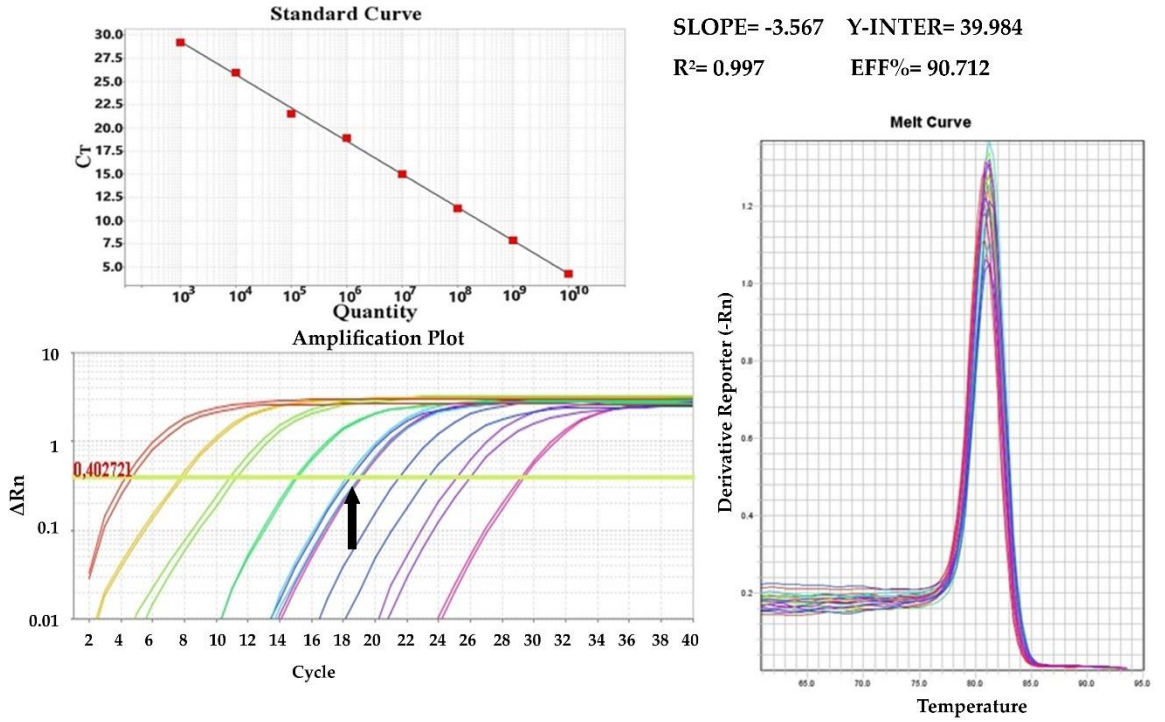


**Figure 28.** "qPCR standard curve using the PPV1_Set_1 primer set (NS1 gene) and the amplification plot with reference samples indicated with the black arrow."

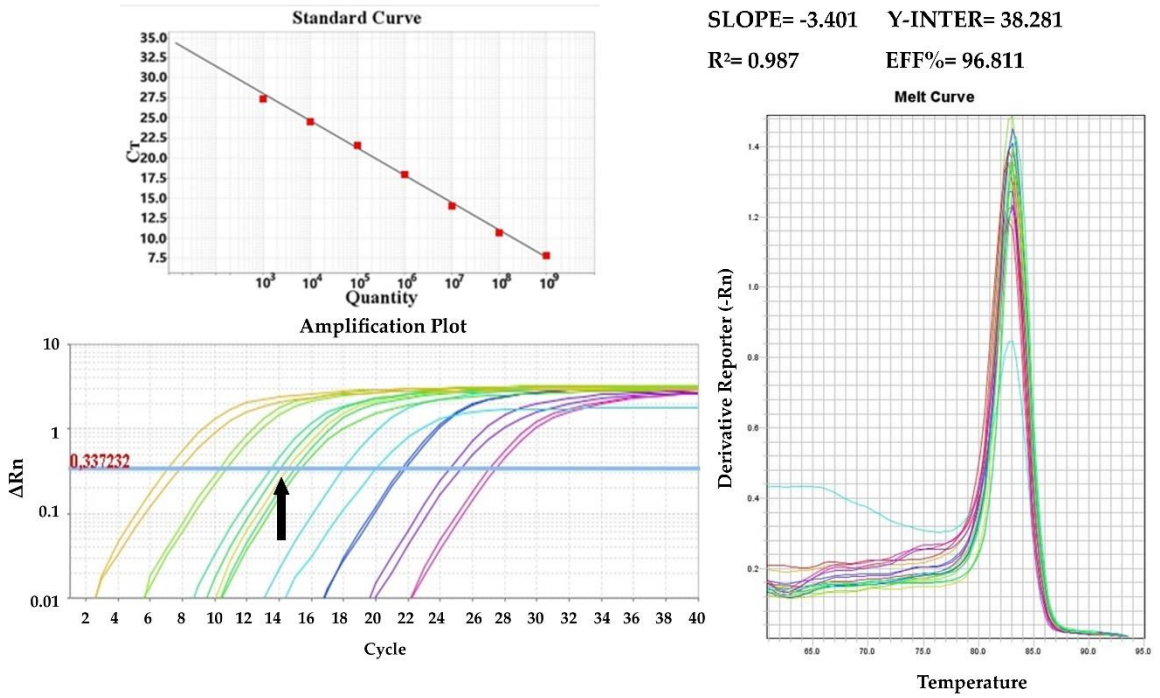


**Figure 29.** "qPCR standard curve using PCV-2_Set_1 primer set (capsid protein gene) and amplification plot with reference samples indicated with the black arrow."

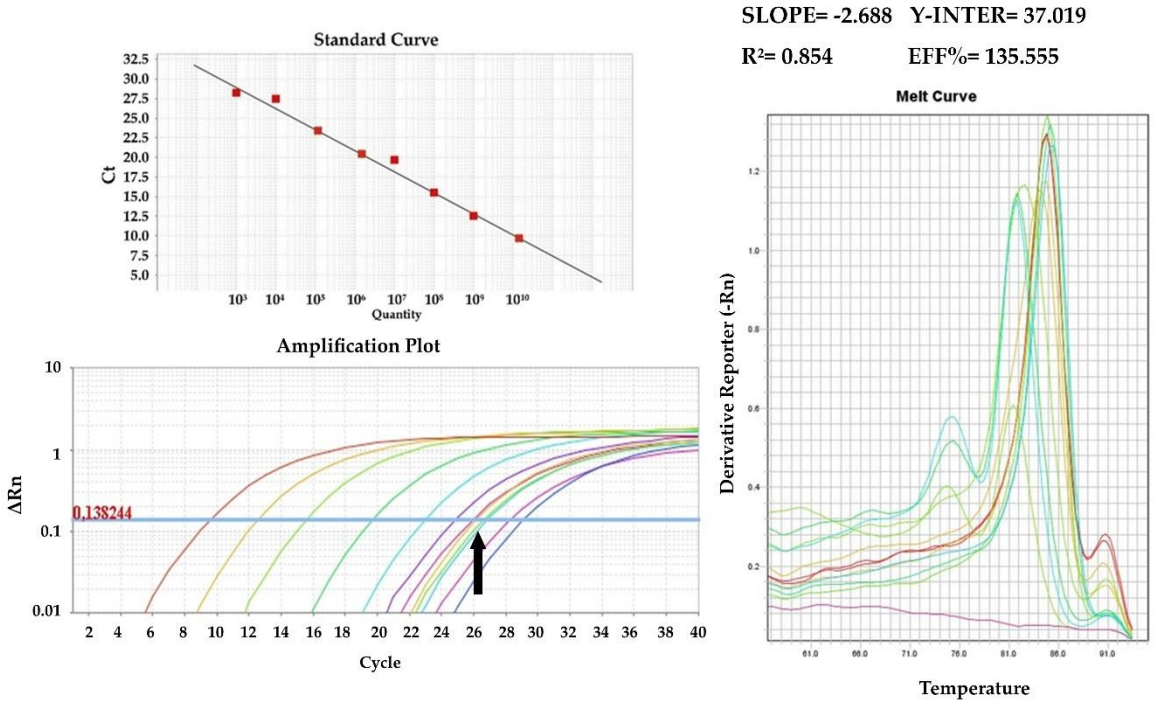


**Figure 30.** "RT-qPCR standard curve using the PRRS_Set_1 (ORF1b gene) primer set and the amplification plot with reference samples indicated with the black arrow."

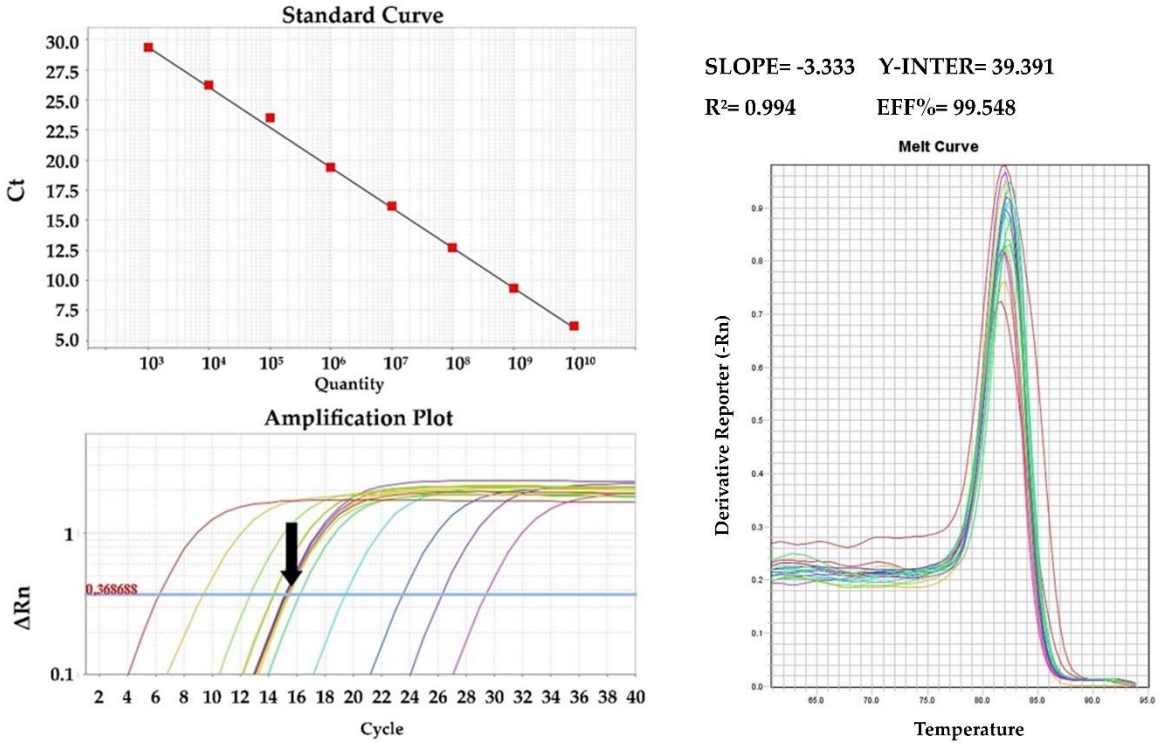


**Figure 31. "**RT-qPCR standard curve using the SIV_Set_1 (M gene) primer set and the amplification plot with reference samples indicated with the black arrow."

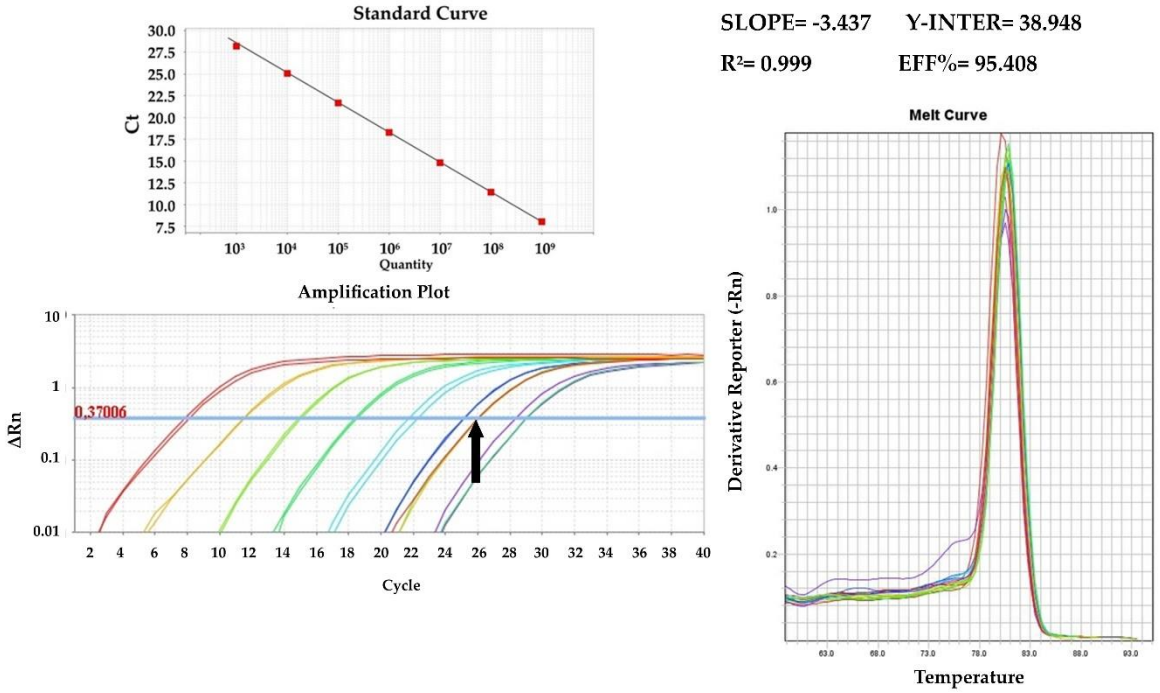


**Figure 32.** "qPCR standard curve using the ASF_Set_1 (VP72 gene) primer set and the amplification plot with reference samples indicated with the black arrow."

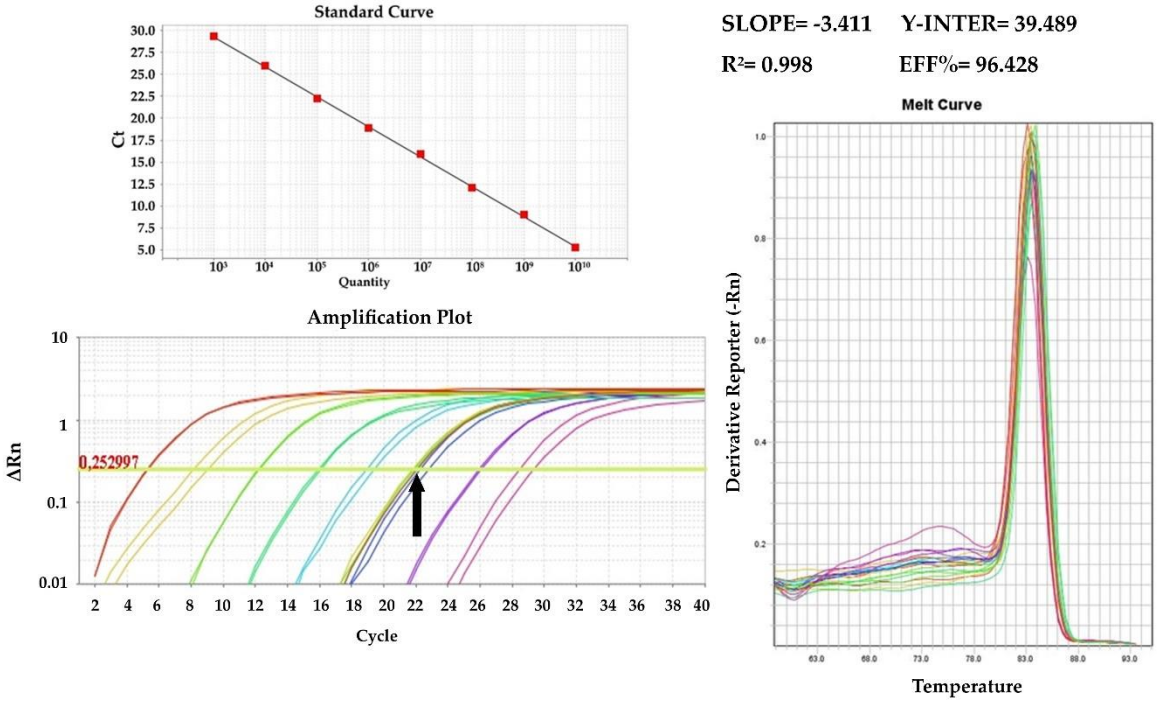


**Figure 33.** "qPCR standard curve using the CSF_Set_1_Nested2 (E2 gene) primer set and the amplification plot with reference samples indicated with the black arrow."

## 4.2 Data fitting

The application of the LOWESS algorithm to raw data (measurements with functionalized rings) resulted to the optimization of the visual interpretation of results and the accurate shift estimation as presented in the following image (Figure 34).

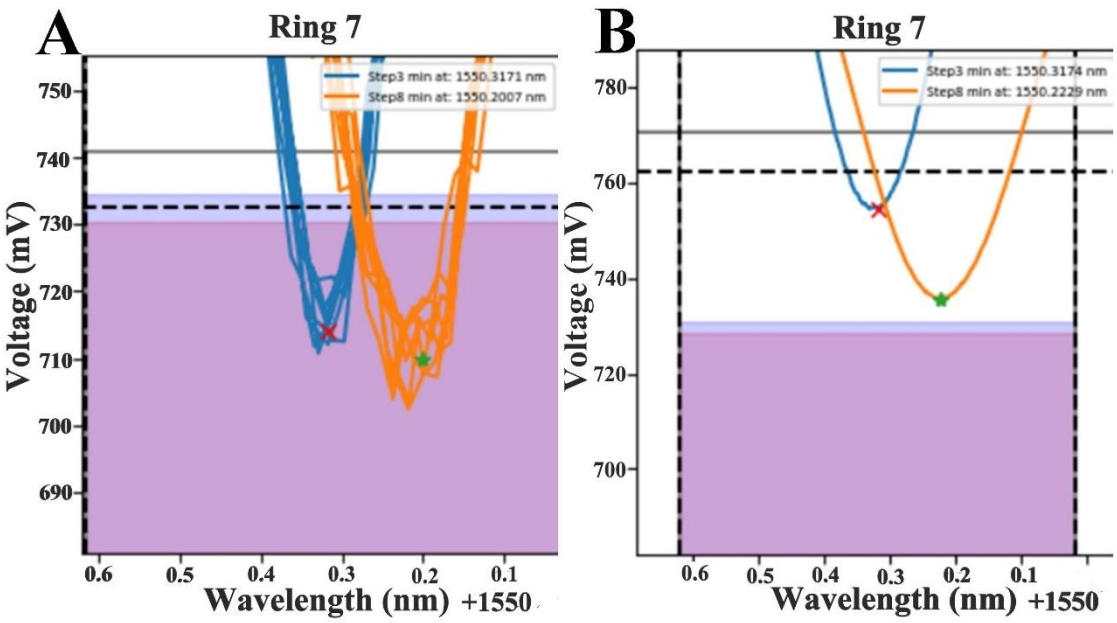


**Figure 34.** "Application of the LOWESS algorithm to raw data: (A) data prior to algorithm implementation, (B) data after the implementation of LOWESS. The wavelength values (x-axis) used for shift estimation remained identical."

In fact, the minimum values (x axis, wavelength in nm) selected after the implementation of the algorithm were closer to the mean value of repeated measurements. The variation in the x-axis (wavelength used for the estimation of shifts) was non-existent, as the algorithm weighs the data based on their $x_i$ values. On the contrary, there was a significant variation in the y axis values. Nevertheless, the variation of the y axis values does not affect the estimation of the shifts, and consequently is irrelevant to viral detection/quantification.

## 4.3 Limit of Detection – LOD

In the following images (Figures 35, 36 & 37), the shift responses in pm of the PPV1, PCV-2, PRRSV, SIV, ASF and CSF functionalized PICs are plotted against the corresponding viral concentrations (in $Log_{10}$(viral genome copies/mL)) of samples. The error bars represent the standard errors of the shifts in each viral concentration. The lowest detectable viral concentration (i.e. the LOD) is indicated by shift values approaching zero.

PPV1 functionalized sensors showed LOD values of $10^6$ viral genome copies/mL. PCV-2, PRRSV and CSF functionalized sensors showed LOD values of $3.3 \times 10^5$ viral genome copies/mL, whereas SIV and ASF functionalized sensors showed LOD values of $3.3 \times 10^4$ viral genome copies/mL. For all functionalization types, shift responses in pm were not dose-dependent due to the prozone effect (also known as hook effect). This realization led to the adoption of a qualitative response (yes or no) system suitable for virus detection but did not allow viral quantification. Additionally, it was observed that ASFV-spiked oral fluids produced greater shift responses than ASFV-spiked sera, indicating that oral fluids were more appropriate for photonic measurements. Finally, the lower LOD of SIV and ASF functionalized sensors and their better performance may be related to the fact that they were produced at a later stage of the project and previous experience was exploited during manufacturing.

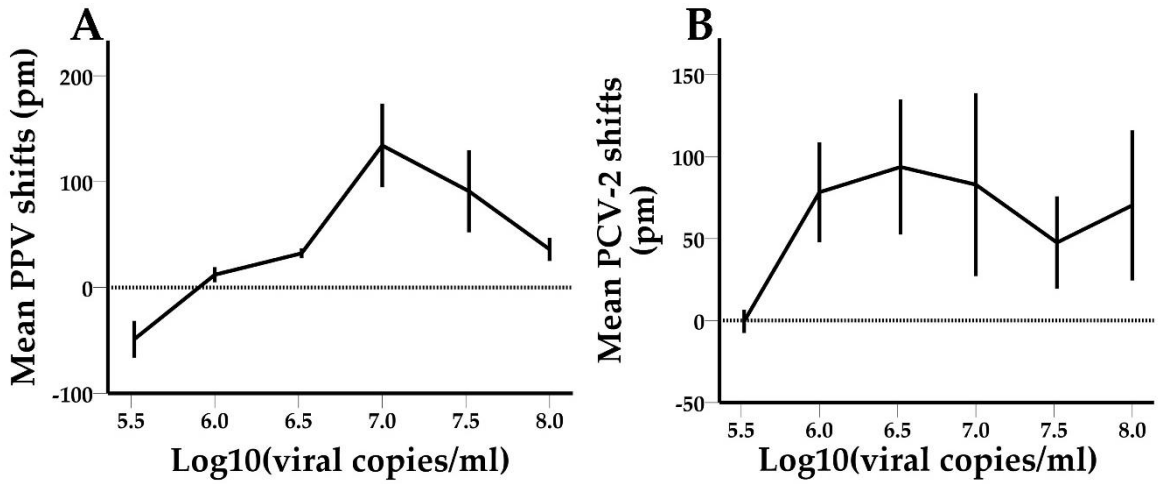


**Figure 35.** "(A) PPV1 and (B) PCV-2 shift responses (in pm) plotted against oral fluid viral concentrations [$Log_{10}$(viral genome copies/mL)]. PPV1 LOD was $10^6$ viral genome copies/mL and PCV-2 LOD was $3.3 \times 10^5$ viral genome copies/mL."

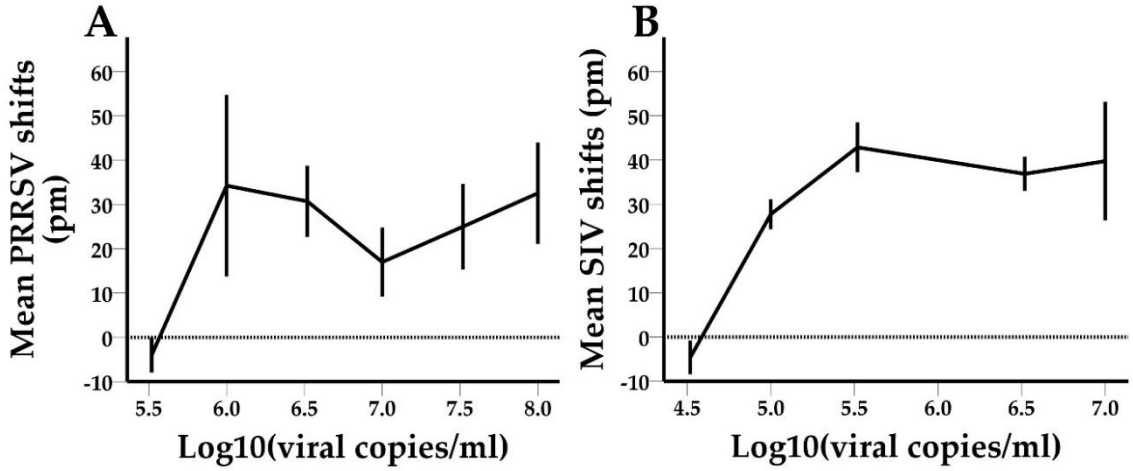


**Figure 36.** "(A) PRRSV and (B) SIV shift responses (in pm) plotted against oral fluid viral concentrations [$Log_{10}$(viral genome copies/mL)]. PRRSV LOD was $3.3 \times 10^5$ viral genome copies/mL and SIV LOD was $3.3 \times 10^4$ viral genome copies/mL."

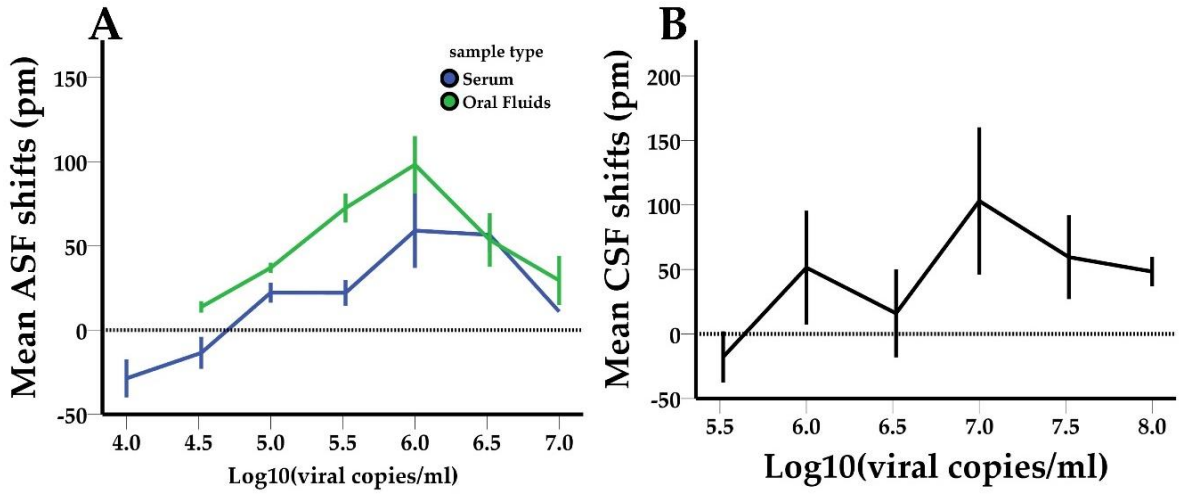


**Figure 37.** "(A) ASF and (B) CSF shift responses (in pm) plotted against viral concentrations [$Log_{10}$(viral genome copies/mL)]. In the LOD figure for ASF (A) the green line represents oral fluids and the blue line represents serum. ASF LOD was $3.3 \times 10^4$ viral genome copies/mL and CSF LOD was $3.3 \times 10^5$ viral genome copies/mL."

## 4.4 Receiver Operating Characteristic (ROC) Curve

AUC represents the chances that the device will correctly distinguish the positive class values from the negative class values. In all cases, optimal thresholds were considered those with positive values (i.e. viral detection, positive shifts) and were selected using Youden's index (= sensitivity + specificity - 1). For the estimation of AUC, 191 and 193 shift values were used for PPV1 and PCV-2, respectively. In the case of PPV1, an AUC value of 0.820 (95% CI: 0.760 to 0.880, $p < 0.0001$) and an optimal shift efficiency threshold equal to 4.5 pm (68.6% sensitivity, 77.1% specificity) were calculated (Figure 38). PCV-2 had an AUC value of 0.742 (CI: 0.670 to 0.815, $p < 0.0001$) and an optimal shift efficiency threshold equal to 6.5 pm (69.5% sensitivity and 70.3% specificity) (Figure 38).

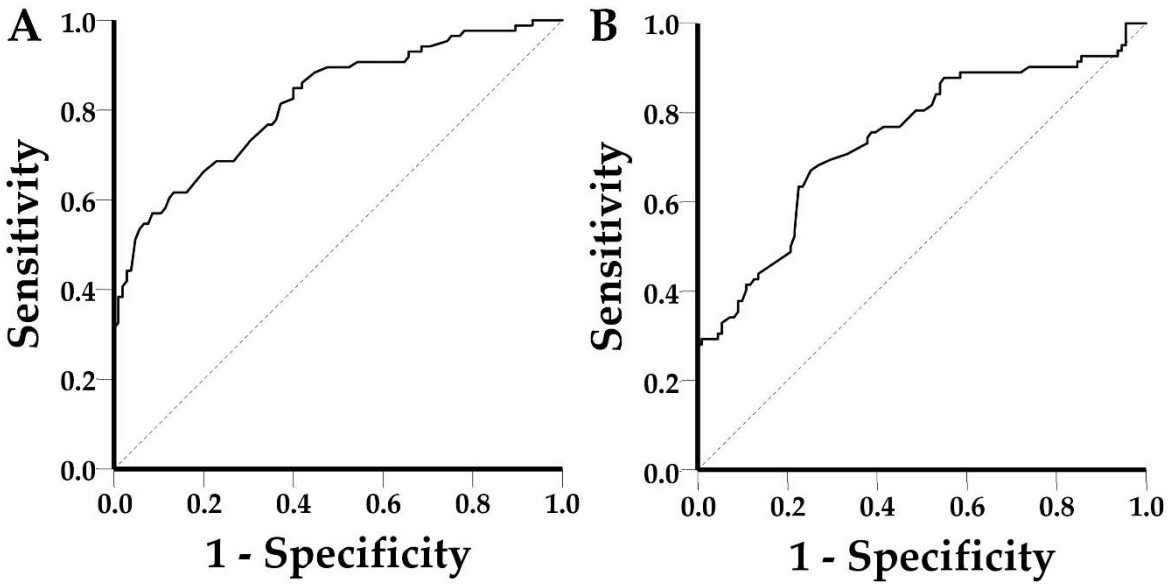


**Figure 38. "**ROC curve for PPV1 and PCV-2. The dashed line represents the diagonal reference line. (A) PPV1 ROC curve, AUC = 0.820, CI: 0.760 to 0.880, p < 0.0001 and (B) PCV-2 ROC curve, AUC = 0.742, CI: 0.670 to 0.815, p < 0.0001."

Among the PPV1/PCV-2 functionalized PICs used in the ROC curve analysis, PIC #45 showed extremely poor performance, affecting AUC values for both PPV1 and PCV-2. Excluding PIC #45 from the ROC analysis as an outlier (and consequently, from the system's diagnostic performance assessment) significantly improved the device's performance. In detail, PPV1 functionalized sensors achieved an AUC value of 0.892 (CI: 0.840 to 0.944, $p < 0.0001$) and an optimal shift efficiency threshold equal to 4.5 pm (77.1% sensitivity, 81.5% specificity) (Figure 39). PCV-2 functionalized sensors showed an AUC value of 0.788 (CI:0.712 to 0.863, $p < 0.0001$) and an optimal shift efficiency threshold equal to 6.5 pm (71.6% sensitivity and 79.7% specificity) (Figure 39).

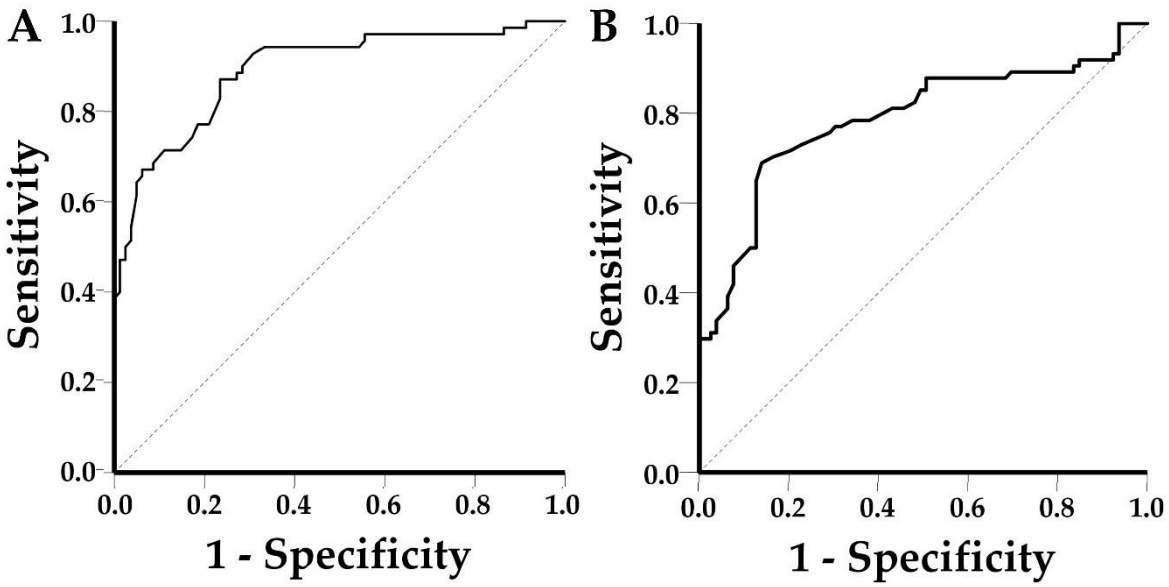


**Figure 39.** "ROC curve for PPV1 and PCV-2 excluding PIC #45 as an outlier. The dashed line represents the diagonal reference line. (A) PPV1 ROC curve, AUC = 0.892, CI: 0.840 to 0.944, p < 0.0001 and (B) PCV-2 ROC curve, AUC = 0.788, CI: 0.712 to 0.863, p < 0.0001."

AUC estimation for PPRSV and SIV included 277 and 100 valid shift responses, respectively. PRRSV sensors achieved an AUC value of 0.812 (95% CI: 0.759 to 0.866, $p < 0.0001$) and an optimal shift threshold equal to 5.5 pm (83.5% sensitivity, 77.8% specificity) (Figure 40). SIV testing resulted in an AUC value of 0.816 (95% CI: 0.719 to 0.912, $p < 0.0001$) and an optimal shift threshold equal to 3 pm (81.8% sensitivity and 82.2% specificity) (Figure 40).

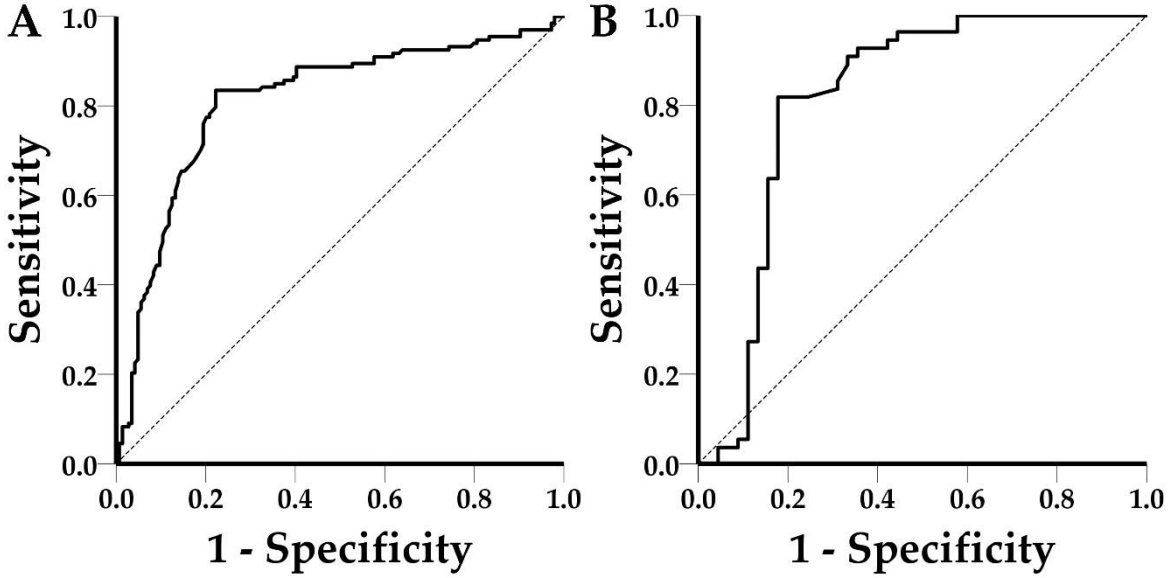


**Figure 40. "**(A) PRRSV ROC curve, AUC: 0.812, 95% CI: 0.759–0.866, p < 0.0001 and (B) SIV ROC curve, AUC: 0.816, 95% CI: 0.719–0.912, p < 0.0001."

For the estimation of the AUC values and the optimal detection threshold of ASF and CSF 177 and 272 valid results at the ring level were used, respectively. ASF

functionalized sensors achieved an AUC value of 0.832 (95% CI: 0.758 – 0.906) and an optimal shift detection threshold of 5.2 pm which corresponds to 80.8% sensitivity and to 88.5% specificity (Figure 41). Respectively, CSF functionalized sensors achieved an AUC value of 0.830 (95% CI: 0.781 – 0.880) and an optimal shift detection threshold of 5.5 pm which corresponds to 79% sensitivity and to 79.1% specificity (Figure 41).

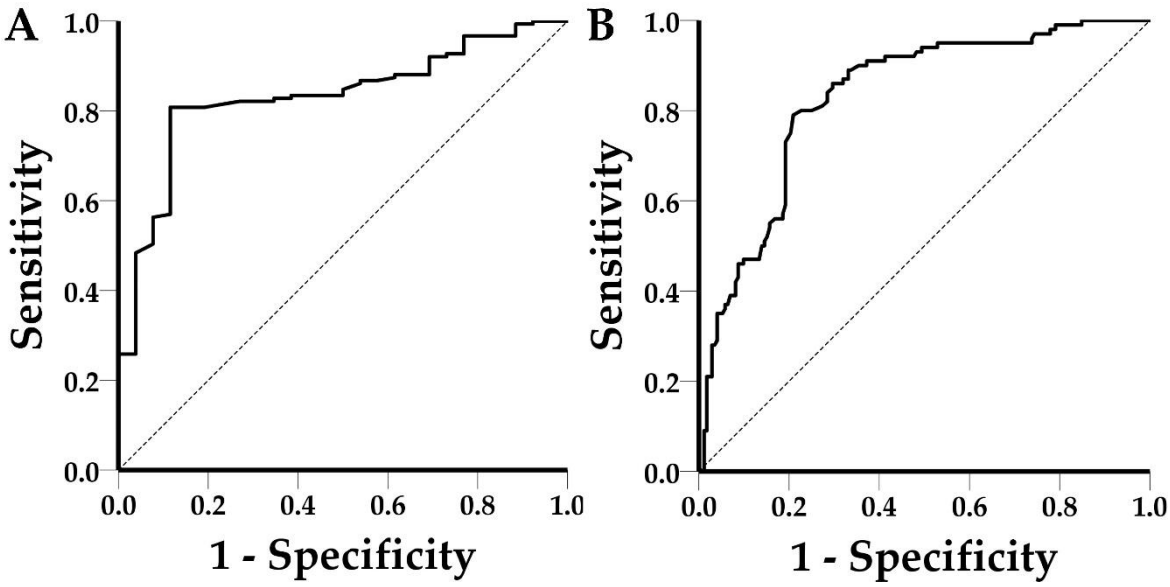


**Figure 41.** "(A) ASF ROC curve, AUC: 0.832, 95% CI: 0.758–0.906, p < 0.0001 and (B) CSF ROC curve, AUC: 0.830, 95% CI: 0.781–0.880, p < 0.0001."

## 4.5 Validation and System Performance

Sample shift responses were classified to TP, TN, FP, and FN using the optimum shift thresholds calculated in the ROC analysis. The optimum threshold values (best combination of sensitivity and specificity) were 4.5 pm for PPV1, 6.5 pm for PCV-2 (for PPV1 and PCV-2 the most conservative scenario was selected which included the low performing PIC #45), 5.5 pm for PRRSV, 3 pm for SIV, 5.2 pm for ASF and 5.5 pm for CSF. The screening results obtained for each virus using the POC device are summarized in Table 6. The performance metrics (sensitivity, specificity, accuracy, precision, PLR, NLR, DOR), along with their 95% CI, are shown in Tables 7, 8 & 9. The presented ASF results include both oral fluid and serum samples, even though serum samples showed lower overall performance. However, the overall evaluation of the POS device using both sample types is necessary, as serum testing for ASF is currently a standard diagnostic practice.

Additionally, 10 PPV1-positive, 10 PPV1-negative and 16 PCV-2 positive fecal samples were tested with the device. Out of the ten (n = 10) PPV1 positive samples, seven (n = 7) gave a true positive result and three (n = 3) were false negatives, while out of the ten (n = 10) PPV1 negative samples, nine (n = 9) gave a true negative result and one (n = 1)

gave a false positive result. Nine of the PCV-2 positive fecal samples (n = 9) gave a true positive result and seven (n = 7) gave a false negative result. One should also keep in mind that samples were consider positive based on qPCR, a technique that detects nucleic acids. It is well known that during a viral infection and subsequent recovery, viral nucleic acids remain longer in circulation than fully assembled virions. The majority of the antibodies used in the study recognize conformational epitopes on fully assembled particles. It is worth noting that the only antibody recognizing a linear epitope is that of PPV, which displayed the lowest sensitivity.

**Table 5.** "Screening results for PPV1, PCV-2, PRRSV, SIV, ASF and CSF obtained with the novel POS device versus the PCR or RT-PCR results, showing the number of TP, TN, FP, and FN for each disease."

| | | **PPV1 sample status (PCR)** | | |
|---|---|---|---|---|
| | | *Positives* | *Negatives* | *Total* |
| **Screening results obtained with the novel POS device** | *Positives* | 59 (TP) | 24 (FP) | 83 |
| | *Negatives* | 27 (FN) | 81 (TN) | 108 |
| | *Total* | 86 | 105 | 191 |
| | | **PCV-2 sample status (PCR)** | | |
| | | *Positives* | *Negatives* | *Total* |
| **Screening results obtained with the novel POS device** | *Positives* | 57 (TP) | 33 (FP) | 90 |
| | *Negatives* | 25 (FN) | 78 (TN) | 103 |
| | *Total* | 82 | 111 | 193 |
| | | **PRRSV sample status (RT-PCR)** | | |
| | | *Positives* | *Negatives* | *Total* |
| **Screening results obtained with the novel POS device** | *Positives* | 111 (TP) | 32 (FP) | 143 |
| | *Negatives* | 22 (FN) | 112 (TN) | 134 |
| | *Total* | 133 | 144 | 277 |
| | | **SIV sample status (RT-PCR)** | | |
| | | *Positives* | *Negatives* | *Total* |

| | | | | |
|---|---|---|---|---|
| **Screening results obtained with the novel POS device** | *Positives* | 45 (TP) | 8 (FP) | 53 |
| | *Negatives* | 10 (FN) | 37 (TN) | 47 |
| | *Total* | 55 | 45 | 100 |
| | | **ASF sample status (PCR)** | | |
| | | *Positives* | *Negatives* | *Total* |
| **Screening results obtained with the novel POS device** | *Positives* | 122 (TP) | 3 (FP) | 125 |
| | *Negatives* | 29 (FN) | 23 (TN) | 52 |
| | *Total* | 151 | 26 | 177 |
| | | **CSF sample status (RT-PCR)** | | |
| | | *Positives* | *Negatives* | *Total* |
| **Screening results obtained with the novel POS device** | *Positives* | 79 (TP) | 36 (FP) | 115 |
| | *Negatives* | 21 (FN) | 136 (TN) | 157 |
| | *Total* | 100 | 172 | 272 |

**Table 6.** "Performance metrics of the novel POS device for PPV1 and PCV-2 functionalized sensors."

| **Performance metrics** | **PPV1** | | **PCV-2** | |
|---|---|---|---|---|
| | **Value** | **95% CI** | **Value** | **95% CI** |
| *Sensitivity* | 68.60% | 57.70% - 78.19% | 69.51% | 58.36% - 79.20% |
| *Specificity* | 77.14% | 67.93% - 84.77% | 70.27% | 60.85% - 78.57% |
| *Accuracy*[1] | 73.30% | 66.43% - 79.43% | 69.95% | 62.95% - 76.32% |
| *Precision*[1] | 71.08% | 62.72% - 78.23% | 63.33% | 55.64% - 70.40% |
| *Positive Likelihood Ratio* | 3.00 | 2.05 - 4.39 | 2.34 | 1.70 - 3.22 |
| *Negative Likelihood Ratio* | 0.41 | 0.29 - 0.57 | 0.43 | 0.31 - 0.61 |

| | | | | |
|---|---|---|---|---|
| *Diagnostic Odds Ratio* | 7.38 | 2.97 - 11.79 | 5.39 | 1.2 - 9.58 |

[1] "Accuracy and Precision values are affected by disease prevalence in the studied sample."

**Table 7.** "Performance metrics of the novel POS device for PRRSV and SIV functionalized sensors."

| **Performance metrics** | **PRRSV** | | **SIV** | |
|---|---|---|---|---|
| | **Value** | **95% CI** | **Value** | **95% CI** |
| *Sensitivity* | 83.5% | 76.03% - 89.33% | 81.8% | 69.10% - 90.92% |
| *Specificity* | 77.8% | 70.10% - 84.28% | 82.2% | 67.95% - 92.00% |
| *Accuracy*[1] | 80.5% | 75.34% - 85.00% | 82% | 73.05% - 88.97% |
| *Precision*[1] | 77.6% | 71.69% - 82.62% | 84.9% | 74.77% - 91.43% |
| *Positive Likelihood Ratio* | 3.76 | 2.74 - 5.15 | 4.60 | 2.43 - 8.73 |
| *Negative Likelihood Ratio* | 0.21 | 0.14 - 0.31 | 0.22 | 0.12 - 0.39 |
| *Diagnostic Odds Ratio* | 17.66 | 13.98 - 21.64 | 20.81 | 10.66 - 30.96 |

[1] "Accuracy and Precision values are affected by disease prevalence in the studied sample."

**Table 8.** "Performance metrics of the novel POS device for ASF and CSF functionalized sensors."

| **Performance metrics** | **ASF** | | **CSF** | |
|---|---|---|---|---|
| | **Value** | **95% CI** | **Value** | **95% CI** |
| *Sensitivity* | 80.79% | 73.60% - 86.74% | 79.00% | 69.71% - 86.51% |
| *Specificity* | 88.46% | 69.85% - 97.55% | 79.07% | 72.22% - 84.89% |
| *Accuracy*[1] | 81.92% | 75.45% - 87.29% | 79.04% | 73.72% - 83.72% |
| *Precision*[1] | 97.60% | 93.33% - 99.16% | 68.70% | 61.74% - 74.90% |
| *Positive Likelihood Ratio* | 7.00 | 2.41 - 20.36 | 3.77 | 2.78 - 5.13 |
| *Negative Likelihood Ratio* | 0.22 | 0.15 - 0.31 | 0.27 | 0.18 - 0.39 |
| *Diagnostic Odds Ratio* | 32.25 | 13.63 - 50.87 | 14.21 | 10.17 - 18.28 |

[1] "Accuracy and Precision values are affected by disease prevalence in the studied sample."

# Chapter 5. Discussion

## 5.1 Performance summary

This work demonstrated that PICs, photonics, microfluidics, and communication technologies can be integrated into a single device for the detection of swine viral diseases in oral fluids and serum samples. PIC sensitivity and selectivity have been previously exploited in gas sensing, biomedical diagnostics, and biochemical detection (Wang *et al.*, 2016; Chandrasekar *et al.*, 2019; Hänsel and Heck, 2020). However, this is the first attempt to exploit PICs for the detection of swine viral pathogens in a POS setting. The novel device achieved LOD values ranging from $3.3 \times 10^4$ viral genome copies/mL for ASF and SIV to $3.3 \times 10^5$ viral genome copies/mL for PCV-2, PRRSV and CSF. The LOD of PPV1 functionalized sensors was higher reaching approximately $10^6$ viral genome copies/mL. In general, PIC performance was satisfactory at ring level. Sensitivity ranged from 68.60% (PPV1) to 83.50 (PRRSV), specificity from 70.27% (PCV-2) to 88.46% (ASFV), accuracy from 69.95% (PCV-2) to 82% (SIV), precision from 63.33& (PCV-2) to 97.60% (ASFV), PLR from 2.34 (PCV-2) to 7 (ASFV), NLR from 0.21 (PRRSV) to 0.43 (PCV-2) and DOR from 5.39 (PCV-2) to 32.25 (ASFV). At first glance, PRRSV, SIV, ASF and CSF sensors seem to outperform PPV1 and PCV-2 sensors in terms of sensitivity, specificity and likelihood ratios, however, the 95% CIs of the aforementioned metrics overlapped, indicating that the recorded differences were not statistically significant. PRRSV, SIV, ASF and CSF sensors showed statistically significant higher DOR values than PCV-2 sensors, whereas only PRRSV and ASF sensors had statistically significant higher DOR values than PPV1 sensors. DOR value differences between PPV1 and PCV-2 sensors, as well as between PRRSV, SIV, ASF and CSF, were not statistically significant. Excluding PIC #45 from the DOR analysis eliminated the statistically significant differences.

In another study, an integrated microfluidic platform developed for the multiplex detection of the anti-PRRSV, -CSFV, and -PCV-2 circulatory antibodies in serum achieved sensitivity of 89.74%, 96.61%, and 88.89%; specificity of 96.61%, 97.22%, and 98.31%; accuracy values of 93.88%, 96.84%, and 94.74%; and AUC values of 0.968, 0.992, and 0.989, respectively, when tested with 100 samples (Fu *et al.*, 2020). Nevertheless, direct comparisons with this study could not be made as the 95% CIs were not presented to establish statistically significant samples. Furthermore, the study does not provide sufficient information on samples and if those samples represented a wide spectrum of antibody concentrations.

## 5.2 POS device concept

Reliable POS diagnostics and tests can play a crucial role in controlling swine viral diseases and limiting their socioeconomic impact. Among the major drawbacks of POS test is the inferior performance when executed by untrained personnel. To mitigate this risk, the novel device utilized microfluidics, photonics, and information and communications technology to completely automate the analysis (delivery of fluids, measurements, and data analysis) and detect the targeted diseases. To use the novel device, oral fluid collection with cotton ropes was followed by sample dilution to a 1:1 ratio with PBS + 0.05% v/v Tween 20 + 1% w/v BSA at pH = 7.4 and filtering with 5 μm and 0.45 μm pore size syringe filters. Following this process, end-users were only required to place the sensors and add pipette tips, buffers and samples to the device, thus minimizing the user-introduced bias in the photonic measurements. Device handling was performed via a tablet using a user-friendly android application. Data analysis was also automated, and the device provided simple positive or negative results. Consequently, the device could be used by non-specialized personnel with limited, if any, impact from mishandling.

Data analysis and shift calculations were simplified by using the LOWESS algorithm to smoothen the detection plots. The algorithm provided a single “minimum” in each step facilitating the automated shift calculations and improving the efficiency of the detection algorithm. Results generated by the device were stored online using a cloud platform and appropriate data transferring applications. Cloud storage provided the capabilities for meta-analysis of results and the establishment of effective surveillance protocols against the targeted diseases. Such technological advancements can contribute to the development of telemedicine in animal production. The system followed a modular approach allowing easy servicing and replacement of broken or faulty components. The proposed syringe-based fluid delivery system is inexpensive and simple in comparison with other solutions for fluid delivery such as peristaltic pumps. The overall architecture and design of the system could potentially allow the device to be deployed directly in farms, peripheral and mobile laboratories, and border checkpoints.

From a biological perspective, the efficiency of the bio-recognition event on the sensor’s surface with the selection of appropriate antibodies largely affects the performance of the device. All antibodies were carefully selected to recognize conserved viral proteins, which are expressed in sufficient quantities, for the detection of a wide range of circulating viral strains. Mild detergents were included in the buffer solutions for the partial disassembly

of the virus envelope (in the case of enveloped viruses), thus enabling the biorecognitions of antigens in the interior of the virions. The PICs used in this work were not functionalized in an oriented way, i.e. the binding of the antibody Fc region on the sensor surface. Despite this fact, the quantity of antibodies used for functionalization sufficed for the biorecognition event to take place.

Throughout this study, the device validation and the calculation of performance metrics was done on the ring level. Three ring resonators were functionalized for a given disease in each PIC. The compilation of the information retrieved from all of the three rings for each targeted analyte could lead to a much better performance (about 90% sensitivity and specificity) at test level for all viruses, similar to the performance achieved in other studies (Fu *et al.*, 2020). This was performed by considering the response of the majority of the functionalized ring resonators as the valid result (Manessis *et al.*, 2022). For example, suppose that two out of the three functionalized rings for a given disease provided a negative output and one out of the three provided a positive output. In this case, the valid results at the test level should be considered as negative, (i.e., the absence of the targeted analyte, no detection). Even though this seems like an attractive alternative, it is far from the original planning of using a single ring resonator for each disease which would allow the multiplex detection of all of the six targeted pathogens with a single sensor.

## 5.3 LOD values

The LOD values (ranging from $3.3 \times 10^4$ viral genome copies/mL for SIV and ASF to $3.3 \times 10^5$ viral genome copies/mL for PCV-2, PRRSV and CSF) achieved in this study were sufficient for the identification of clinical cases for all of the targeted diseases. This applies to the LOD of PPV1 ($10^6$ viral genome copies/mL) as well. It is known that high levels of viral copies, exceeding $10^6$ viral genome copies/mL, in oral fluids for PPV1 or PCV-2 are linked with clinical symptoms in animals, even for these diseases that are not in general associated with clinical disease or high mortality rates (Olvera *et al.*, 2004; Miao *et al.*, 2009; Zhou *et al.*, 2016). At this point, it is important to mention that the samples were directly used in the device without a pretreatment or sample enrichment step, except syringe filtering for large particulate matter removal. In comparison, PCR and RT-LAMP assays translated into Lab-on-Chip devices using microfluidic chips showed LOD values of $10^3$ or $10^4$ viral genome copies/mL, respectively (Fu *et al.*, 2020; Jiang *et al.*, 2021). However, both assays required laboratory-based isolation of nucleic acids, which is considered a labor-intensive sample pretreatment step. As it was also mentioned earlier, the device detects fully

or partially assembled particles, meaning that using PCR as a reference method probably overestimates the viral load of samples used for the LOD experiments. It is a well-known issue in virology that viral genome copies do not always correspond to the number of infectious virions (Sender *et al.*, 2021).

## 5.4 ROC curves, sensitivity, and specificity

The recorded number of TP, FN, TN and FP relies on the following conditions: i) the selected threshold that classifies the device's response to positive or negative, ii) the inherent characteristics of the device (this includes antibodies used, the analysis protocol, mechanics/microfluidics, photonics, algorithms etc.) and iii) the balance between the tested positive and negative samples (for example the inclusion of a very limited number of positive samples would result in fewer false negatives). The ROC curves and Youden's index were exploited to identify the signal threshold that provided the best combination of sensitivity and specificity. The ROC curves practicality in the assessment of the sensitivity-specificity tradeoff is undisputed, as they can help in establishing the desired levels of sensitivity or specificity based on disease characteristics and epidemiology. For example, a POS test for the ASF virus should be highly sensitive, or in other words have high negative predictive values, considering that missing positive cases could devastate the swine sector in the infected areas and have severe socioeconomic impact. Optimum shift thresholds ranged from 3 pm for SIV to 6.5 pm for PCV-2, the corresponding sensitivities ranged from 68.60% for PPV1 to 83.5% for PRRSV and the specificities ranged from 70.27% for PCV-2 to 88.46% for ASF. At first glance, the achieved sensitivities and specificities may seem suboptimal, however, it is important to note that low positive calibrators (samples with low copy number and Ct values equal to or larger than 30) were used in the study. The inclusion of low positive samples helps to avoid the disease spectrum bias (disease spectrum bias in diagnostics refers to the inclusion of only the "best" samples with high viral load that are easily classified by the device) and consequently, the overestimation of the performance of the device (Pewsner *et al.*, 2004). Furthermore, PCR, the current diagnostic "golden standard" in swine viral disease is highly sensitive and specific, thus a lower performance was expected for the novel POS device.

Sensitivity and specificity are the two most used metrics of the performance of a diagnostic device or assay. Both metrics are intrinsic test characteristics and easily understood. Despite this, their values may change when the test is carried out in different settings and/or populations than the validation study. In fact, the assessment of the

performance of a diagnostic test should concurrently take under consideration both sensitivity and specificity. Additionally these two metrics do not suffice to assess the post-test probability and interpret test results (Pewsner *et al.*, 2004). Consequently, the calculation of other performance metrics is imperative to provide a more complete view of the performance of a diagnostic test.

## 5.5 Accuracy and precision

Accuracy is a performance metric that includes the estimates of both pre- and post-test probabilities and is defined as the proportion of true classification out of all the recorded classifications. Accuracy values ranged from 69.95% for PCV-2 to 82.00% for SIV. Accuracy can be useful in evaluating diagnostic tests through one metric but is slightly affected by disease prevalence (in this study accuracy was affected at about 1% when results were tested at various prevalence levels using Medcalc) and weighs equally the effects of false positives and false negatives. Additionally, accuracy is affected by the study population and setting. As a result, comparisons of diagnostic performance solely based on accuracy can be misleading.

The novel POS device had precision (also known as positive predictive value) values ranging from 63.33% for PCV-2 to 97.60% for ASF. The ASF sensors had statistically significant higher precision in comparison with the rest of the functionalization types. However, this can probably be explained by the ratio of positive and negative samples in the ASF group. In reality, increased prevalence in the screened population increases precision values TP/(TP + FP)) by reducing false positives as less negatives are tested. Vice versa, low prevalence resulted in reduced precision (by increasing the FP). In another study two SARS-CoV-2 nucleic acid amplification tests (PCR based) used for screening in a low-prevalence (0.14–0.41%) population achieved precision values of 61.8–89.8% and 20.1–73.8% (Skittrall *et al.*, 2021). Both precision and negative predictive values are susceptible to prevalence differences, making them unsuitable for the evaluation of diagnostic tests in different populations. In most cases, the lack of surveillance epidemiological data for swine diseases between animal groups, farms, regions, and/or countries render precision and negative predictive value impractical for the estimation of post-test probability in animal POS diagnostics (Manessis *et al.*, 2022).

## 5.6 Positive and negative likelihood ratios

To counter the issue of prevalence-induced bias in the estimation of post-probabilities through precision and negative predictive value, prevalence-independent

markers of diagnostic performance such as PLR and NLR have been suggested. The PLR and NLR utility lies in the fact that both metrics are capable to link pre- and post-test probabilities of diagnostic tests by showing how many more times a particular test result is likely to occur in the "diseased" group in comparison with the "healthy" group. PLR values greater than 1 indicate that the test result is truly associated with presence of disease. Respectively, NLR values lower than 1 indicate that the test results are associated with the absence of disease (Deeks and Altman, 2004). A general rule is that likelihood ratios above 10 or less than 0.1 are considered sufficient to rule-in or rule-out a disease, respectively (Deeks and Altman, 2004). PLR values ranged from 2.34 for PCV-2 to 7 for ASF. NLR values ranged from 0.21 for PRRSV to 0.43 for PCV-2. Although the achieved PLR and NLR values for all viruses were not ideal, especially for PPV1 and PCV-2, still the 95% CIs did not include the value 1, indicating that test results are truly associated with the sample status (negative, positive).

## 5.7 Diagnostic odds ratio

The DOR is not likely to be a test-specific constant, but its main utility is that of a global measure for the diagnostic performance of a test. It can be exploited in diagnostic test comparisons across populations regardless of disease prevalence, making DOR suitable for meta-analyses (Glas *et al.*, 2003). Based on its definition, DOR values can range from 0 to infinity. DOR values higher than 1 indicate a good test performance, values equal to 1 indicate that the test cannot discriminate the healthy and diseased groups and values lower than 1 suggest improper test result interpretation. The novel POS device achieved DOR values ranging from 5.39 for PCV-2 to 32.25 for ASF. For all viruses, DOR values were statistically significant higher than 1, implying that the system could successfully discriminate negative from positive samples. DOR, as well as the rest of the performance metrics, still relies on the spectrum of the disease in the population study, i.e. the inclusion of low positives. Moreover, DOR is not defined in 2 × 2 tables that contain zeros, and two tests with identical DOR can have very different sensitivity and specificity (Glas *et al.*, 2003).

## 5.8 Proper validation of POS diagnostics

It is important to notice that to provide a complete view of the utility and the performance of a given diagnostic test, the calculation of all the aforementioned metrics is required. Moving a step beyond, properly designed POS validation studies should also provide the framework of decision making after test result interpretation. However, this task

is rather challenging considering that to do so, detailed description of the targeted diseases, their clinical manifestation, epidemiological data, and surveillance systems must be available. It is obvious that the acquisition of these types of information is rather expensive and time consuming. This was demonstrated in a real-world example with the effort and money put in the epidemiological surveillance of SARS-Cov-2. However, the market of animal POS diagnostics and the profit margins of animal production, despite the socioeconomic impact of some animal diseases, could not easily justify the cost of full-scale surveillance programs. Unavoidably, this often results in POS devices and test validated in laboratory settings being largely ineffective in practice, as the proper diagnostic tool is not used in the proper framework and/or setting. For example, a test with 95% sensitivity and specificity would only achieve positive predictive values of only 50% in a population setting with 5% disease prevalence. This means that the hypothetical test is not appropriate to rule in the disease given a positive result. This has a significant impact as the end-user (e.g. veterinarian, farmer etc.) relies on positive predictive values to make "evidence-based" decisions. Consequently, POS manufacturers and traders should not only focus on achieving "perfect" sensitivity and specificity values, but also on providing the proper framework to maximize the effectiveness of POS testing.

Moreover, most POS tests for animal (and some cases human) diseases do not undergo sufficient validation with field trials and clinical utility evaluation, providing even less financial incentive for commercial exploitation due to the high risk of failure of diagnostic tests (Kumar *et al.*, 2015). This creates a vicious cycle of scarce investments, low-quality tests and few novel POS devices. This phenomenon is further aggravated in animal production due to the slim profit margins of both farmers, and consequently commercial companies launching POS devices. Given that the presented diagnostic device has not been sufficiently validated in the field, commercialization attempts have not yet been made.

Taking under consideration the above, it is suggested that validation studies for novel POS devices should focus on the following three points: (i) proof of concept experiments with reference samples; (ii) extensive laboratory testing with negative and positive samples that represent the whole spectrum of the disease for the calculation of the performance metrics of the device; and (iii) field testing to investigate the utility of the device for stakeholders (Manessis *et al.*, 2022). It is worth mentioning that the novel POS device underwent limited field testing, nevertheless the present study focused on the proof-of-

concept of the proposed system, as well as on the first laboratory experiment with complex sample matrices (oral fluids and serum).

## 5.9 Study impact on POS diagnostics and livestock biosecurity

Effective and timely control of swine viral diseases to mitigate transmission risks is heavily dependent on early and reliable diagnosis (Belák, 2007). The need for reliable, next-generation POS devices with extended capabilities for the detection of swine viral diseases is reflected by the willingness of consumers to invest up to 5000 euros for such a test (Nannucci *et al.*, 2020). Researchers and commercial companies aspire to meet this demand by developing cost-effective, reliable (in farm conditions), POS tests and devices. However, many methodologies and tests suffer from limitations such as low performance, cost, complexity, limited number of targeted analytes, extended analytical times, improper validation, and lack of field testing, thus resulting sometimes in low-quality tests entering the market (Hobbs *et al.*, 2021).

It was demonstrated through the present work that the novel device is a promising tool for the sensitive and specific detection of swine viral pathogens at the POS setting, given that the proper framework is provided, and specific objectives have been set. The proposed device paves the way for the integration of emerging technologies such as advanced materials, communications, microfluidics, microfabrication and photonics into portable, user-centered POS device, thus allowing the translation of core laboratory techniques into field diagnostics. Microfabrication allows the production of sensors at the μm or even the nm scale for the transduction of biomolecule interactions into measurable signals. PICs, fabricated with this technology, receive an increased research interest as an ultra-sensitive platform for the detection of pathogens and other analytes. However, this device is the first attempt to detect viral pathogens using PICs.

Overall, the system can contribute to reducing screening costs and minimize the effort and time required for the diagnosis of viral diseases. The current cost estimate for the analysis of a single sample (screening for two diseases) is EUR 0.60. The device can test up to four samples simultaneously within approximately 1 hour. The main advantage of the device is the ability of performing at farms, in the actual POS setting. The device can be used for the evaluation of the health status of animals, slightly prior or during the onset of the disease, thus supporting evidence-based disease control strategies. For example, POS tests with mediocre performance (70% sensitivity and specificity such as this device for PCV-2) are used to manage disease outbreaks with high prevalence where rapid and

inexpensive testing can help reduce the impact of the disease by eradicating "superspreaders" i.e. animals with high viral load that shed the virus in the environment and infect a large number of animals. Finally, the device could be exploited at border checkpoints or during the purchase of animals for disease screening. In this case, the rapid and reliable identification of negative animals, i.e. a high negative predictive value/high sensitivity, is of utmost importance so that the import or purchase can take place immediately. On the other hand, if suspected cases are detected the import/purchase can be delayed until the necessary laboratory confirmation takes place without posing any risk for the buyer.

The device also focused on oral fluids as the main sample type for the detection of the targeted diseases. Oral fluids are non-intrusive, easy to collect, cost-effective and suitable for herd screening (Ramirez *et al.*, 2012; Bjustrom-Kraft *et al.*, 2018; Henao-Diaz *et al.*, 2020). Despite the unquestionable utility of oral fluids, other sample types such as serum, fecal samples or nasal swabs can be exploited with adaptions in the analysis protocol such as sample pre-treatment, different dilution factors, and the use of alternative buffers. Serum samples, although more complicated to collect, remain popular and are integral parts of standard diagnostic practice for disease surveillance. On the other hand, fecal samples are necessary for monitoring Enterobacteriaceae pathogens or some swine viral pathogens such as PPV1 or PCV-2. Considering that the use of antibodies that recognize different antigens (viruses, circulatory antibodies, etc.) typically found in other sample types could potentially widen the panel of analytes that could be detected with the novel POS device, the investigation of alternative sample types should remain a priority.

Although the presented results are indeed promising and a multitude of novelties were introduced in the field of veterinary POS diagnostics, the device failed to quantify the samples as presented in the LOD experiments. The proposed solutions to this issue include the immobilization of the antibodies on the sensor surface in an oriented way and increasing PIC uniformity. As it was previously demonstrated, the PPV1 and PCV-2 values could be significantly improved from 0.820 and 0.742 to 0.892 and 0.788, respectively, just by excluding the low performing PIC #45. Another study limitation is the relatively wide 95% CIs for each performance metrics, especially for SIV. To reduce the 95% CIs and provide a much more precise performance assessment of the device, the number of tested samples should be increased. The main restrictive factor was the number of available sensors, as the work done mainly focused on proving the concept of the device and providing the first validation data.

Future research on the proposed concept should focus on three main aspects: MREs, PICs and increased study size. The targeting of different antigen epitopes with alternative MREs could allow the identification of other viral strains, viruses or other analytes to widen the panel of detectable diseases and improve the performance of the device. Epidemiological surveillance and using antibodies that recognize the majority of circulating viral strains is necessary to constantly keep the device updated. Additionally, the oriented immobilization of antibodies could improve both the performance of the device and its quantification capabilities. The use of 3D microprinters in the functionalization procedure of both antibodies (detection ring resonators) and blocking proteins (reference ring resonators) can reduce the background and refine signal resolution. The standardization of materials and procedures and completely automated PIC fabrication processes could further reduce the tolerances in PIC manufacturing and improve the performance of the device. Future studies should focus on testing different sample types and increasing the number of tests to reduce the CIs and unveil any system/sensor limitations that were not detected in this work. Finally, extensive field validation studies are required to increase the technology readiness level (TRL) of the device and successfully translate the research results into a commercially successful POS device.

## 5.10 Challenges of POS testing in farm animals

POS testing is slowly gaining popularity as an integral part of standard veterinary practice. This phenomenon could probably be attributed to the popularization and globalization of POS testing in human medicine, especially through the COVID-19 crisis. Despite the success and development of various POS tests in human medicine, the adoption of POS testing in animal production is still lacking due to the unique socioeconomic status of the sector.

Firstly, the profit margin in animal production remains slim, thus limiting the disposable income of farmers (Manessis, Gelasakis and Bossis, 2019). Consequently, with the exception of devastating disease outbreaks, the investments in POS diagnostics or the prolonged use of field tests is uncommon and sometimes unjustified. Substantial investments are required to develop novel POS devices including research, validation and marketing costs. As a result, and given the limited market share, POS manufacturers usually lack the financial incentives to commercially launch new devices and tests or even maintain the supply of developed diagnostics. The transition of proof-of-concept prototypes to commercial devices is further hampered by the unwillingness of private companies to share

technological advancements and intellectual property constraints (Teles and Fonseca, 2015). For these reasons, this study received funding for the European Commission through the Horizon 2020 program. Apart from the aforementioned challenges, POS development and production is stalled by the incompatibility of certain fabrication methods with scaled up manufacturing processes and/or by the cost of raw materials such as glass, thermoplastics etc. (Chin, Linder and Sia, 2012), thus making the production costs of POS diagnostics prohibitive for animal farming (Manessis, Gelasakis and Bossis, 2019). The main challenge faced during the production of PICs was the standardization of the fabrication method which resulted initially in PICs with tolerances. However, the PICs used in this study were fabricated using a standardized protocol. Other limitations during PIC fabrication included the use of specialized equipment (such as clean rooms and machinery for aligning the optic fibers with the grating couplers of the sensors) as well as delayed supply chains for raw materials due to the Covid-19 crisis.

Portability and the ability to perform analytical diagnostic procedures in the field are the very essence of POS devices and tests. Despite that, many proposed POS methodologies fail to meet these key requirements. Among the most important factors that limit portability and POS testing outside laboratory settings are the complex sample pretreatment (the isolation of nucleic acids, enrichment, labeling etc.) and handling, the limited lifetime of reagents, the integration level and device packaging and size, powering, user friendliness and complex interpretation of test results and data sharing capabilities (Srinivasan and Tung, 2015). Although the majority of these challenges were addressed with the suggested approach the device remains somewhat bulky. During the work done in this thesis, an alternative design which reduced length by 10 cm and width and height by 5 cm was suggested which was partially implemented for the devices delivered to Italy, Hungary and Poland. Processivity is critical for farmers or field veterinarians that usually must test hundreds, or even thousands of animals for screening and epidemiological surveillance purposes (Manessis, Gelasakis and Bossis, 2019). This device could test up to 4 samples simultaneously within 1 hour. Although some level of processivity was achieved it remained suboptimal. Finally, multiplexing can be critical for successful POS testing, especially to facilitate differential diagnosis given that most animal diseases lack pathognomonic signs and symptoms. This device offered some multiplexing, and a sample could be tested simultaneously for all of the six diseases using three out of the four sample slots, however it was far from the original concept and theoretical capability of testing all of the 6 diseases in one PIC/slot (this is why the validation was done at the ring level). Increasing the level of

multiplexing could potentially further reduce screening costs, by reducing the number of the sensors required for the testing against all of the six viral diseases.

As it was previously mentioned, several POS devices and tests enter the market without being adequately validated (Hobbs *et al.*, 2021). Most validation studies are not transparent in terms of study design, sample inclusion criteria, and differences between the study and target populations, whereas most of the time present overoptimistic results (Hobbs *et al.*, 2021). Moreover, the 95% confidence intervals of the various performance metrics are rarely presented or discussed hampering the comparisons with other tests or the robust evaluation of test performance. Evaluation studies of POS methodologies or even sometimes POS devices and tests, exclude clinical, complex sample matrices, which usually include contaminants (particulate matter, blood, mucus, or feces), thus overestimating the performance of these methods. This study was designed to address this issue. It is crucial that research focuses on improving the automated, on-chip sample pretreatment and handling to facilitate the translation of POS methods to actual field devices. The proposed POS device is practically completely automated with minimal user interference apart from adding the sample. Finally, disease epidemiology also affects the performance of POS devices and tests in field conditions. Including high prevalence populations in the validation studies can artificially inflate positive predictive value and vice versa, rendering these values irrelevant to real world scenarios (Hobbs *et al.*, 2021). Considering that this thesis focuses on the laboratory validation of the device with complex, clinical samples, epidemiological data were not acquired but rather a balanced approach between the testing of positive and negative samples was followed to investigate the performance metrics of the device and reveal any limitations on the diagnostic protocol.

End-users and especially farmers are often characterized by the inability to exploit new avenues, requiring extensive evidence before investing in new technologies (Manessis, Gelasakis and Bossis, 2019). To successfully promote POS testing, farmers should be familiarized with novel, sensor-based technologies in livestock management (Neethirajan, 2020). Additionally, POS manufacturers should also provide the necessary framework, tailored to local conditions and disease epidemiology, for efficient testing. As most farmers lack the scientific background to interpret test results in conjunction with disease characteristics and epidemiology, they usually rely on veterinarians, animal scientists or POS manufacturers to fully exploit the added value of novel diagnostic tools. Achieving this goal exceeded the objectives of the present thesis. However, in case of future commercial exploitation further investigations to define the proper framework will be performed.

Finally, it is important to notice that existing legislation can be pivotal in the successful adoption of POS testing. Very strict regulation may inhibit the development and marketing of novel technological solutions, as the alignment with strict legal requirements can be costly. On the contrary, the absence of regulation may result in the introduction of poorly validated, low-quality POS devices entering the market, thus further limiting the adoption of POS testing. A balanced regulatory approach can both promote the development and marketing of novel POS devices and also protect and safeguard consumers from low quality products.

## 5.11 Future perspectives

The development of nanomaterials and microfabrication and their integration with novel instrumentation approaches and sensors into POS devices and tests present exciting opportunities for the non-intrusive, real-time monitoring of animal health, behavior, and physiology (Neethirajan, 2020). For example, nanomaterials including colloidal gold, noble metals, fluorescent and magnetic nanoparticles, quantum dots, nanozymes, conjugated polymers, surface-enhanced Raman scattering (SERS)-active nanomaterials, and carbon nanomaterials have been exploited to label the targeted analytes and improve the sensitivity of LFA tests, as well as to allow the integration of LFAs with miniaturized reading equipment (Nguyen and Kim, 2020; Guo *et al.*, 2021; Lou *et al.*, 2022). Under the same concept, plasmonic nanoparticles combined with photothermal and photoacoustic methodologies have been exploited in LFA testing (Ye *et al.*, 2020). Additionally, novel materials used in biosensing such as molecularly imprinted polymers, carbon-allotrope-based nanomaterials, nanocages, nanoshells, nanowires, nanostructured films and hydrogels, dendrimers, hyperbranched polymeric nanoparticles, and covalent organic frameworks, offer new opportunities in methodology development and analyte detection (Pirzada and Altintas, 2019; Denmark, Mohapatra and Mohapatra, 2020). To limit the reliance on specialized and often expensive materials for the creation of sensors, the current methodology focused on the label-free detection of viral pathogens. Provided that further studies and improvement of PICs will be performed, the device could actually limit the reliance on labeling or complex and expensive signal-enhancement techniques.

Advanced materials such as PDMS and thermoplastic materials, and cutting-edge production techniques such as soft lithography, 3D printing, paper microfluidics and the automated laser-printer deposition of hydrophobic ink allow the mass production of POS devices and tests (Mejía-Salazar *et al.*, 2020; S.-M. Yang *et al.*, 2022). Mass production is

associated with significant reduction of manufacturing costs, and consequently testing costs. Furthermore, mass production can maintain a steady supply of POS diagnostics in the market and meet demand surges. Although mass production was not attempted, antibodies were 3D printed on the sensor surfaces, thus greatly reducing the functionalization times. Apart from performance and production costs, the disposal of biological materials and waste is another important aspect of POS devices and tests. Microfluidic devices can reduce the total waste in POS application due to the low requirements in sample and reagents. In microfluidic devices, waste is usually collected in tanks, making disinfection and disposal easier. This approach was also followed in the proposed device. In fact, the analysis of one sample, including PIC regeneration and sample volumes, required only 2.4 ml of fluids. Incineration can be also used to dispose paper-based diagnostics tests. Such approaches can minimize biohazards, simplify waste control and reduce waste management costs.

Miniaturization of device components and reading equipment is essential to achieve a higher level of integration in POS devices (D. Liu *et al.*, 2020). Simple reading equipment from thermometers and pH meters to low-cost microscopes, SPR readers, and portable SERS readers have already been integrated into POS devices to improve portability and enable full sample analyses into single platforms (Tran *et al.*, 2019; D. Liu *et al.*, 2020). Although the size of the device is not optimal, the used methodology achieved to integrate all the necessary equipment into a single device which was capable of operating in the field. Smartphones have been used as instrumental interfaces, dongles, microscopes, or test result readers (bright-field, colorimetric, and fluorescent measurements. Enhancement of the signal detection properties of smartphones with 3D-printed modules, mobile applications, and various accessories, can make them powerful platforms for POS testing allowing the exploitation of their high-quality digital cameras, computer processors, touchscreen interfaces, wireless-data-transfer capabilities, as well as their wide adoption (Vashist *et al.*, 2015; Ong and Poljak, 2020). The combination of smartphone data-transfer capabilities and cloud-based POS platforms can facilitate data sharing to specialists and health centers, thus facilitating the development of telemedicine (Xu *et al.*, 2015). This device exploited a cloud-based platform for data storage and sharing. This paves the way for the integration of telemedicine and animal tracking to allow the real-time epidemiological surveillance and the implementation of evidence-based disease-control strategies.

To date, multiplex pathogen detection and identification is performed in centralized laboratories using specialized equipment and trained personnel, as veterinary services usually lack field tests with these characteristics (Teles and Fonseca, 2015). Multiplexing in

POS devices is critical as the detection of a single analyte may not be informative for the diagnosis of some diseases, and often does not suffice to assess the progress of diseases (Gil Rosa *et al.*, 2022). The detection of a multitude of discriminative biomarkers using multiplexed sensors and POS devices can improve the detection accuracy of complex diseases. Furthermore, multiplexing in general requires fewer materials, reduces the required sample and reagent volumes and analysis times and offers higher throughput (Vashist, 2021; Gil Rosa *et al.*, 2022). Approaches such as microarrays, antibody spotting, spatial multiplexing, time division, frequency division, and particle-based and barcoded multiplexing have already been used in some multiplexed POS applications (Gil Rosa *et al.*, 2022, p. 20). In our case, better PIC fabrication and oriented functionalization could improve the performance of ring resonators and consequently allow a higher level of multiplexing.

To summarize, the development of nanomaterials and microfabrication technologies, along with miniaturization, smartphones and multiplexing methodologies can reduce production costs, improve the performance and commercialization of POS devices and lead to the decentralization of disease diagnosis (Teles and Fonseca, 2015). However, to achieve these objectives researchers and POS manufacturers must first overcome the multitude of POS testing challenges.

# Chapter 6. Conclusions

POS devices can contribute to the optimization of livestock biosecurity by providing fast, reliable and low-cost tests in field conditions to diagnose animal diseases and identify risk factors. Towards this goal, various technologies and novel materials have been used to produce a multitude of POS tests, from LFAs and microfluidic paper-based devices to sensors and fully integrated Lab-on-Chip devices. In the present work, photonics, microfluidics, and information and communications technologies were integrated into a single and portable device paving the way for the next generation of animal POS diagnostics. The first validation data showed that the novel device is a promising tool with satisfactory performance that can potentially reduce the time and costs required for the diagnosis of swine viral diseases, and at the same time enable rapid and local decision making for the implementation of evidence-based disease control measures. Future research should focus on reducing the current system limitations, improving PIC fabrication processes, the performance of the device and multiplexing, implementing large-scale field validation studies, providing the necessary framework for proper usage of the device and increasing the Technology Readiness Level TRL of the device for successful commercialization. The development and the commercialization of advanced POS devices through the exploitation of recent technological breakthroughs is expected to overcome the current limitations of POS methodologies, and finally realize the translation of cutting-edge laboratory techniques to accessible and user-friendly devices and tests that improve the biosecurity, resilience, and sustainability of animal farming. This work is a small contribution towards this goal.

The development and validation of the device, as well as a large portion of this work was funded by EU's "H2020 SWINOSTICS project under the grant agreement ID 771649".

# References


Abd El Wahed, A., Weidmann, M. and Hufert, F.T. (2015) 'Diagnostics-in-a-Suitcase: Development of a portable and rapid assay for the detection of the emerging avian influenza A (H7N9) virus', *Journal of Clinical Virology*, 69, pp. 16–21. Available at: https://doi.org/10.1016/j.jcv.2015.05.004.

Agrawal, A. *et al.* (2020) 'Gold nanoparticle based immunochromatographic biosensor for rapid diagnosis of Mycobacterium avium subspecies paratuberculosis infection using recombinant protein', *Journal of Microbiological Methods*, 177, p. 106024. Available at: https://doi.org/10.1016/j.mimet.2020.106024.

Ahmed, S.R. *et al.* (2018) 'Optoelectronic fowl adenovirus detection based on local electric field enhancement on graphene quantum dots and gold nanobundle hybrid', *Biosensors and Bioelectronics*, 103, pp. 45–53. Available at: https://doi.org/10.1016/j.bios.2017.12.028.

Ahmed, S.R., Nagy, É. and Neethirajan, S. (2017) 'Self-assembled star-shaped chiroplasmonic gold nanoparticles for an ultrasensitive chiro-immunosensor for viruses', *RSC Advances*, 7(65), pp. 40849–40857. Available at: https://doi.org/10.1039/C7RA07175B.

Åkerstedt, M. *et al.* (2006) 'Biosensor assay for determination of haptoglobin in bovine milk', *Journal of Dairy Research*, 73(3), pp. 299–305. Available at: https://doi.org/10.1017/S0022029906001774.

Akyazi, T., Basabe-Desmonts, L. and Benito-Lopez, F. (2018) 'Review on microfluidic paper-based analytical devices towards commercialisation', *Analytica Chimica Acta*, 1001, pp. 1–17. Available at: https://doi.org/10.1016/j.aca.2017.11.010.

Ali, M.M. *et al.* (2017) 'A Printed Multicomponent Paper Sensor for Bacterial Detection', *Scientific Reports*, 7(1), p. 12335. Available at: https://doi.org/10.1038/s41598-017-12549-3.

Antonis, A.F.G. *et al.* (2006) 'A novel recombinant virus-like particle vaccine for prevention of porcine parvovirus-induced reproductive failure', *Vaccine*, 24(26), pp. 5481–5490. Available at: https://doi.org/10.1016/j.vaccine.2006.03.089.

Arora, K. *et al.* (2007) '*Escherichia coli* Genosensor Based on Polyaniline', *Analytical Chemistry*, 79(16), pp. 6152–6158. Available at: https://doi.org/10.1021/ac070403i.

Bahadır, E.B. and Sezgintürk, M.K. (2016) 'Lateral flow assays: Principles, designs and labels', *TrAC Trends in Analytical Chemistry*, 82, pp. 286–306. Available at: https://doi.org/10.1016/j.trac.2016.06.006.

Barman, N.N. *et al.* (2010) 'Molecular Characterization of Classical swine fever virus Involved in the Outbreak in Mizoram', *Indian Journal of Virology*, 21(1), pp. 76–81. Available at: https://doi.org/10.1007/s13337-010-0006-z.

Barnett, J.M. *et al.* (2020) 'Initial trail results of a magnetic biosensor for the rapid detection of Porcine Reproductive and Respiratory Virus (PRRSV) infection', *Sensing and Bio-Sensing Research*, 27, p. 100315. Available at: https://doi.org/10.1016/j.sbsr.2019.100315.

Bayramoglu, G. *et al.* (2019) 'Rapid and label-free detection of Brucella melitensis in milk and milk products using an aptasensor', *Talanta*, 200, pp. 263–271. Available at: https://doi.org/10.1016/j.talanta.2019.03.048.

Belák, S. (2007) 'Molecular diagnosis of viral diseases, present trends and future aspects', *Vaccine*, 25(30), pp. 5444–5452. Available at: https://doi.org/10.1016/j.vaccine.2006.11.068.

Bellini, S. (2021) '7. The pig sector in the European Union', in L. Iacolina et al. (eds) *Understanding and combatting African Swine Fever*. The Netherlands: Wageningen Academic Publishers, pp. 183–195. Available at: https://doi.org/10.3920/978-90-8686-910-7_7.

Bhatta, D. *et al.* (2012) 'Rapid Detection of Foot-and-Mouth Disease Virus with Optical Microchip Sensors', *Procedia Chemistry*, 6, pp. 2–10. Available at: https://doi.org/10.1016/j.proche.2012.10.124.

Bhattacharya, M. *et al.* (2011) 'Carbon nanotube based sensors for the detection of viruses', *Sensors and Actuators B: Chemical*, 155(1), pp. 67–74. Available at: https://doi.org/10.1016/j.snb.2010.11.025.

Bjustrom-Kraft, J. *et al.* (2018) 'The use of oral fluid diagnostics in swine medicine', *Journal of Swine Health and Production*, 26(5).

Blome, S. *et al.* (2017) 'Classical Swine Fever—An Updated Review', *Viruses*, 9(4), p. 86. Available at: https://doi.org/10.3390/v9040086.

Bonin, E. *et al.* (2018) 'Molecular subtyping of European swine influenza viruses and scaling to high-throughput analysis', *Virology Journal*, 15(1), p. 7. Available at: https://doi.org/10.1186/s12985-018-0920-z.

Borisov, S.M. and Wolfbeis, O.S. (2008) 'Optical Biosensors', *Chemical Reviews*, 108(2), pp. 423–461. Available at: https://doi.org/10.1021/cr068105t.

Brady, M.A., Dennis, J.S. and Wagner-Mann, C. (2003) 'Evaluating the use of plasma hematocrit samples to detect ketones utilizing urine dipstick colorimetric methodology in diabetic dogs and cats: Use of plasma hematocrit samples', *Journal of Veterinary Emergency and Critical Care*, 13(1), pp. 1–6. Available at: https://doi.org/10.1046/j.1435-6935.2003.00057.x.

Brunborg, I.M. *et al.* (2007) 'Association of Myocarditis with High Viral Load of Porcine Circovirus Type 2 in Several Tissues in Cases of Fetal Death and High Mortality in Piglets. A Case Study', *Journal of Veterinary Diagnostic Investigation*, 19(4), pp. 368–375. Available at: https://doi.org/10.1177/104063870701900405.

Brüning-Richardson, A. *et al.* (2011) 'Improvement and development of rapid chromatographic strip-tests for the diagnosis of rinderpest and peste des petits ruminants viruses', *Journal of Virological Methods*, 174(1–2), pp. 42–46. Available at: https://doi.org/10.1016/j.jviromet.2011.03.016.

Busin, V. *et al.* (2016) 'Opportunities and challenges for the application of microfluidic technologies in point-of-care veterinary diagnostics', *Molecular and Cellular Probes*, 30(5), pp. 331–341. Available at: https://doi.org/10.1016/j.mcp.2016.07.004.

Caglayan, M.G. *et al.* (2016) 'Fluorescent zinc and copper complexes for detection of adrafinil in paper-based microfluidic devices', *Chemical Communications*, 52(53), pp. 8279–8282. Available at: https://doi.org/10.1039/C6CC03640F.

Carrier, J. *et al.* (2004) 'Evaluation and Use of Three Cowside Tests for Detection of Subclinical Ketosis in Early Postpartum Cows', *Journal of Dairy Science*, 87(11), pp. 3725–3735. Available at: https://doi.org/10.3168/jds.S0022-0302(04)73511-0.

Carrilho, E., Martinez, A.W. and Whitesides, G.M. (2009) 'Understanding Wax Printing: A Simple Micropatterning Process for Paper-Based Microfluidics', *Analytical Chemistry*, 81(16), pp. 7091–7095. Available at: https://doi.org/10.1021/ac901071p.

Chai, Y. *et al.* (2012) 'Rapid and Sensitive Detection of Salmonella Typhimurium on Eggshells by Using Wireless Biosensors', *Journal of Food Protection*, 75(4), pp. 631–636. Available at: https://doi.org/10.4315/0362-028X.JFP-11-339.

Chand, R.J., Trible, B.R. and Rowland, R.R. (2012) 'Pathogenesis of porcine reproductive and respiratory syndrome virus', *Current Opinion in Virology*, 2(3), pp. 256–263. Available at: https://doi.org/10.1016/j.coviro.2012.02.002.

Chandrasekar, R. *et al.* (2019) 'Photonic integrated circuits for Department of Defense-relevant chemical and biological sensing applications: state-of-the-art and future outlooks', *Optical Engineering*, 58(02), p. 1. Available at: https://doi.org/10.1117/1.OE.58.2.020901.

Chang'a, J.S. *et al.* (2019) 'Symptomatic and asymptomatic cases of African swine fever in Tanzania', *Transboundary and Emerging Diseases*, 66(6), pp. 2402–2410. Available at: https://doi.org/10.1111/tbed.13298.

Chen, C. and Wang, J. (2020) 'Optical biosensors: an exhaustive and comprehensive review', *The Analyst*, 145(5), pp. 1605–1628. Available at: https://doi.org/10.1039/C9AN01998G.

Chen, J.Y., Penn, L.S. and Xi, J. (2018) 'Quartz crystal microbalance: Sensing cell-substrate adhesion and beyond', *Biosensors and Bioelectronics*, 99, pp. 593–602. Available at: https://doi.org/10.1016/j.bios.2017.08.032.

Chen, L. *et al.* (2015) 'An aqueous platinum nanotube based fluorescent immuno-assay for porcine reproductive and respiratory syndrome virus detection', *Talanta*, 144, pp. 324–328. Available at: https://doi.org/10.1016/j.talanta.2015.06.061.

Chin, C.D., Linder, V. and Sia, S.K. (2012) 'Commercialization of microfluidic point-of-care diagnostic devices', *Lab on a Chip*, 12(12), p. 2118. Available at: https://doi.org/10.1039/c2lc21204h.

Cho, J.G. and Dee, S.A. (2006) 'Porcine reproductive and respiratory syndrome virus', *Theriogenology*, 66(3), pp. 655–662. Available at: https://doi.org/10.1016/j.theriogenology.2006.04.024.

Choi, E.-J. *et al.* (2012) 'A survey of porcine reproductive and respiratory syndrome among wild boar populations in Korea', *Journal of Veterinary Science*, 13(4), p. 377. Available at: https://doi.org/10.4142/jvs.2012.13.4.377.

Choi, J.R. *et al.* (2016) 'An integrated paper-based sample-to-answer biosensor for nucleic acid testing at the point of care', *Lab on a Chip*, 16(3), pp. 611–621. Available at: https://doi.org/10.1039/C5LC01388G.

Choi, J.-W. *et al.* (2006) 'Lab-on-a-Chip for Monitoring the Quality of Raw Milk', *Journal of Microbiology and Biotechnology*, 16(8), pp. 1229–1235. Available at: https://koreascience.kr/article/JAKO200634718411415.pdf

Chowdry, V.K. *et al.* (2014) 'Development of a loop-mediated isothermal amplification assay combined with a lateral flow dipstick for rapid and simple detection of classical swine fever virus in the field', *Journal of Virological Methods*, 197, pp. 14–18. Available at: https://doi.org/10.1016/j.jviromet.2013.11.013.

Cino-Ozuna, A.G. *et al.* (2011) 'Characterization of a New Disease Syndrome Associated with Porcine Circovirus Type 2 in Previously Vaccinated Herds', *Journal of Clinical Microbiology*, 49(5), pp. 2012–2016. Available at: https://doi.org/10.1128/JCM.02543-10.

Cleveland, W.S. (1979) 'Robust Locally Weighted Regression and Smoothing Scatterplots', *Journal of the American Statistical Association*, 74(368), pp. 829–836. Available at: https://doi.org/10.1080/01621459.1979.10481038.

Correa-Fiz, F. *et al.* (2020) 'Porcine circovirus 2 (PCV2) population study in experimentally infected pigs developing PCV2-systemic disease or a subclinical infection', *Scientific Reports*, 10(1), p. 17747. Available at: https://doi.org/10.1038/s41598-020-74627-3.

Corzo, C.A. *et al.* (2010) 'Control and elimination of porcine reproductive and respiratory syndrome virus', *Virus Research*, 154(1–2), pp. 185–192. Available at: https://doi.org/10.1016/j.virusres.2010.08.016.

Creedon, N. *et al.* (2018) 'Label-free impedimetric nanoband sensor for detection of both Bovine Viral Diarrhoea virus (BVDV) and antibody (BVDAb) in serum', *ChemRxiv*. Available at: 10.26434/chemrxiv.7326719.v1

Cui, S. *et al.* (2008) 'A simple and rapid immunochromatographic strip test for detecting antibody to porcine reproductive and respiratory syndrome virus', *Journal of Virological Methods*, 152(1–2), pp. 38–42. Available at: https://doi.org/10.1016/j.jviromet.2008.05.029.

Cui, X. *et al.* (2016) 'A volumetric meter chip for point-of-care quantitative detection of bovine catalase for food safety control', *Analytica Chemica Acta*, 935, pp. 207–212. Available at: https://doi.org/10.1016/j.aca.2016.07.046.

Cummins, B.M., Ligler, F.S. and Walker, G.M. (2016) 'Point-of-care diagnostics for niche applications', *Biotechnology Advances*, 34(3), pp. 161–176. Available at: https://doi.org/10.1016/j.biotechadv.2016.01.005.

Davaji, B. and Lee, C.H. (2014) 'A paper-based calorimetric microfluidics platform for bio-chemical sensing', *Biosensors and Bioelectronics*, 59, pp. 120–126. Available at: https://doi.org/10.1016/j.bios.2014.03.022.

Deeks, J.J. and Altman, D.G. (2004) 'Diagnostic tests 4: likelihood ratios', *BMJ* 17, pp. 329. Available at: 10.1136/bmj.329.7458.168.

Delaney, J.L. *et al.* (2011) 'Electrogenerated Chemiluminescence Detection in Paper-Based Microfluidic Sensors', *Analytical Chemistry*, 83(4), pp. 1300–1306. Available at: https://doi.org/10.1021/ac102392t.

Denmark, D.J., Mohapatra, S. and Mohapatra, S.S. (2020) 'Point-of-Care Diagnostics: Molecularly Imprinted Polymers and Nanomaterials for Enhanced Biosensor Selectivity and Transduction', *The EuroBiotech Journal*, 4(4), pp. 184–206. Available at: https://doi.org/10.2478/ebtj-2020-0023.

Diouani, M.F. *et al.* (2008) 'Miniaturized biosensor for avian influenza virus detection', *Materials Science and Engineering: C*, 28(5–6), pp. 580–583. Available at: https://doi.org/10.1016/j.msec.2007.10.043.

Dittrich, P.S., Tachikawa, K. and Manz, A. (2006) 'Micro Total Analysis Systems. Latest Advancements and Trends', *Analytical Chemistry*, 78(12), pp. 3887–3908. Available at: https://doi.org/10.1021/ac0605602.

Dixon, L.K. *et al.* (2020) 'African Swine Fever Epidemiology and Control', *Annual Review of Animal Biosciences*, 8(1), pp. 221–246. Available at: https://doi.org/10.1146/annurev-animal-021419-083741.

Dokland, T. (2010) 'The structural biology of PRRSV', *Virus Research*, 154(1–2), pp. 86–97. Available at: https://doi.org/10.1016/j.virusres.2010.07.029.

Donadeu, M. (1999) 'Using polymerase chain reaction to obtain PRRSV-free piglets from endemically infected herds', *Swine Health and Production*, 7(6). Available at: http://hdl.handle.net/10261/289321

Dong, S. *et al.* (2015) 'Electrochemical DNA Biosensor Based on a Tetrahedral Nanostructure Probe for the Detection of Avian Influenza A (H7N9) Virus', *ACS Applied Materials & Interfaces*, 7(16), pp. 8834–8842. Available at: https://doi.org/10.1021/acsami.5b01438.

Drain, P.K. *et al.* (2014) 'Diagnostic point-of-care tests in resource-limited settings', *The Lancet Infectious Diseases*, 14(3), pp. 239–249. Available at: https://doi.org/10.1016/S1473-3099(13)70250-0.

Drolet, R. (1999) 'Porcine dermatitis and nephropathy syndrome (PDNS): An overview of the disease', *Swine Health and Production*, 7(6). Available at: https://www.aasv.org/jshap/issues/v7n6/v7n6p283.pdf

Duarte, C. *et al.* (2016) 'Semi-Quantitative Method for Streptococci Magnetic Detection in Raw Milk', *Biosensors*, 6(2), p. 19. Available at: https://doi.org/10.3390/bios6020019.

Edwards, S. *et al.* (2000) 'Classical swine fever: the global situation', *Veterinary Microbiology*, 73(2–3), pp. 103–119. Available at: https://doi.org/10.1016/S0378-1135(00)00138-3.

El Ichi, S. *et al.* (2014) 'Microconductometric immunosensor for label-free and sensitive detection of Gram-negative bacteria', *Biosensors and Bioelectronics*, 54, pp. 378–384. Available at: https://doi.org/10.1016/j.bios.2013.11.016.

Eltzov, E. *et al.* (2015) 'Lateral Flow Immunoassays - from Paper Strip to Smartphone Technology', *Electroanalysis*, 27(9), pp. 2116–2130. Available at: https://doi.org/10.1002/elan.201500237.

Eltzov, E. and Marks, R.S. (2016) 'Miniaturized Flow Stacked Immunoassay for Detecting *Escherichia coli* in a Single Step', *Analytical Chemistry*, 88(12), pp. 6441–6449. Available at: https://doi.org/10.1021/acs.analchem.6b01034.

Eltzov, E. and Marks, R.S. (2017) 'Colorimetric stack pad immunoassay for bacterial identification', *Biosensors and Bioelectronics*, 87, pp. 572–578. Available at: https://doi.org/10.1016/j.bios.2016.08.044.

Fan, X. *et al.* (2008) 'Sensitive optical biosensors for unlabeled targets: A review', *Analytica Chimica Acta*, 620(1–2), pp. 8–26. Available at: https://doi.org/10.1016/j.aca.2008.05.022.

Fang, X. *et al.* (2010) 'Loop-Mediated Isothermal Amplification Integrated on Microfluidic Chips for Point-of-Care Quantitative Detection of Pathogens', *Analytical Chemistry*, 82(7), pp. 3002–3006. Available at: https://doi.org/10.1021/ac1000652.

Fang, Y. and Snijder, E.J. (2010) 'The PRRSV replicase: Exploring the multifunctionality of an intriguing set of nonstructural proteins', *Virus Research*, 154(1–2), pp. 61–76. Available at: https://doi.org/10.1016/j.virusres.2010.07.030.

Fang, Z. *et al.* (2014) 'Lateral flow biosensor for DNA extraction-free detection of salmonella based on aptamer mediated strand displacement amplification', *Biosensors and Bioelectronics*, 56, pp. 192–197. Available at: https://doi.org/10.1016/j.bios.2014.01.015.

Fei, J., Dou, W. and Zhao, G. (2016) 'Amperometric immunoassay for the detection of Salmonella pullorum using a screen - printed carbon electrode modified with gold nanoparticle-coated reduced

graphene oxide and immunomagnetic beads', *Microchimica Acta*, 183(2), pp. 757–764. Available at: https://doi.org/10.1007/s00604-015-1721-3.

Fernandes, A. *et al.* (2014) 'Lab-on-Chip Cytometry Based on Magnetoresistive Sensors for Bacteria Detection in Milk', *Sensors*, 14(8), pp. 15496–15524. Available at: https://doi.org/10.3390/s140815496.

Ferris, N.P. *et al.* (2009) 'Development and laboratory validation of a lateral flow device for the detection of foot-and-mouth disease virus in clinical samples', *Journal of Virological Methods*, 155(1), pp. 10–17. Available at: https://doi.org/10.1016/j.jviromet.2008.09.009.

Ferris, N.P. *et al.* (2010) 'Development and laboratory validation of a lateral flow device for the detection of serotype SAT 2 foot-and-mouth disease viruses in clinical samples', *Journal of Virological Methods*, 163(2), pp. 474–476. Available at: https://doi.org/10.1016/j.jviromet.2009.09.022.

Fila, M. and Woźniakowski, G. (2020) 'African swine fever virus – the possible role of flies and other insects in virus transmission', *Journal of Veterinary Research*, 64(1), pp. 1–7. Available at: https://doi.org/10.2478/jvetres-2020-0001.

Fritz, J. (2008) 'Cantilever biosensors', *The Analyst*, 133(7), p. 855. Available at: https://doi.org/10.1039/b718174d.

Fu, L.-M. and Wang, Y.-N. (2018) 'Detection methods and applications of microfluidic paper-based analytical devices', *TrAC Trends in Analytical Chemistry*, 107, pp. 196–211. Available at: https://doi.org/10.1016/j.trac.2018.08.018.

Fu, Q. *et al.* (2021) 'Lateral flow strip biosensor based on streptavidin-coated gold nanoparticles with recombinase polymerase amplification for the quantitative point-of-care testing of Salmonella', *Microchemical Journal*, 171, p. 106859. Available at: https://doi.org/10.1016/j.microc.2021.106859.

Fu, Y. *et al.* (2014) 'Exploiting Enzyme Catalysis in Ultra-Low Ion Strength Media for Impedance Biosensing of Avian Influenza Virus Using a Bare Interdigitated Electrode', *Analytical Chemistry*, 86(4), pp. 1965–1971. Available at: https://doi.org/10.1021/ac402550f.

Fu, Y. *et al.* (2020) 'Diagnosis of mixed infections with swine viruses using an integrated microfluidic platform', *Sensors and Actuators B: Chemical*, 312, p. 128005. Available at: https://doi.org/10.1016/j.snb.2020.128005.

Ganges, L. *et al.* (2020) 'Classical swine fever virus: the past, present and future', *Virus Research*, 289, p. 198151. Available at: https://doi.org/10.1016/j.virusres.2020.198151.

Garcia-Cordero, J.L. *et al.* (2010) 'Microfluidic sedimentation cytometer for milk quality and bovine mastitis monitoring', *Biomedical Microdevices*, 12(6), pp. 1051–1059. Available at: https://doi.org/10.1007/s10544-010-9459-5.

Ge, L. *et al.* (2014) 'Lab-on-paper-based devices using chemiluminescence and electrogenerated chemiluminescence detection', *Analytical and Bioanalytical Chemistry*, 406(23), pp. 5613–5630. Available at: https://doi.org/10.1007/s00216-014-7756-1.

Gil Rosa, B. *et al.* (2022) 'Multiplexed immunosensors for point-of-care diagnostic applications', *Biosensors and Bioelectronics*, 203, p. 114050. Available at: https://doi.org/10.1016/j.bios.2022.114050.

Gilbert, S.A. *et al.* (1997) 'Typing of porcine reproductive and respiratory syndrome viruses by a multiplex PCR assay', *Journal of Clinical Microbiology*, 35(1), pp. 264–267. Available at: https://doi.org/10.1128/jcm.35.1.264-267.1997.

Glas, A.S. *et al.* (2003) 'The diagnostic odds ratio: a single indicator of test performance', *Journal of Clinical Epidemiology*, 56(11), pp. 1129–1135. Available at: https://doi.org/10.1016/S0895-4356(03)00177-X.

Gómez-Gómez, M. *et al.* (2022) 'Photonic Label-Free Biosensors for Fast and Multiplex Detection of Swine Viral Diseases', *Sensors*, 22(3), p. 708. Available at: https://doi.org/10.3390/s22030708.

Grenvall, C. *et al.* (2012) 'Label-free somatic cell cytometry in raw milk using acoustophoresis', *Cytometry Part A*, 81A(12), pp. 1076–1083. Available at: https://doi.org/10.1002/cyto.a.22214.

Griol, A. *et al.* (2019) 'Design and Development of Photonic Biosensors for Swine Viral Diseases Detection', *Sensors*, 19(18), p. 3985. Available at: https://doi.org/10.3390/s19183985.

Guo, Jiuchuan *et al.* (2021) 'Nanomaterial Labels in Lateral Flow Immunoassays for Point-of-Care-Testing', *Journal of Materials Science & Technology*, 60, pp. 90–104. Available at: https://doi.org/10.1016/j.jmst.2020.06.003.

Guo, Y. *et al.* (2016) 'Label-free and highly sensitive electrochemical detection of E. coli based on rolling circle amplifications coupled peroxidase-mimicking DNAzyme amplification', *Biosensors and Bioelectronics*, 75, pp. 315–319. Available at: https://doi.org/10.1016/j.bios.2015.08.031.

Hammond, J.L. *et al.* (2016) 'Electrochemical biosensors and nanobiosensors', *Essays in Biochemistry*. Edited by P. Estrela, 60(1), pp. 69–80. Available at: https://doi.org/10.1042/EBC20150008.

Hanon, J.-B. *et al.* (2016) 'Inter-laboratory evaluation of the performance parameters of a Lateral Flow Test device for the detection of Bluetongue virus-specific antibodies', *Journal of Virological Methods*, 228, pp. 140–150. Available at: https://doi.org/10.1016/j.jviromet.2015.12.001.

Hänsel, A. and Heck, M.J.R. (2020) 'Opportunities for photonic integrated circuits in optical gas sensors', *Journal of Physics: Photonics*, 2(1), p. 012002. Available at: https://doi.org/10.1088/2515-7647/ab6742.

Haun, J.B. *et al.* (2010) 'Magnetic nanoparticle biosensors: Magnetic nanoparticle biosensors', *Wiley Interdisciplinary Reviews: Nanomedicine and Nanobiotechnology*, 2(3), pp. 291–304. Available at: https://doi.org/10.1002/wnan.84.

He, Q. *et al.* (2020) 'High-throughput and all-solution phase African Swine Fever Virus (ASFV) detection using CRISPR-Cas12a and fluorescence based point-of-care system', *Biosensors and Bioelectronics*, 154, p. 112068. Available at: https://doi.org/10.1016/j.bios.2020.112068.

Heinze, B.C. *et al.* (2009) 'Microfluidic immunosensor for rapid and sensitive detection of bovine viral diarrhea virus', *Sensors and Actuators B: Chemical*, 138(2), pp. 491–496. Available at: https://doi.org/10.1016/j.snb.2009.02.058.

Henao-Diaz, A. *et al.* (2020) 'Guidelines for oral fluid-based surveillance of viral pathogens in swine', *Porcine Health Management*, 6(1), p. 28. Available at: https://doi.org/10.1186/s40813-020-00168-w.

Hideshima, S. *et al.* (2013) 'Attomolar Detection of Influenza A Virus Hemagglutinin Human H1 and Avian H5 Using Glycan-Blotted Field Effect Transistor Biosensor', *Analytical Chemistry*, 85(12), pp. 5641–5644. Available at: https://doi.org/10.1021/ac401085c.

Hobbs, E.C. *et al.* (2021) 'The potential of diagnostic point-of-care tests (POCTs) for infectious and zoonotic animal diseases in developing countries: Technical, regulatory and sociocultural considerations', *Transboundary and Emerging Diseases*, 68(4), pp. 1835–1849. Available at: https://doi.org/10.1111/tbed.13880.

Holtkamp, D. *et al.* (2013) 'Assessment of the economic impact of porcine reproductive and respiratory syndrome virus on United States pork producers', *Journal of Swine Health and Production*, 21(2). Available at: https://www.aasv.org/shap/issues/v21n2/v21n2p72.pdf

Hou, P. *et al.* (2018) 'Development of a recombinase polymerase amplification combined with lateral-flow dipstick assay for detection of bovine ephemeral fever virus', *Molecular and Cellular Probes*, 38, pp. 31–37. Available at: https://doi.org/10.1016/j.mcp.2017.12.003.

Hu, J. *et al.* (2012) 'Development of a label-free and innovative approach based on surface plasmon resonance biosensor for on-site detection of infectious bursal disease virus (IBDV)', *Biosensors and Bioelectronics*, 31(1), pp. 475–479. Available at: https://doi.org/10.1016/j.bios.2011.11.019.

Hu, Jie *et al.* (2014) 'Advances in paper-based point-of-care diagnostics', *Biosensors and Bioelectronics*, 54, pp. 585–597. Available at: https://doi.org/10.1016/j.bios.2013.10.075.

Hu, Jiandong *et al.* (2014) 'Development of a Surface Plasmon Resonance Biosensing Approach for the Rapid Detection of Porcine Circovirus Type 2 in Sample Solutions', *PLoS ONE*. Edited by S. D'Auria, 9(10), p. e111292. Available at: https://doi.org/10.1371/journal.pone.0111292.

Hu, J. *et al.* (2019) 'Sensitive and rapid visual detection of Salmonella Typhimurium in milk based on recombinase polymerase amplification with lateral flow dipsticks', *Journal of Microbiological Methods*, 158, pp. 25–32. Available at: https://doi.org/10.1016/j.mimet.2019.01.018.

Huan, T.N. *et al.* (2009) 'Square wave voltammetric detection of Anthrax utilizing a peptide for selective recognition of a protein biomarker', *Biosensors and Bioelectronics*, 25(2), pp. 469–474. Available at: https://doi.org/10.1016/j.bios.2009.08.002.

Huang, C. *et al.* (2004) 'Multiplex PCR for rapid detection of pseudorabies virus, porcine parvovirus and porcine circoviruses', *Veterinary Microbiology*, 101(3), pp. 209–214. Available at: https://doi.org/10.1016/j.vetmic.2004.04.007.

Huang, L. *et al.* (2021) 'Miniaturized Paper-Based Smartphone Biosensor for Differential Diagnosis of Wild-type Pseudorabies Virus Infection versus Vaccination Immunization', *Sensors and Actuators B: Chemical*, 327, p. 128893. Available at: https://doi.org/10.1016/j.snb.2020.128893.

Jaffrezic-Renault, N. *et al.* (2007) 'Biosensors and Bio-Bar Code Assays Based on Biofunctionalized Magnetic Microbeads', *Sensors*, 7(4), pp. 589–614. Available at: https://doi.org/10.3390/s7040589.

Jain, B. *et al.* (2018) 'Development of a rapid test for detection of foot-and-mouth disease virus specific antibodies using gold nanoparticles', *VirusDisease*, 29(2), pp. 192–198. Available at: https://doi.org/10.1007/s13337-018-0450-8.

James, H.E. *et al.* (2010) 'Detection of African swine fever virus by loop-mediated isothermal amplification', *Journal of Virological Methods*, 164(1–2), pp. 68–74. Available at: https://doi.org/10.1016/j.jviromet.2009.11.034.

Jangid, A.R. *et al.* (2019) 'Chronometric Quantitation of Analytes in Paper-Based Microfluidic Devices (MicroPADs) via Enzymatic Degradation of a Metastable Biomatrix', *Inventions*, 4(3), p. 48. Available at: https://doi.org/10.3390/inventions4030048.

Jiang, Y. *et al.* (2021) 'Multiplex and on-site PCR detection of swine diseases based on the microfluidic chip system', *BMC Veterinary Research*, 17(1), p. 117. Available at: https://doi.org/10.1186/s12917-021-02825-w.

Jin, Q. *et al.* (2012) 'Development of an immunochromatographic strip for the detection of antibodies against *Porcine circovirus-2*', *Journal of Veterinary Diagnostic Investigation*, 24(6), pp. 1151–1157. Available at: https://doi.org/10.1177/1040638712462374.

Jung, J.H. *et al.* (2015) 'Integrated centrifugal reverse transcriptase loop-mediated isothermal amplification microdevice for influenza A virus detection', *Biosensors and Bioelectronics*, 68, pp. 218–224. Available at: https://doi.org/10.1016/j.bios.2014.12.043.

Jung, W. *et al.* (2015) 'Point-of-care testing (POCT) diagnostic systems using microfluidic lab-on-a-chip technologies', *Microelectronic Engineering*, 132, pp. 46–57. Available at: https://doi.org/10.1016/j.mee.2014.09.024.

Kameyama, K. *et al.* (2006) 'Development of an immunochromatographic test kit for rapid detection of bovine viral diarrhea virus antigen', *Journal of Virological Methods*, 138(1–2), pp. 140–146. Available at: https://doi.org/10.1016/j.jviromet.2006.08.005.

Kappes, M.A. and Faaberg, K.S. (2015) 'PRRSV structure, replication and recombination: Origin of phenotype and genotype diversity', *Virology*, 479–480, pp. 475–486. Available at: https://doi.org/10.1016/j.virol.2015.02.012.

Karash, S. *et al.* (2016) 'Rapid detection of avian influenza virus H5N1 in chicken tracheal samples using an impedance aptasensor with gold nanoparticles for signal amplification', *Journal of Virological Methods*, 236, pp. 147–156. Available at: https://doi.org/10.1016/j.jviromet.2016.07.018.

Kedkovid, R., Sirisereewan, C. and Thanawongnuwech, R. (2020) 'Major swine viral diseases: an Asian perspective after the African swine fever introduction', *Porcine Health Management*, 6(1), p. 20. Available at: https://doi.org/10.1186/s40813-020-00159-x.

Khan, S. *et al.* (2018) 'Synthesis and Application of Cu-Doped Nickel and Zirconium Oxide Nanoparticles as *Brucella abortus* Electrochemical Device Development', *Sensor Letters*, 16(4), pp. 267–276. Available at: https://doi.org/10.1166/sl.2018.3949.

Kim, B. *et al.* (2017) 'A portable somatic cell counter based on a multi-functional counting chamber and a miniaturized fluorescence microscope', *Talanta*, 170, pp. 238–243. Available at: https://doi.org/10.1016/j.talanta.2017.04.014.

Kim, S.H. *et al.* (2019) 'Specific detection of avian influenza H5N2 whole virus particles on lateral flow strips using a pair of sandwich-type aptamers', *Biosensors and Bioelectronics*, 134, pp. 123–129. Available at: https://doi.org/10.1016/j.bios.2019.03.061.

Kim, T.-H. *et al.* (2014) 'Fully Integrated Lab-on-a-Disc for Nucleic Acid Analysis of Food-Borne Pathogens', *Analytical Chemistry*, 86(8), pp. 3841–3848. Available at: https://doi.org/10.1021/ac403971h.

Kimura, S. *et al.* (2012) 'On-chip diagnosis of subclinical mastitis in cows by electrochemical measurement of neutrophil activity in milk', *Lab on a Chip*, 12(7), p. 1309. Available at: https://doi.org/10.1039/c2lc20952g.

Klungthong, C. *et al.* (2010) 'The impact of primer and probe-template mismatches on the sensitivity of pandemic influenza A/H1N1/2009 virus detection by real-time RT-PCR', *Journal of Clinical Virology*, 48(2), pp. 91–95. Available at: https://doi.org/10.1016/j.jcv.2010.03.012.

Ko, S. and Grant, S.A. (2006) 'A novel FRET-based optical fiber biosensor for rapid detection of Salmonella typhimurium', *Biosensors and Bioelectronics*, 21(7), pp. 1283–1290. Available at: https://doi.org/10.1016/j.bios.2005.05.017.

Kothalawala, H., Toussaint, M.J.M. and Gruys, E. (2006) 'An overview of swine influenza', *Veterinary Quarterly*, 28(2), pp. 45–53. Available at: https://doi.org/10.1080/01652176.2006.9695207.

Krakowka, S. *et al.* (2001) 'Activation of the Immune System is the Pivotal Event in the Production of Wasting Disease in Pigs Infected with Porcine Circovirus-2 (PCV-2)', *Veterinary Pathology*, 38(1), pp. 31–42. Available at: https://doi.org/10.1354/vp.38-1-31.

Krejcova, L. *et al.* (2014) '3D printed chip for electrochemical detection of influenza virus labeled with CdS quantum dots', *Biosensors and Bioelectronics*, 54, pp. 421–427. Available at: https://doi.org/10.1016/j.bios.2013.10.031.

Krishna, V.D. *et al.* (2016) 'Giant Magnetoresistance-based Biosensor for Detection of Influenza A Virus', *Frontiers in Microbiology*, 7. Available at: https://doi.org/10.3389/fmicb.2016.00400.

Kumar, A.A. *et al.* (2015) 'From the Bench to the Field in Low-Cost Diagnostics: Two Case Studies', *Angewandte Chemie International Edition*, 54(20), pp. 5836–5853. Available at: https://doi.org/10.1002/anie.201411741.

Kumar, N. *et al.* (2020) 'Label-free peptide nucleic acid biosensor for visual detection of multiple strains of influenza A virus suitable for field applications', *Analytica Chimica Acta*, 1093, pp. 123–130. Available at: https://doi.org/10.1016/j.aca.2019.09.060.

Kun Jia, Toury, T. and Ionescu, R.E. (2012) 'Fabrication of an atrazine acoustic immunosensor based on a drop-deposition procedure', *IEEE Transactions on Ultrasonics, Ferroelectrics and Frequency Control*, 59(9), p. 6306023. Available at: https://doi.org/10.1109/TUFFC.2012.2421.

Kuntz-Simon, G. and Madec, F. (2009) 'Genetic and Antigenic Evolution of Swine Influenza Viruses in Europe and Evaluation of Their Zoonotic Potential', *Zoonoses and Public Health*, 56(6–7), pp. 310–325. Available at: https://doi.org/10.1111/j.1863-2378.2009.01236.x.

Larochelle, R. *et al.* (2000) 'PCR Detection and Evidence of Shedding of Porcine Circovirus Type 2 in Boar Semen', *Journal of Clinical Microbiology*, 38(12), pp. 4629–4632. Available at: https://doi.org/10.1128/JCM.38.12.4629-4632.2000.

Li, H. *et al.* (2009) 'Applications of Nanomaterials in Electrochemical Enzyme Biosensors', *Sensors*, 9(11), pp. 8547–8561. Available at: https://doi.org/10.3390/s91108547.

Li, M. *et al.* (2021) 'Rapid, on-site, and sensitive detection of aflatoxin M1 in milk products by using time-resolved fluorescence microsphere test strip', *Food Control*, 121, p. 107616. Available at: https://doi.org/10.1016/j.foodcont.2020.107616.

Li, S. *et al.* (2019) 'Rapid Detection of Brucella spp. and Elimination of Carryover Using Multiple Cross Displacement Amplification Coupled With Nanoparticles-Based Lateral Flow Biosensor', *Frontiers in Cellular and Infection Microbiology*, 9, p. 78. Available at: https://doi.org/10.3389/fcimb.2019.00078.

Li, X. *et al.* (2012) 'A fast and sensitive immunoassay of avian influenza virus based on label-free quantum dot probe and lateral flow test strip', *Talanta*, 100, pp. 1–6. Available at: https://doi.org/10.1016/j.talanta.2012.08.041.

Liébana, S. *et al.* (2009) 'Rapid detection of Salmonella in milk by electrochemical magneto-immunosensing', *Biosensors and Bioelectronics*, 25(2), pp. 510–513. Available at: https://doi.org/10.1016/j.bios.2009.07.022.

Lin, J. *et al.* (2015) 'An impedance immunosensor based on low-cost microelectrodes and specific monoclonal antibodies for rapid detection of avian influenza virus H5N1 in chicken swabs', *Biosensors and Bioelectronics*, 67, pp. 546–552. Available at: https://doi.org/10.1016/j.bios.2014.09.037.

Link, N., Weber, W. and Fussenegger, M. (2007) 'A novel generic dipstick-based technology for rapid and precise detection of tetracycline, streptogramin and macrolide antibiotics in food samples', *Journal of Biotechnology*, 128(3), pp. 668–680. Available at: https://doi.org/10.1016/j.jbiotec.2006.11.011.

Lisowski, P. and Zarzycki, P.K. (2013) 'Microfluidic Paper-Based Analytical Devices (μPADs) and Micro Total Analysis Systems (μTAS): Development, Applications and Future Trends', *Chromatographia*, 76(19–20), pp. 1201–1214. Available at: https://doi.org/10.1007/s10337-013-2413-y.

Liu, D. *et al.* (2020) 'Trends in miniaturized biosensors for point-of-care testing', *TrAC Trends in Analytical Chemistry*, 122, p. 115701. Available at: https://doi.org/10.1016/j.trac.2019.115701.

Liu, Y. *et al.* (2020) 'Identification of a dominant linear epitope on the VP2 capsid protein of porcine parvovirus and characterization of two monoclonal antibodies with neutralizing abilities', *International Journal of Biological Macromolecules*, 163, pp. 2013–2022. Available at: https://doi.org/10.1016/j.ijbiomac.2020.09.055.

Lopez, C.A. *et al.* (2011) 'Label-free multiplexed virus detection using spectral reflectance imaging', *Biosensors and Bioelectronics*, 26(8), pp. 3432–3437. Available at: https://doi.org/10.1016/j.bios.2011.01.019.

Lou, D. *et al.* (2022) 'Advances in nanoparticle-based lateral flow immunoassay for point-of-care testing', *VIEW*, 3(1), p. 20200125. Available at: https://doi.org/10.1002/VIW.20200125.

Lu, L. and Jun, S. (2012) 'Evaluation of a microwire sensor functionalized to detect Escherichia coli bacterial cells', *Biosensors and Bioelectronics*, 36(1), pp. 257–261. Available at: https://doi.org/10.1016/j.bios.2012.04.033.

Lu, T. *et al.* (2018) 'Selection of an aptamer against Muscovy duck parvovirus for highly sensitive rapid visual detection by label-free aptasensor', *Talanta*, 176, pp. 214–220. Available at: https://doi.org/10.1016/j.talanta.2017.08.037.

Luo, B. *et al.* (2016) 'Label-free immunoassay for porcine circovirus type 2 based on excessively tilted fiber grating modified with staphylococcal protein A', *Biosensors and Bioelectronics*, 86, pp. 1054–1060. Available at: https://doi.org/10.1016/j.bios.2016.07.100.

Luo, Y. *et al.* (2017) 'Development of an updated PCR assay for detection of African swine fever virus', *Archives of Virology*, 162(1), pp. 191–199. Available at: https://doi.org/10.1007/s00705-016-3069-3.

Lv, S. *et al.* (2018) 'The detection of brucellosis antibody in whole serum based on the low-fouling electrochemical immunosensor fabricated with magnetic Fe3O4@Au@PEG@HA nanoparticles', *Biosensors and Bioelectronics*, 117, pp. 138–144. Available at: https://doi.org/10.1016/j.bios.2018.06.010.

Maes, D.G.D. *et al.* (2020) 'A critical reflection on intensive pork production with an emphasis on animal health and welfare', *Journal of Animal Science*, 98(Supplement_1), pp. S15–S26. Available at: https://doi.org/10.1093/jas/skz362.

Mahato, K., Srivastava, A. and Chandra, P. (2017) 'Paper based diagnostics for personalized health care: Emerging technologies and commercial aspects', *Biosensors and Bioelectronics*, 96, pp. 246–259. Available at: https://doi.org/10.1016/j.bios.2017.05.001.

Manessis, G. *et al.* (2021) 'Integration of Microfluidics, Photonic Integrated Circuits and Data Acquisition and Analysis Methods in a Single Platform for the Detection of Swine Viral Diseases', *Animals*, 11(11), p. 3193. Available at: https://doi.org/10.3390/ani11113193.

Manessis, G. *et al.* (2022) 'Point-of-Care and Label-Free Detection of Porcine Reproductive and Respiratory Syndrome and Swine Influenza Viruses Using a Microfluidic Device with Photonic Integrated Circuits', *Viruses*, 14(5), p. 988. Available at: https://doi.org/10.3390/v14050988.

Manessis, G., Gelasakis, A. and Bossis, I. (2019) 'The challenge of introducing Point of Care Diagnostics in Farm Animal Health Management', *Biomedical Journal of Scientific & Technical Research*, 14(5). Available at: https://doi.org/10.26717/BJSTR.2019.14.002601.

Manessis, G., Gelasakis, A.I. and Bossis, I. (2022) 'Point-of-Care Diagnostics for Farm Animal Diseases: From Biosensors to Integrated Lab-on-Chip Devices', *Biosensors*, 12(7), p. 455. Available at: https://doi.org/10.3390/bios12070455.

Marie-Laure, A.-G. (2020) 'The EU pig meat sector', *European parliament Briefing*. Available at: https://www.europarl.europa.eu/RegData/etudes/BRIE/2020/652044/EPRS_BRI(2020)652044_EN.pdf

accessed: 28/10/2022

Martinez, A.W. *et al.* (2010) 'Diagnostics for the Developing World: Microfluidic Paper-Based Analytical Devices', *Analytical Chemistry*, 82(1), pp. 3–10. Available at: https://doi.org/10.1021/ac9013989.

McCutcheon, K. *et al.* (2019) 'The Application of a Nanomaterial Optical Fiber Biosensor Assay for Identification of Brucella Nomenspecies', *Biosensors*, 9(2), p. 64. Available at: https://doi.org/10.3390/bios9020064.

McDonald, J.C. *et al.* (2000) 'Fabrication of microfluidic systems in poly(dimethylsiloxane)', *Electrophoresis*, 21(1), pp. 27–40. Available at: https://doi.org/10.1002/(SICI)1522-2683(20000101)21:1<27::AID-ELPS27>3.0.CO;2-C.

Mei, X. *et al.* (2019) 'Development and application of a visual loop-mediated isothermal amplification combined with lateral flow dipstick (LAMP-LFD) method for rapid detection of Salmonella strains in food samples', *Food Control*, 104, pp. 9–19. Available at: https://doi.org/10.1016/j.foodcont.2019.04.014.

Mejía-Salazar, J.R. *et al.* (2020) 'Microfluidic Point-of-Care Devices: New Trends and Future Prospects for eHealth Diagnostics', *Sensors*, 20(7), p. 1951. Available at: https://doi.org/10.3390/s20071951.

Mészáros, I. *et al.* (2017) 'Biology of Porcine Parvovirus (Ungulate parvovirus 1)', *Viruses*, 9(12), p. 393. Available at: https://doi.org/10.3390/v9120393.

Meulenberg, J.J.M. (2000) 'PRRSV, the virus', *Veterinary Research*, 31(1), pp. 11–21. Available at: https://doi.org/10.1051/vetres:2000103.

Miao, F. *et al.* (2019) 'Rapid and Sensitive Recombinase Polymerase Amplification Combined With Lateral Flow Strip for Detecting African Swine Fever Virus', *Frontiers in Microbiology*, 10, p. 1004. Available at: https://doi.org/10.3389/fmicb.2019.01004.

Miao, L. *et al.* (2009) 'Real-time PCR to detect and analyze virulent PPV loads in artificially challenged sows and their fetuses', *Veterinary Microbiology*, 138(1–2), pp. 145–149. Available at: https://doi.org/10.1016/j.vetmic.2009.02.006.

Mohankumar, P. *et al.* (2021) 'Recent developments in biosensors for healthcare and biomedical applications: A review', *Measurement*, 167, p. 108293. Available at: https://doi.org/10.1016/j.measurement.2020.108293.

Mohd Hanafiah, K. *et al.* (2017) 'Development of Multiplexed Infectious Disease Lateral Flow Assays: Challenges and Opportunities', *Diagnostics*, 7(3), p. 51. Available at: https://doi.org/10.3390/diagnostics7030051.

Montrose, A. *et al.* (2015) 'Novel Single Gold Nanowire-based Electrochemical Immunosensor for Rapid Detection of Bovine Viral Diarrhoea Antibodies in Serum', *Journal of Biosensors & Bioelectronics*, 06(03). Available at: https://doi.org/10.4172/2155-6210.1000174.

Moon, J.S. *et al.* (2007) 'Application of a New Portable Microscopic Somatic Cell Counter with Disposable Plastic Chip for Milk Analysis', *Journal of Dairy Science*, 90(5), pp. 2253–2259. Available at: https://doi.org/10.3168/jds.2006-622.

Morbioli, G.G. *et al.* (2017) 'Technical aspects and challenges of colorimetric detection with microfluidic paper-based analytical devices (μPADs) - A review', *Analytica Chimica Acta*, 970, pp. 1–22. Available at: https://doi.org/10.1016/j.aca.2017.03.037.

Morgan, A.P. (1998) 'Regulatory control of veterinary diagnostic test kits', *Rev. Sci. Tech.*, (17), pp. 562–567.

Morgan, N. and Prakash, A. (2006) 'International livestock markets and the impact of animal disease', *Rev. sci. tech. Off. int. Epiz.*, 25 (2), pp. 517-528. Available at: http://dx.doi.org/10.20506/rst.25.2.1685

Mudumba, S. *et al.* (2017) 'Photonic ring resonance is a versatile platform for performing multiplex immunoassays in real time', *Journal of Immunological Methods*, 448, pp. 34–43. Available at: https://doi.org/10.1016/j.jim.2017.05.005.

Nannucci, L. *et al.* (2020) 'Point-of-service diagnostic technology for detection of swine viral diseases', *Journal of Veterinary Research*, 64(1), pp. 15–23. Available at: https://doi.org/10.2478/jvetres-2020-0016.

Nasseri, B. *et al.* (2018) 'Point-of-care microfluidic devices for pathogen detection', *Biosensors and Bioelectronics*, 117, pp. 112–128. Available at: https://doi.org/10.1016/j.bios.2018.05.050.

Neethirajan, S. (2020) 'Transforming the Adaptation Physiology of Farm Animals through Sensors', *Animals*, 10(9), p. 1512. Available at: https://doi.org/10.3390/ani10091512.

Nguyen, Q.H. and Kim, M.I. (2020) 'Nanomaterial-mediated paper-based biosensors for colorimetric pathogen detection', *TrAC Trends in Analytical Chemistry*, 132, p. 116038. Available at: https://doi.org/10.1016/j.trac.2020.116038.

Nidzworski, D. *et al.* (2014) 'Universal biosensor for detection of influenza virus', *Biosensors and Bioelectronics*, 59, pp. 239–242. Available at: https://doi.org/10.1016/j.bios.2014.03.050.

Olmos, C.M. *et al.* (2019) 'Epoxy resin mold and PDMS microfluidic devices through photopolymer flexographic printing plate', *Sensors and Actuators B: Chemical*, 288, pp. 742–748. Available at: https://doi.org/10.1016/j.snb.2019.03.062.

Olsen, C.W. (2002) 'The emergence of novel swine influenza viruses in North America', *Virus Research*, 85(2), pp. 199–210. Available at: https://doi.org/10.1016/S0168-1702(02)00027-8.

Olvera, A. *et al.* (2004) 'Comparison of porcine circovirus type 2 load in serum quantified by a real time PCR in postweaning multisystemic wasting syndrome and porcine dermatitis and nephropathy syndrome naturally affected pigs', *Journal of Virological Methods*, 117(1), pp. 75–80. Available at: https://doi.org/10.1016/j.jviromet.2003.12.007.

Ong, D.S.Y. and Poljak, M. (2020) 'Smartphones as mobile microbiological laboratories', *Clinical Microbiology and Infection*, 26(4), pp. 421–424. Available at: https://doi.org/10.1016/j.cmi.2019.09.026.

de-Paris, F. *et al.* (2012) 'Optimization of one-step duplex real-time RT-PCR for detection of influenza and respiratory syncytial virus in nasopharyngeal aspirates', *Journal of Virological Methods*, 186(1–2), pp. 189–192. Available at: https://doi.org/10.1016/j.jviromet.2012.07.008.

Peduru Hewa, T.M. *et al.* (2009) 'The detection of influenza A and B viruses in clinical specimens using a quartz crystal microbalance', *Journal of Virological Methods*, 162(1–2), pp. 14–21. Available at: https://doi.org/10.1016/j.jviromet.2009.07.001.

Peedel, D. and Rinken, T. (2014) 'Rapid biosensing of Staphylococcus aureus bacteria in milk', *Analytical Methods*, 6(8), p. 2642. Available at: https://doi.org/10.1039/c3ay42036a.

Perry, B.D., Grace, D. and Sones, K. (2013) 'Current drivers and future directions of global livestock disease dynamics', *Proceedings of the National Academy of Sciences*, 110(52), pp. 20871–20877. Available at: https://doi.org/10.1073/pnas.1012953108.

Petrakova, A.V. *et al.* (2019) 'Gold nanoparticles of different shape for bicolor lateral flow test', *Analytical Biochemistry*, 568, pp. 7–13. Available at: https://doi.org/10.1016/j.ab.2018.12.015.

Pewsner, D. *et al.* (2004) 'Ruling a diagnosis in or out with "SpPIn" and "SnNOut": a note of caution', *BMJ*, 329(7459), pp. 209–213. Available at: https://doi.org/10.1136/bmj.329.7459.209.

Pirzada, M. and Altintas, Z. (2019) 'Nanomaterials for Healthcare Biosensing Applications', *Sensors*, 19(23), p. 5311. Available at: https://doi.org/10.3390/s19235311.

Postel, A. *et al.* (2018) 'Epidemiology, diagnosis and control of classical swine fever: Recent developments and future challenges', *Transboundary and Emerging Diseases*, 65, pp. 248–261. Available at: https://doi.org/10.1111/tbed.12676.

Potockova, H., Dohnal, J. and Thome-Kromer, B. (2020) 'Regulation of veterinary point-of-care testing in the European Union, the United States of America and Japan, *Revue Scientifique et Technique de l'OIE*, 39(3), pp. 699–709. Available at: https://doi.org/10.20506/rst.39.3.3171.

Qi, C. *et al.* (2010) 'Detection of avian influenza virus subtype H5 using a biosensor based on imaging ellipsometry', *Biosensors and Bioelectronics*, 25(6), pp. 1530–1534. Available at: https://doi.org/10.1016/j.bios.2009.10.030.

Qi, J. *et al.* (2017) 'Three-dimensional paper-based microfluidic chip device for multiplexed fluorescence detection of Cu2+ and Hg2+ ions based on ion imprinting technology', *Sensors and Actuators B: Chemical*, 251, pp. 224–233. Available at: https://doi.org/10.1016/j.snb.2017.05.052.

Quesada-González, D. and Merkoçi, A. (2018) 'Nanomaterial-based devices for point-of-care diagnostic applications', *Chemical Society Reviews*, 47(13), pp. 4697–4709. Available at: https://doi.org/10.1039/C7CS00837F.

Rabenau, H.F. *et al.* (2007) 'Verification and validation of diagnostic laboratory tests in clinical virology', *Journal of Clinical Virology*, 40(2), pp. 93–98. Available at: https://doi.org/10.1016/j.jcv.2007.07.009.

Rahi, A., Sattarahmady, N. and Heli, H. (2016) 'An ultrasensitive electrochemical genosensor for Brucella based on palladium nanoparticles', *Analytical Biochemistry*, 510, pp. 11–17. Available at: https://doi.org/10.1016/j.ab.2016.07.012.

Ramirez, A. *et al.* (2012) 'Efficient surveillance of pig populations using oral fluids', *Preventive Veterinary Medicine*, 104(3–4), pp. 292–300. Available at: https://doi.org/10.1016/j.prevetmed.2011.11.008.

Reyes, D.R. *et al.* (2002) 'Micro Total Analysis Systems. 1. Introduction, Theory, and Technology', *Analytical Chemistry*, 74(12), pp. 2623–2636. Available at: https://doi.org/10.1021/ac0202435.

Rincón Monroy, M.A. *et al.* (2014) 'Detection and molecular characterization of porcine circovirus type 2 from piglets with Porcine Circovirus Associated Diseases in Colombia', *Virology Journal*, 11(1), p. 143. Available at: https://doi.org/10.1186/1743-422X-11-143.

Ronkainen, N.J., Halsall, H.B. and Heineman, W.R. (2010) 'Electrochemical biosensors', *Chemical Society Reviews*, 39(5), p. 1747. Available at: https://doi.org/10.1039/b714449k.

Rossier, J., Reymond, F. and Michel, P.E. (2002) 'Polymer microfluidic chips for electrochemical and biochemical analyses', *ELECTROPHORESIS*, 23(6), pp. 858–867. Available at: https://doi.org/10.1002/1522-2683(200203)23:6<858::AID-ELPS858>3.0.CO;2-3.

Rovira, A. *et al.* (2002) 'Experimental Inoculation of Conventional Pigs with Porcine Reproductive and Respiratory Syndrome Virus and Porcine Circovirus 2', *Journal of Virology*, 76(7), pp. 3232–3239. Available at: https://doi.org/10.1128/JVI.76.7.3232-3239.2002.

Segalés, J. (2012) 'Porcine circovirus type 2 (PCV2) infections: Clinical signs, pathology and laboratory diagnosis', *Virus Research*, 164(1–2), pp. 10–19. Available at: https://doi.org/10.1016/j.virusres.2011.10.007.

Sender, R. *et al.* (2021) 'The total number and mass of SARS-CoV-2 virions', *Proceedings of the National Academy of Sciences*, 118(25), p. e2024815118. Available at: https://doi.org/10.1073/pnas.2024815118.

Shao, K. *et al.* (2017) 'Near–infrared electrochemiluminesence biosensor for high sensitive detection of porcine reproductive and respiratory syndrome virus based on cyclodextrin-grafted porous Au/PtAu nanotube', *Sensors and Actuators B: Chemical*, 240, pp. 586–594. Available at: https://doi.org/10.1016/j.snb.2016.08.162.

Shao, Y. *et al.* (2010) 'Graphene Based Electrochemical Sensors and Biosensors: A Review', *Electroanalysis*, 22(10), pp. 1027–1036. Available at: https://doi.org/10.1002/elan.200900571.

Sharma, S. *et al.* (2015) 'Point-of-Care Diagnostics in Low Resource Settings: Present Status and Future Role of Microfluidics', *Biosensors*, 5(3), pp. 577–601. Available at: https://doi.org/10.3390/bios5030577.

Shen, H. *et al.* (2018) 'A novel fluorescent immunochromatographic strip combined with pocket fluorescence observation instrument for rapid detection of PRV', *Analytical and Bioanalytical Chemistry*, 410(29), pp. 7655–7661. Available at: https://doi.org/10.1007/s00216-018-1379-x.

Sher, M. *et al.* (2017) 'Paper-based analytical devices for clinical diagnosis: recent advances in the fabrication techniques and sensing mechanisms', *Expert Review of Molecular Diagnostics*, 17(4), pp. 351–366. Available at: https://doi.org/10.1080/14737159.2017.1285228.

Silva, M.G. *et al.* (2008) 'An impedance spectroscopy method for the detection and evaluation of Babesia bovis antibodies in cattle', *Sensors and Actuators B: Chemical*, 135(1), pp. 206–213. Available at: https://doi.org/10.1016/j.snb.2008.08.019.

Singh, A. *et al.* (2018) 'Paper-Based Sensors: Emerging Themes and Applications', *Sensors*, 18(9), p. 2838. Available at: https://doi.org/10.3390/s18092838.

Skittrall, J.P. *et al.* (2021) 'Specificity and positive predictive value of SARS-CoV-2 nucleic acid amplification testing in a low-prevalence setting', *Clinical Microbiology and Infection*, 27(3), p. 469.e9-469.e15. Available at: https://doi.org/10.1016/j.cmi.2020.10.003.

Soares, R.M. *et al.* (1999) 'Detection of porcine parvovirus DNA by the polymerase chain reaction assay using primers to the highly conserved nonstructural protein gene, NS-1', *Journal of Virological Methods*, 78(1–2), pp. 191–198. Available at: https://doi.org/10.1016/S0166-0934(98)00177-3.

Soin, N. *et al.* (2021) 'Triboelectric Effect Enabled Self-Powered, Point-of-Care Diagnostics: Opportunities for Developing ASSURED and REASSURED Devices', *Micromachines*, 12(3), p. 337. Available at: https://doi.org/10.3390/mi12030337.

Srinivasan, B. and Tung, S. (2015) 'Development and Applications of Portable Biosensors', *SLAS Technology*, 20(4), pp. 365–389. Available at: https://doi.org/10.1177/2211068215581349.

Streck, A.F., Canal, C.W. and Truyen, U. (2015) 'Molecular epidemiology and evolution of porcine parvoviruses', *Infection, Genetics and Evolution*, 36, pp. 300–306. Available at: https://doi.org/10.1016/j.meegid.2015.10.007.

Stringer, R.C. *et al.* (2008) 'Development of an optical biosensor using gold nanoparticles and quantum dots for the detection of Porcine Reproductive and Respiratory Syndrome Virus', *Sensors and Actuators B: Chemical*, 134(2), pp. 427–431. Available at: https://doi.org/10.1016/j.snb.2008.05.018.

Su, L.-C. *et al.* (2012) 'Rapid and Highly Sensitive Method for Influenza A (H1N1) Virus Detection', *Analytical Chemistry*, 84(9), pp. 3914–3920. Available at: https://doi.org/10.1021/ac3002947.

Sun, Y. *et al.* (2016) 'Control of swine pseudorabies in China: Opportunities and limitations', *Veterinary Microbiology*, 183, pp. 119–124. Available at: https://doi.org/10.1016/j.vetmic.2015.12.008.

Taberham, A. *et al.* (2008) 'The fabrication of lab-on-chip devices from fluoropolymers', *Journal of Micromechanics and Microengineering*, 18(6), p. 064011. Available at: https://doi.org/10.1088/0960-1317/18/6/064011.

Takekawa, J.Y. *et al.* (2010) 'Field detection of avian influenza virus in wild birds: Evaluation of a portable rRT-PCR system and freeze-dried reagents', *Journal of Virological Methods*, 166(1–2), pp. 92–97. Available at: https://doi.org/10.1016/j.jviromet.2010.02.029.

Tan, X. *et al.* (2012) 'Development of an immunosensor assay for detection of haptoglobin in mastitic milk', *Veterinary Clinical Pathology*, 41(4), pp. 575–581. Available at: https://doi.org/10.1111/j.1939-165X.2012.00468.x.

Tarasov, A. *et al.* (2016) 'A potentiometric biosensor for rapid on-site disease diagnostics', *Biosensors and Bioelectronics*, 79, pp. 669–678. Available at: https://doi.org/10.1016/j.bios.2015.12.086.

Teh, S.-Y. *et al.* (2008) 'Droplet microfluidics', *Lab on a Chip*, 8(2), p. 198. Available at: https://doi.org/10.1039/b715524g.

Teles, F. and Fonseca, L. (2015) 'Nucleic-Acid Testing, New Platforms and Nanotechnology for Point-of-Decision Diagnosis of Animal Pathogens', in M.V. Cunha and J. Inácio (eds) *Veterinary Infection Biology: Molecular Diagnostics and High-Throughput Strategies*. New York, NY: Springer New York (Methods in Molecular Biology), pp. 253–283. Available at: https://doi.org/10.1007/978-1-4939-2004-4_20.

Tran, V. *et al.* (2019) 'Rapid, Quantitative, and Ultrasensitive Point-of-Care Testing: A Portable SERS Reader for Lateral Flow Assays in Clinical Chemistry', *Angewandte Chemie International Edition*, 58(2), pp. 442–446. Available at: https://doi.org/10.1002/anie.201810917.

Trible, B.R. *et al.* (2012) 'Recognition of the Different Structural Forms of the Capsid Protein Determines the Outcome following Infection with Porcine Circovirus Type 2', *Journal of Virology*, 86(24), pp. 13508–13514. Available at: https://doi.org/10.1128/JVI.01763-12.

Tseng, Y.-T. *et al.* (2016) 'Integrated microfluidic system for rapid detection of influenza H1N1 virus using a sandwich-based aptamer assay', *Biosensors and Bioelectronics*, 82, pp. 105–111. Available at: https://doi.org/10.1016/j.bios.2016.03.073.

Tuteja, S.K. and Neethirajan, S. (2018) 'Exploration of two-dimensional bio-functionalized phosphorene nanosheets (black phosphorous) for label free haptoglobin electro-immunosensing applications', *Nanotechnology*, 29(13), p. 135101. Available at: https://doi.org/10.1088/1361-6528/aaab15.

Ungur, A. *et al.* (2021) 'Genotyping of African Swine Fever Virus (ASFV) Isolates in Romania with the First Report of Genotype II in Symptomatic Pigs', *Veterinary Sciences*, 8(12), p. 290. Available at: https://doi.org/10.3390/vetsci8120290.

VanderWaal, K. and Deen, J. (2018) 'Global trends in infectious diseases of swine', *Proceedings of the National Academy of Sciences*, 115(45), pp. 11495–11500. Available at: https://doi.org/10.1073/pnas.1806068115.

Vashist, S.K. *et al.* (2015) 'Emerging Technologies for Next-Generation Point-of-Care Testing', *Trends in Biotechnology*, 33(11), pp. 692–705. Available at: https://doi.org/10.1016/j.tibtech.2015.09.001.

Vashist, S.K. (2021) 'Trends in Multiplex Immunoassays for In Vitro Diagnostics and Point-of-Care Testing', *Diagnostics*, 11(9), p. 1630. Available at: https://doi.org/10.3390/diagnostics11091630.

Veerapandian, M., Hunter, R. and Neethirajan, S. (2016) 'Lipoxygenase-modified Ru-bpy/graphene oxide: Electrochemical biosensor for on-farm monitoring of non-esterified fatty acid', *Biosensors and Bioelectronics*, 78, pp. 253–258. Available at: https://doi.org/10.1016/j.bios.2015.11.058.

Vidic, J. *et al.* (2017) 'Advanced biosensors for detection of pathogens related to livestock and poultry', *Veterinary Research*, 48(1), p. 11. Available at: https://doi.org/10.1186/s13567-017-0418-5.

Vincent, A.L. *et al.* (2008) 'Chapter 3 Swine Influenza Viruses', in *Advances in Virus Research*. Elsevier, pp. 127–154. Available at: https://doi.org/10.1016/S0065-3527(08)00403-X.

Wadhwa, A. *et al.* (2012) 'Bead-based microfluidic immunoassay for diagnosis of Johne's disease', *Journal of Immunological Methods*, 382(1–2), pp. 196–202. Available at: https://doi.org/10.1016/j.jim.2012.06.006.

Wadl, M. *et al.* (2009) 'Easy-to-Use Rapid Test for Direct Detection of Campylobacter spp. in Chicken Feces', *Journal of Food Protection*, 72(12), pp. 2483–2488. Available at: https://doi.org/10.4315/0362-028X-72.12.2483.

Wagner, A.M. *et al.* (2019) 'Quantum dots in biomedical applications', *Acta Biomaterialia*, 94, pp. 44–63. Available at: https://doi.org/10.1016/j.actbio.2019.05.022.

Wang, G. *et al.* (2021) 'Structures and Functional Diversities of ASFV Proteins', *Viruses*, 13(11), p. 2124. Available at: https://doi.org/10.3390/v13112124.

Wang, H. *et al.* (2013) 'An ultrasensitive peroxydisulfate electrochemiluminescence immunosensor for Streptococcus suis serotype 2 based on l-cysteine combined with mimicking bi-enzyme synergetic catalysis to in situ generate coreactant', *Biosensors and Bioelectronics*, 43, pp. 63–68. Available at: https://doi.org/10.1016/j.bios.2012.11.038.

Wang, H. *et al.* (2018) 'Rapid detection of foot-and-mouth disease virus using reverse transcription recombinase polymerase amplification combined with a lateral flow dipstick', *Journal of Virological Methods*, 261, pp. 46–50. Available at: https://doi.org/10.1016/j.jviromet.2018.07.011.

Wang, J. (2005) 'Carbon-Nanotube Based Electrochemical Biosensors: A Review', *Electroanalysis*, 17(1), pp. 7–14. Available at: https://doi.org/10.1002/elan.200403113.

Wang, R. *et al.* (2017) 'A nanowell-based QCM aptasensor for rapid and sensitive detection of avian influenza virus', *Sensors and Actuators B: Chemical*, 240, pp. 934–940. Available at: https://doi.org/10.1016/j.snb.2016.09.067.

Wang, S. *et al.* (2016) 'Advances in addressing technical challenges of point-of-care diagnostics in resource-limited settings', *Expert Review of Molecular Diagnostics*, 16(4), pp. 449–459. Available at: https://doi.org/10.1586/14737159.2016.1142877.

Wang, T.T. and Palese, P. (2009) 'Unraveling the Mystery of Swine Influenza Virus', *Cell*, 137(6), pp. 983–985. Available at: https://doi.org/10.1016/j.cell.2009.05.032.

Waters, R.A. *et al.* (2014) 'Preliminary Validation of Direct Detection of Foot-And-Mouth Disease Virus within Clinical Samples Using Reverse Transcription Loop-Mediated Isothermal Amplification Coupled with a Simple Lateral Flow Device for Detection', *PLoS ONE*. Edited by L. Menéndez-Arias, 9(8), p. e105630. Available at: https://doi.org/10.1371/journal.pone.0105630.

Weng, X. *et al.* (2015) 'Development of quantum dots-based biosensor towards on-farm detection of subclinical ketosis', *Biosensors and Bioelectronics*, 72, pp. 140–147. Available at: https://doi.org/10.1016/j.bios.2015.05.008.

Weng, X. and Neethirajan, S. (2018) 'Immunosensor Based on Antibody-Functionalized $MoS_2$ for Rapid Detection of Avian Coronavirus on Cotton Thread', *IEEE Sensors Journal*, 18(11), pp. 4358–4363. Available at: https://doi.org/10.1109/JSEN.2018.2829084.

Wu, F. *et al.* (2016) 'Multiplexed detection of influenza A virus subtype H5 and H9 via quantum dot-based immunoassay', *Biosensors and Bioelectronics*, 77, pp. 464–470. Available at: https://doi.org/10.1016/j.bios.2015.10.002.

Wu, H. *et al.* (2013) 'Rapid Quantitative Detection of Brucella melitensis by a Label-Free Impedance Immunosensor Based on a Gold Nanoparticle-Modified Screen-Printed Carbon Electrode', *Sensors*, 13(7), pp. 8551–8563. Available at: https://doi.org/10.3390/s130708551.

Xia, Y., Si, J. and Li, Z. (2016) 'Fabrication techniques for microfluidic paper-based analytical devices and their applications for biological testing: A review', *Biosensors and Bioelectronics*, 77, pp. 774–789. Available at: https://doi.org/10.1016/j.bios.2015.10.032.

Xiao, W. *et al.* (2018) 'A simple and compact smartphone-based device for the quantitative readout of colloidal gold lateral flow immunoassay strips', *Sensors and Actuators B: Chemical*, 266, pp. 63–70. Available at: https://doi.org/10.1016/j.snb.2018.03.110.

Xie, K. *et al.* (2021) 'On-Site Determination of Classical Swine Fever Virus (CSFV) by a Fluorescent Microsphere-Based Lateral Flow Immunoassay Strip (FM-LFIAs) Based on Monoclonal Antibodies', *Analytical Letters*, 54(14), pp. 2347–2362. Available at: https://doi.org/10.1080/00032719.2020.1860998.

Xu, X. *et al.* (2015) 'Advances in Smartphone-Based Point-of-Care Diagnostics', *Proceedings of the IEEE*, 103(2), pp. 236–247. Available at: https://doi.org/10.1109/JPROC.2014.2378776.

Yang, K. *et al.* (2019) 'Development of a multiplex PCR to detect and discriminate porcine circoviruses in clinical specimens', *BMC Infectious Diseases*, 19(1), p. 778. Available at: https://doi.org/10.1186/s12879-019-4398-0.

Yang, M. *et al.* (2015) 'Development of a multiplex lateral flow strip test for foot-and-mouth disease virus detection using monoclonal antibodies', *Journal of Virological Methods*, 221, pp. 119–126. Available at: https://doi.org/10.1016/j.jviromet.2015.05.001.

Yang, M. *et al.* (2022) 'Combining a Universal Capture Ligand and Pan-Serotype Monoclonal Antibody to Develop a Pan-Serotype Lateral Flow Strip Test for Foot-and-Mouth Disease Virus Detection', *Viruses*, 14(4), p. 785. Available at: https://doi.org/10.3390/v14040785.

Yang, S. *et al.* (2010) 'Development of an immunochromatographic strip for the detection of antibodies against foot-and-mouth disease virus serotype O', *Journal of Virological Methods*, 165(2), pp. 139–144. Available at: https://doi.org/10.1016/j.jviromet.2010.01.001.

Yang, S.-M. *et al.* (2022) 'Microfluidic Point-of-Care (POC) Devices in Early Diagnosis: A Review of Opportunities and Challenges', *Sensors*, 22(4), p. 1620. Available at: https://doi.org/10.3390/s22041620.

Ye, H. *et al.* (2020) 'Signal amplification and quantification on lateral flow assays by laser excitation of plasmonic nanomaterials', *Theranostics*, 10(10), pp. 4359–4373. Available at: https://doi.org/10.7150/thno.44298.

Ye, X. *et al.* (2019) 'Microfluidic-CFPA Chip for the Point-of-Care Detection of African Swine Fever Virus with a Median Time to Threshold in about 10 min', *ACS Sensors*, 4(11), pp. 3066–3071. Available at: https://doi.org/10.1021/acssensors.9b01731.

Yehia, A.M., Farag, M.A. and Tantawy, M.A. (2020) 'A novel trimodal system on a paper-based microfluidic device for on-site detection of the date rape drug "ketamine"', *Analytica Chimica Acta*, 1104, pp. 95–104. Available at: https://doi.org/10.1016/j.aca.2020.01.002.

Yetisen, A.K., Akram, M.S. and Lowe, C.R. (2013) 'Paper-based microfluidic point-of-care diagnostic devices', *Lab on a Chip*, 13(12), p. 2210. Available at: https://doi.org/10.1039/c3lc50169h.

Young, M., Cunningham, G. and Sanford, E. (2011) 'Circovirus vaccination in pigs with subclinical porcine circovirus type 2 infection complicated by ileitis', *Journal of Swine Health and Production*, 19(3).

Zarei, M. (2017) 'Portable biosensing devices for point-of-care diagnostics: Recent developments and applications', *TrAC Trends in Analytical Chemistry*, 91, pp. 26–41. Available at: https://doi.org/10.1016/j.trac.2017.04.001.

Zhang, J. *et al.* (2019) 'Loop-mediated isothermal amplification-lateral-flow dipstick (LAMP-LFD) to detect Mycoplasma ovipneumoniae', *World Journal of Microbiology and Biotechnology*, 35(2), p. 31. Available at: https://doi.org/10.1007/s11274-019-2601-5.

Zhao, G. *et al.* (2018) 'Development of a recombinase polymerase amplification combined with a lateral flow dipstick assay for rapid detection of the Mycoplasma bovis', *BMC Veterinary Research*, 14(1), p. 412. Available at: https://doi.org/10.1186/s12917-018-1703-x.

Zhou, W. *et al.* (2016) 'Molecular investigations on the prevalence and viral load of enteric viruses in pigs from five European countries', *Veterinary Microbiology*, 182, pp. 75–81. Available at: https://doi.org/10.1016/j.vetmic.2015.10.019.

# Appendix

## Reference samples

The vaccine strain NADL-2 was provided by Professor I. Bossis (University of Maryland, College Park, MD, USA) and was used as a reference sample for PPV1. “In brief, the PPV1 NADL-2 strain was propagated in swine testicular cells. The cells were cultured at 37° C and 5% $CO_2$ atmosphere in Dulbecco’s Modified Eagle Medium (DMEM) supplemented with 10% heat-inactivated FBS, 100 U/mL penicillin, and 100 μg/mL streptomycin. PPV1 was collected in the supernatant. Finally, the number of viral genome copies per ml of supernatant was calculated at 72 hours post-inoculation with real-time PCR”.

The PCV-2 samples were provided by the University of Veterinary Medicine Budapest (UVMB, Budapest, Hungary). “In brief, PCV-2 strain R15, isolated from pig lung tissue in 2009 using swine testicular cells, was used in the experiments. The isolate was stored at -80 °C in DMEM. Afterwards, it was propagated on the same cell line in 25 $cm^2$ flasks with 15 mL DMEM. The cell culture medium was supplemented with 10% inactivated FBS, 50 U/mL penicillin, and 0.05 mg/mL streptomycin. Phosphate buffer saline (PBS) containing 0.5% trypsin was used for cell resuspension. Before every passage, cells were washed with 5 mL PBS. Incubation was performed at 37 °C in a 5% $CO_2$ atmosphere, and virus growth was assessed by real-time PCR”.

The PRRSV type 1 Lelystad strain was provided by Professor I. Bossis (University of Maryland, College Park, MD, USA). “The virus was propagated in sub-confluent cultures of primary alveolar macrophages (PAMs) and maintained in RPMI medium supplemented with 1% glutamine, 10% fetal bovine serum, and 1% antibiotic mixture (100 × pen-strep). Using a 96-well plate, 100 μL cell suspension per well were inoculated with 50 μL of 10-fold serial dilutions of PRRSV positive sera (tested with reverse transcription PCR) to titrate the sample. Cytopathic effect (CPE) was observed daily. At day 2 post-inoculation, 25 μL of the supernatant were transferred to freshly seeded PAM cells and CPE was observed every day (second pass). The cells were incubated at 37 °C and in a 5% $CO_2$ atmosphere. Positives were considered those in which PAM cells showed CPE at both passages. The viral genome copies per mL of the supernatant were estimated by real-time reverse transcription PCR”.

Swine influenza H1N1 and H3N2 field isolates (laboratory confirmation and isolation was conducted at the “Department of Pathology, University of Veterinary

Medicine, Budapest") were used in the study. "The samples were isolated from clinical cases of swine influenza in Hungary. Isolates were serially propagated in 9-day old embryonated chicken eggs by inoculating 100 μL of the field sample (swabs in viral transport media) in the chorionic space of eggs. Chorioallantoic fluids were collected 72 h post-inoculation, diluted 1:10 with phosphate buffered saline (PBS) and re-inoculated on 9-day old embryonated eggs. Chorioallantoic fluids were then collected 48 h post inoculation and clarified by high-speed centrifugation. SIV particles were precipitated using 5.5% w/v PEG-6000. Total protein concentration was determined using a spectrophotometer and absorbance values at 215 and 225 nm. Viral precipitates and chorio-allantoic fluids were stored at -80 °C. The viral genome copies per mL of sample were estimated by real-time reverse transcription PCR".

Reference, heat inactivated ASF samples were received from the National Veterinary Research Institute of Poland (PIWET). In short, ASF field isolate (outbreak #111, Poland 2018) was propagated in sub-confluent cultures of pulmonary alveolar macrophages (PAMs) grown in RPMI with 10% FBS. The medium was replaced with virus inoculum 18-24 h post-seeding and PAMs were incubated for 2 hours at 37°C to allow the absorption of the virus. Subsequently the virus inoculum was removed; cells were washed twice with medium and incubated for 72-120h. Cell culture aliquots were collected daily for DNA extraction and real-time PCR analysis to monitor virus propagation. After the development of CPE, the culture media was collected and clarified by centrifugation. The clarified, heat inactivated supernatant served as the reference sample in the device validation. The same organization (PIWET) provided heat inactivated CSF reference samples. Strain Alfort 187 was propagated in confluent monolayers of the swine kidney cell line SK-6 and cultured in MEM supplemented with 7% horse serum. After the development of CPE, both the released and cell-associated virus was collected using 3 freeze-thaw cycles and centrifugal clarification.

## ELISA experiments for the validation of anti-SIV and anti-ASFV antibodies

Two commercial antibodies for ASF and one for SIV were tested with an indirect ELISA assay to evaluate their reactivity with reference samples. The antibodies tested were:

1) Anti-ASFV antibody Ingenasa M.11.PPA.I1BC11 (anti - VP72)
2) Anti-ASFV antibody Ingenasa M.11.PPA.I17AH2 (anti - VP220/150)
3) Anti-SIV antibody Invitrogen MA5-17101

The indirect ELISA assay protocol was the following:

A) Plate coating of antigens in carbonate/bicarbonate buffer pH = 9.2 at 4 °C, overnight. Both ASFV antigen and SIV antigen (PEG-6000 purified) were diluted in a ratio 1/100 for the coating.

B) 2 washes with PBS + 0.05% Tween 20

4) Blocking with PBS + 2.5% BSA + 0.05% Tween 20 for 90 minutes at room temperature
5) 2 washes with PBS + 0.05% Tween 20
6) Incubation of the primary antibody for 90 minutes at room temperature, at a dilution of 1/500 in PBS + 0.5% BSA + Tween 20
7) 6 washes with PBS+0.05% Tween 20
8) Incubation of the secondary antibody for 60 minutes at room temperature, at a dilution of 1/2000 in PBS + 0.5% BSA + Tween 20
9) 6 washes with PBS+0.05% Tween 20
10) PBS for 10 min
11) Incubation of the substrate for 12-15 min and stop solution ($H_2SO_4$)

The antibodies could be used for the detection of antigens with high selectivity and without background. ELISA testing indicated that the best performing antibodies were:

1) Anti-ASFV: M.11.PPA.I1BC11 (Anti PPA VP72) for ASFV

2) Anti-SIV: Invitrogen MA5-17101 for SIV.

We were able to detect SIV using the Invitrogen MA5-17101 antibody in complex samples with a high protein content such as chorioallantoic fluids of embryonated chicken eggs at 1/10 dilution in carbonate/bicarbonate buffer, pH=9.2

## Assessment of the regeneration protocol

The efficiency of the regeneration protocol was assessed prior to the finalization of the analysis protocol. HRP-conjugated goat/anti-rabbit antibodies were deployed on PIC surfaces to capture the immobilized MREs. Buffer (to wash the excessive antibodies) and TMB substrate were consecutively passed through the sensor and collected in Eppendorf tubes, resulting on the formation of blue-colored product (HRP-mediated oxidization of TMB). $H_2SO_4$ was added immediately to the flow-through to stop the oxidizing of TMB. Washing buffer and 300 μl (the same amount is used in the analysis protocol of the

diagnostic device) of regeneration buffer, 50 mM Glycine + 50 % Ethylene Glycol, pH=3, were passed through the PIC, followed again by washing buffer and TMB substrate. After the regeneration step, TMB substrate did not develop any color (figure below), indicating that HRP-conjugated antibodies were released, and consequently that the regeneration protocol was efficient.


## Sanitization protocol

Sanitization is an important procedure during on-site testing for viral pathogens, especially in the case of ASF and CSF. Residues and waste during testing were discarded in a waste tank for UV light sterilization. During experimentation a 10% bleach solution was also added in the waste tank for sterilization.

Approximately 40 days, after initiation of the experiments with high protein content samples, the development of fungi in the interior of the microfluidic channels was observed. This was caused by the accumulation of proteins on the interior surface of the microfluidic channels.

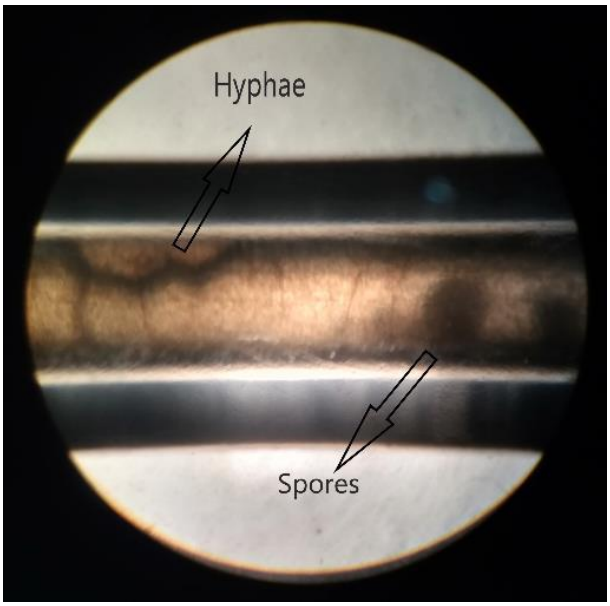


The microscopic image of the microfluidic channel depicts the development of fungal hyphae and spores. As a result, the microfluidic channel was replaced. The channel was washed with warm soapy water and was sterilized with a 10% bleach solution. Considering the aforementioned, the application of a sanitization procedure/protocol for the elimination of fungi or other contaminants is suggested at the end of the experimentations, especially in the case of long-term storage of the device.

The application of bleach, ionic detergents and acidic/basic solutions for the sanitization of the microfluidic channel, should not be delivered to the PIC surface due to the potential destruction of the immobilized antibodies on the sensor's surface. In fact, after a sanitization protocol, the microfluidic channels should be extensively washed with water and running buffer (PBS + 0.05% Tween 20).